THEORETICAL ASPECTS OF BLUNT BODY MAGNETOAERODYNAMICS

by

Robert W. Porter* and Ali Bulent Cambel**

Gas Dynamics Laboratory

Northwestern University

Evanston, Illinois

NU-GDL REPORT N-1-66

Contract No. NsG 547

National Aeronautics and Space Administration

August, 1966

Approved:_____

Ali Bulent Cambel
Principal Investigator

*Research Assistant in Mechanical Engineering and Astronautical Sciences

**Walter P. Murphy Professor and Chairman, Mechanical Engineering and Astronautical Sciences

ABSTRACT

Theoretical aspects of supersonic magnetoaerodynamic flow about a blunt body with self contained magnetic field source are presented. The effect was studied for a hemisphere nose containing a dipole field source with body and magnetic axis at zero angle-of-attack. Theoretical predictions of the alteration of magnetoaerodynamic coefficients and of the flow field are presented for a range of parameters appropriate for possible application to planetary entry flight control and laboratory simulation. Emphasis was on determining the principal contributing effects for continuum, aerodynamic-like flows.

After a general introductory to flight magnetohydrodynamics and appropriate literature survey, flight and laboratory regimes were delineated and compared. A mathematical model for constant property flow was developed and the equations were non-dimensionalized in terms of parameter groups. Estimates of the expected range of parameters were presented.

The equations were reduced for the stagnation region where the principal effect and local similarity occur. The resulting two point boundary value problem with undetermined boundary point was solved analytically for simple degenerate cases and numerically for more complex combinations of the parameters. The numerical techniques are discussed.

It was found that the shock density ratio and magnetic interaction parameter are of principal importance. Viscous effects are also important for

low density laboratory flows. Results are presented which demonstrate these effects and the influence of magnetic field distortion and the Hall effect.

Comparison with experiment and new avenues for theory are discussed.

TABLE OF CONTENTS

LIST OF TABLES

LIST OF FIGURES

FIGURE PAGE

FIGURE PAGE

CHAPTER I

INTRODUCTION

1.1 Flight Magnetohydrodynamics

It is well known that the bow shock ahead of a blunt body in hypersonic flow results in an ionized region of electrically conducting gas. In entry flight to Earth or other planets, communications blackout may occur, the structural integrity of the vehicle may be impaired and the aerodynamic forces may not be sufficient to maintain control of a high speed vehicle.

Incorporation of magnetic field coils in space vehicles offers interesting possibilities in alleviating some of the problems of space flight. It has been suggested by Kantrowitz (Ref. 1) and by Resler and Sears (Ref. 2) that coupling the flow field with a magnetic field might have salutory effects by increasing the drag experienced by an entry vehicle. Other promising applications of external magnetogasdynamics are: the opening of communications windows, enhanced flexibility of maneuvers through improved flight control, active shielding against radiation, the reduction of convective heat transfer and the elimination of the conventional heat shield.

So far such schemes have not been exploited due to hardware design limitations and due to the fact that current design philosophy has been successful in current programs. However, continuing progress in superconducting magnets and the demands of advanced space programs lend practical significance to equipping space vehicles with electromagnets.

This work is concerned with one of the applications mentioned above, namely magnetoaerodynamic drag. Although categorization often leads to questionable over simplification, a vehicle may be said to encounter three types of drag, i.e., aerodynamic, magnetohydrodynamic and electric. In general, the first two classes are associated with continuum flow while the last occurs at extremely high altitudes where the gas is substantially rarefied. Since the underlying practical application of the study is entry drag and its enhancement in appreciable atmosphere, this study does not concern itself with electric drag. The reader is referred to Wood (Ref. 3) for such a study while the present work is limited from the onset to continuum flow. The regime where such flows exist is discussed in Chapter II. It is natural to further limit the bulk of the discussion to bodies and electromagnets with axis at zero angle-of-attack and to aerodynamic-like flows. Angle-of-attack produces cross-flow and lift but the drag is the same qualitatively. Magnetically dominated flow may occur at extremely high magnetic field strength causing a lift-off of the flow from the body. However, before employment of the phenomena of investigation it is very important to understand the intermediate or aerodynamic-like flow first.

While an analysis of the complete configuration of a blunt vehicle requires knowledge of the flow in the nose region, along the afterbody and in the base region, the point of view taken here is that the principal magnetohydrodynamic effect for braking will occur near the nose. Thus, the theory is principally concerned with the stagnation region. For concreteness we consider a hemisphere nose and an onboard magnetic

dipole field source located at the nose radius center of curviture.

The general configuration of interest is shown in Figure 1a. With no magnetic field, the flow has the well known features associated with hypersonic flight. A bow shock lies forward of the nose and because of the thinness of the shock layer, the layer of gas between the shock and body, the shock is nearly concentric with the nose. Far away from the body, the shock angle approaches that for a small disturbance. The shock has finite thickness but is presumably small in thickness. Other distinctive layers include the inviscid, boundary and sheath layers. These are described in detail in Chapter II. Wake or base flow occurs behind the body. In hypersonic flow, this is a region of low density and little direct effect of it is felt by the body except for suction due to its low pressure. This is the so-called base drag. Most of the drag, however, is due to the pressure on the nose. Friction drag also is important for low Reynolds number flow. These considerations allow one to consider the nose region only and account for most of the drag effect. Base drag is small and can be estimated if desired.

When the magnet is turned on, as in Figure 1b, the flow interacts with the magnetic field to cause a body force on the fluid, $\underset{\sim}{J} \times \underset{\sim}{B}$ where J is current density and B magnetic field strength. The reaction force of these $\underset{\sim}{J} \times \underset{\sim}{B}$ forces (on each fluid element) is felt by the magnet structure and thus by the vehicle as a unit. The drag of the vehicle tends to increase. This is the basic phenomena behind the MHD drag concept.

The shock stand-off distance increases because the flow is slowed down and requires a larger passage area between the shock and body in order to accomodate the flow rate impressed ahead of the shock wave.

Obviously, the flow rate cannot be influenced by anything that occurs downstream of the shock wave (so long as we neglect free stream magnetic interaction). Figure 1b also indicates the currents involved. These are discussed in detail later. Basically, the principal currents run in the azimuthal direction or in rings about the axis. These currents interact with the magnetic field to produce Hall currents. The entire system is highly coupled and the Hall current paths depend on the conductivity of the body. In Figure 1b we show the path near the shock. In this region the path is qualitatively the same for an insulated or conducting body.

The general effects of the applied magnetic field can be summarized as follows. The skin friction and stagnation point heat transfer are decreased due to a reduction of the velocity gradient. The pressure drag is diminished due to a partial support of the flow by the magnetic pressure. The total drag of the body increases because of the Lorentz force on the fluid and the reactive force on the magnet. The body is subjected to a rolling moment due to reaction on the magnet of the Lorentz force in the azimuthal direction.

Most of the literature cited deals with the external flow since the MHD drag force is most conveniently thought of as a body force on the fluid with reactive force on the magnet structure. Thus, one may integrate the fluid body force to obtain the body drag. We purposefully avoid studies limited to the boundary layer because in such a case calculation of the external contribution to the drag can only be made through knowledge of the magnetic stress at the body. In order to obtain the magnetic stress one must first solve the outer flow and supply its

solution as a boundary condition for the boundary layer analysis. Thus, while boundary layer theory is useful for describing boundary phenomena such as skin friction and heat transfer, it is inadequate for predicting the total MHD drag. Further, at high altitudes or in low density laboratory simulation, the boundary layer may cease to exist. This occurs at low Reynolds number. Accordingly, some of the references cited and the theory presented here have some consideration of the viscous shock layer.

Generally, most MHD analyses follow either of two basic viewpoints. One approach is to assume that the plasma is compressible but that its electrical conductivity is infinite. The alternate approach is to appreciate the finite conductivity but to assume that the plasma density is locally constant. The former viewpoint, although practically unrealistic, makes it possible to reduce the problem to a form well exploited in conventional gasdynamics. Analogously, singularities occur at magnetic Mach number of unity instead of simply Mach one. The second approach too has limitations in MHD analyses. The acceptance of finite conductivity is a great improvement since the shock layer conductivity may be low. However, the assumption of constant density is not completely acceptable. This is particularly true in magnetically dominated flows where the density essentially vanishes at the boundary of no flow. However, the constant density approximation has been very useful in aerodynamic-like flow studies where the body supports the shock layer. In such a layer, the density is relatively constant, particularly at hypersonic speeds. The constant density approximation will be discussed in more detail subsequently.

One great simplification that is often made is that the magnetic Reynolds number is small so that wave propagation effects, characteristic

of high magnetic Reynolds number, are not present. The applied magnetic field can also be assumed to be undistorted or only perturbed by the flow for small magnetic Reynolds number. This effect will be studied through the theory developed. Finally one can make the very rough approximation that the flow field is not much effected by the magnetic field. This is valid for very small magnetic interaction.

In almost all analyses it has been assumed that a simple form of Ohm's law applys. Essentially, the Hall effect is neglected. However, depending on the magnitude of the Hall coefficient, which depends on the magnetic field strength linearly, and depending on the geometry currents and electric fields arise and effect the flow and drag. Further, these currents, which lie in meridian planes (planes including the body and magnetic axis), give rise to body forces in the azimuthal direction and a reactive rolling moment on the body.

The Hall effect has been studied in detail for only simple external flows. For example, Levy (Ref. 4) studied the assumption of reduced effective conductivity on the flow past a conducting wire with no perturbation. However, his attention was directed to the alteration of currents that would exist without the Hall effect although one plot of Hall current path lines was presented. In the theory developed here, the Hall effect is studied. Predictions of its effect on the flow and electromagnetic fields, the conventional magnetoaerodynamic coefficients and the torque coefficient are made.

The rest of this chapter concerns a literature survey limited to areas reflecting on the drag problem. In Chapter II the flow regimes are delineated. That is, we attempt to foresee what assumptions are appropriate. This is done not only for flight conditions but for conditions

which exist in low density laboratory plasma facilities. All subsequent development includes such considerations as well.

In Chapter III, a mathematical model for constant property flow is developed. Chapter IV concerns equation reduction for the shock layer stagnation region in terms of local similarity. The explicit solutions are discussed in Chapter V and the results are presented in Chapter VI. Rather than consider all possible variations of all combinations of parameters, the emphasis is on discovering which effects are important by studying them one at a time. Conclusions, based on theory and experiment, are summarized in Chapter VI . At this point we focus on the observations made in course of the present theory and suggest how the MHD effect may be accounted for. Finally, its shortcomings are recalled and recommendations for future study are made.

1.2 Literature Survey

The survey that follows is intended to lend historical perspective to the theoretical development of magnetoaerodynamics related to the drag problem. The principal assumptions are listed in Table 1 for representative studies.

In 1958, Bush (Ref. 5) treated the hypersonic, axisymmetric stagnation point flow about a blunt body with magnetic source. The flow was assumed to be inviscid and incompressible behind the shock. The assumptions of constant density and electrical conductivity in the layer behind a shock concentric with the body allowed reduction of the problem by similarity to two coupled, non-linear ordinary differential equations. The one point boundary value problem was numerically integrated backwards from the shock to the body after the flow properties and magnetic field

intensity were specified at the shock. This approach is convenient but is in terms of rather unnatural parameters such as

$$Rem_s = \sigma_1 V_1 R_s \mu \tag{1-1}$$

$$S_s = \frac{\sigma_1 B_s^2 R_s}{\rho_\infty V_\infty} \tag{1-2}$$

where Rem is the magnetic Reynolds number, S is the magnetic interaction parameter and σ is conductivity V velocity, R radius, B magnetic field intensity and ρ density. The subscripts ∞, s, 1 refer to the flow at infinity, at the shock and in the shock layer respectively. The parameters are unnatural because they are based on a prior unknown shock condition "s" instead of the body reference.

The solution was obtained for $\epsilon = 1/11$ where

$$\epsilon = \rho_\infty/\rho_1 \tag{1-3}$$

and for $Rem_s \epsilon = 0$, .2 and 1. The interaction parameter S_s ranged from 0 to 16. Beyond $S_s = 16$ no solution was found to exist and the approach to this limit was accompanied by a rapid increase in shock stand-off distance. However, the value of the more natural interaction parameter

$$S = \frac{\sigma_1 B_o^2 R_b}{\rho_\infty V_\infty} \tag{1-4}$$

based on stagnation point field and body radius had a value of over 300 near the limit. In a later note (Ref. 6), Bush suggested that arbitrarily large values of S produce correspondingly large stand-off distances

$$\delta = \frac{R_s - R_b}{R_b} \tag{1-5}$$

It is surprising that the net effect is a limiting S_s.

Both the stand-off and pressure relief were found to increase with S_s and Rem_s^{-1}.

In an analytical study of the same basic problem as Bush, Kemp (Ref. 7) extended Lighthill's non-MHD solution (Ref. 8) to the case where a radial magnetic field is present. An expansion technique in ϵ and S required small values of these parameters. Also, the magnetic field was assumed to be undistorted (Rem = 0). While Kemp succeeded in calculating the MHD induced pressure relief, Freeman (Ref. 9) showed Kemp's analysis to be incorrect due to a false assumption of analyticity of the functions concerned. Freeman applied Lighthill's prescription (Ref. 10) for rendering such solutions uniformly valid and determined that the MHD pressure relief is negligible to first order in S. That is, for small interaction the body pressure coefficient is virtually uneffected.

In reply to Freeman, Kemp conceded the analyticity error and extended the earlier work by numerically integrating the equations. For $\epsilon = 1/10$ and S from 0 to 6, the stand-off, velocity gradient and pressure gradient were calculated; the later being small as indicated by Freeman.

Meyer (Ref. 12) extended the MHD hypersonic, stagnation point flow solution to include viscosity and heat transfer. Proposing a similarity solution for small values of Rem/Re, where Re is the Reynolds number

$$Re = \rho VR/\eta \tag{1-6}$$

η is viscosity, Meyer obtained the boundary layer approximation as a function of S for large S. The heat transfer coefficient was reduced

at the wall but increased in the external flow.

Ladyzkenskii (Ref. 13) treated subsonic, incompressible flow over bodies in order to study certain induced effects. For Rem $\rightarrow \infty$, there occured large surface currents and an induced magnetic field which exactly cancelled the applied magnetic field. For large but finite Rem there occurs a Prandtl type "magnetic boundary layer" and a thickened boundary layer with reduced region of external flow.

Ladyzkenskii (Ref. 14) further considered a wedge and cone in hypersonic, constant conductivity flow. Compressibility was included in an approximate way by using the polytropic law along a streamline. He neglected the dissipation term in the modified Bernoulli equation. The deformation of the magnetic field is handled by writing the appropriate Maxwell equation in intergral form and solving for the first successive approximation. An important result of Ladyzkenskii is the prediction of a magnetically induced separation point which is not normally present in conical or wedge flow. The separation, which moves toward the stagnation point with increasing interaction, is accompanied with an inflection in shock curviture such that the shock curves away from the body.

Yen (Ref. 15) reduced the problem of two-dimensional, incompressible subsonic, constant viscosity and conductivity, MHD flow past a wedge. Two ordinary, non-linear differential equations resulted from similarity. The solution was not carried out further.

Ludford and Murray (Ref. 16) also treated the incompressible subsonic problem but for a sphere with a dipole field source enclosed. Fluid properties were uniform including electrical conductivity and magnetic permeability which were also arbitrary constants of the sphere. A product type solution

was found after an expansion process was applied. This was accomplished by first expanding in the magnetic pressure number

$$\beta = \frac{B_o^2}{\mu \rho_\infty V_\infty^2} \tag{1-7}$$

to first order and further expanding that first term in a singular perturbation of the magnetic Reynolds number. The results are valid for small β and Rem. This implies a small value of S. The fluid pressure drag was found to be unchanged from zero to first order in Rem. Further, the MHD drag was independent of the body conductivity so long as it was not infinite. The MHD drag of an infinitely conducting body was still unchanged so long as its permeability μ was equal to the fluid value. A high permeability, infinitely conducting body would have a greatly increased drag. In summary, the MHD drag was unchanged for ordinary body composition according to the results of Ludford and Murray's analysis.

Returning to supersonic analyses, Wu (Ref. 17) extended Bush's solution to include viscosity and heat transfer. The dynamics of the constant property (density, viscosity and conductivities) flow was reduced to two ordinary differential equations. Once these functions were determined, two other differential equations yielded the thermodynamics. The solution was accomplished on a PACE 1631 analog computer. Wu found the same limiting S_s phenomena as Bush. That is, solutions for interaction parameters beyond a point were non-existant. Significant was the fact that the shock stand-off distance increased with the parameters Rem_s, β_s and $1/Re_s$.

Meyer (Ref. 18) utilized the fact that the total enthalpy is constant along a stream line in axisymmetric, adiabatic flow even though Joule heating is present. Treating hypersonic, constant property flow, Meyer developed

a Newtonian-Busemann type theory modified for MHD application. A similarity solution was found for this approximation.

Lykoudis (Ref. 19) also considered the Newtonian-Busemann approximation in the sense that the conventional pressure distribution was used in the momentum equation for a stream line. The assumption is justified for small interaction according to the work of Kemp and Freeman. Constant property, inviscid flow was assumed behind the shock. The radial magnetic field was taken as a constant. An appropriate mean value is suggested by Lykoudis in Reference 20. The solution was in terms of integrals which were functionals of a special variable including S_s and ϵ. Magnetic field deformation was neglected. In addition to sample solutions for ϵ = 1/5, 1/10, 1/15 and 1/20 and for S_s from 0 to 30, Lykoudis gives empirical functions for the stand-off and velocity gradient in closed form in terms of S_s and ϵ.

Pai and Kornowskii (Ref. 21) treated the hypersonic, inviscid, constant property, stagnation flow similarly to Bush but the magnetic field was assumed to appear in an inverse n-power law at the shock. Values of n of 3, 4 and 5 were selected where 3 corresponds to Bush's choice of a dipole. Actual field coils will have a faster drop off or a higher n-power value. The origins of the poles were chosen to be located one body radius behind the shock. Unfortunately this physical location varies in the problem. Thus, while the MHD effect, characterized by the shock stand-off, increased with increasing n, part of the effect must be attributed to the resultant movement of higher n-power poles closer to the flow. While sufficiently high values of S were not used in the numerical examples, the above scheme could result in poles situated outside of the body and in the flow.

Whereas low magnetic Reynolds numbers are expected for flight situations,

Andrade (Ref. 22) dealt with hypersonic, compressible flow with $Re_m \to \infty$. With no heat transfer or other dissipation, the use of

$$\frac{d}{dt}\left(\frac{p}{\rho^{\gamma}}\right) = 0 \tag{1-8}$$

was justified. The Van Dyke transformation led to reduction to second order, non-linear, ordinary differential equations. No results were given.

Power and Turnbridge (Ref. 23) extended Ludford and Murray's analysis of a sphere to the two dinensional case. Both analyses are parallel.

Levy and Petschek (Ref. 24) considered hypersonic flow normal to a conducting cylinder with concentric magnetic field lines. In the stagnation region, this corresponds qualitatively to a dipole with the principle axis normal to the flow rather than the usual case. Both high and low magnetic Reynolds numbers were treated according to appropriate ad hoc approximations. At high enough MHD interaction it was predicted that the shock layer would actually lift off the body and be magnetically supported. This phenomena was verified experimentally by Locke, Petschek and Rose (Ref. 25), but their photographs do not show a sharp no-flow boundary. It was predicted that this lift-off would occur and be accompanied with further lift-off with a constant shock interaction parameter S_s. The theory necessarily included compressibility since a body would no longer be present to back up the flow and the density would vanish at the no-flow boundary. It is interesting to note that Bush's incompressible solution did not exist beyond a critical S_s. Therefore, it would appear that this may be due to a non-existant physical solution.

Smith and Wu (Ref. 26) extended Bush's solution to include viscosity.

Numerical solutions again were non-existant beyond a critical S_s. Smith and Wu suggested that the phenomena may be due to large deformation of the magnetic field at high interaction. This does not appear to be the case since Bush found only a small difference in computations for $\frac{Rem}{\epsilon} = .2$ and 1. The present author has repeated the calculations (to be discussed later) for the limit Rem = 0 and has found again no significant difference for the case of no magnetic deformation.

It seems that the critical S_s occurs naturally with a large field strength, B_o, causing an increase in stand-off coupled with a decrease in B_s such that $S_s = \sigma_1 B_s^2 R_s / \rho_\infty V_\infty$ remains constant. This assumption was used by Ericson and Maciulaitus (Ref. 27) who added a gimbeling magnet in the nose to produce lift for entry flight control. The flow was divided into a longitudinal flow and a cross-flow with respect to the magnetic axis. The longitudinal flow, causing drag, was not considered further. The authors indicate that MHD flight control would be effective enough to trim a 20^o sphere-cone of nose radius 0.5 meter and length 5.5 meters while in interplanetary re-entry.

Levy, Gierasch and Henderson (Ref. 28) extended the work of Levy and Petschek to include a sphere in magnetically dominated flow. The analysis indicated the presense of a no-flow region at large S_s interaction and that the interaction parameter at the shock, S_s, is constant.

It appears as though an increase in interaction parameter (say by increasing the stagnation point field strength) causes an increase in shock stand-off and an increase in shock interaction parameter S_s. While this occurs, the body supports the shock layer and maintains the layer density about constant. Beyond a critical value of S_s, the shock layer is lifted

off the body and is magnetically supported. The density must essentially vanish at the no-flow boundary and so a constant density solution does not exist. Further increase in the interaction parameter S causes an increase in shock stand-off and a decrease in shock magnetic field such that S_s is held constant. Viscosity apparantly does not change the situation except for altering the critical S_s (Ref. 26). The experiments do not show a sharp no-flow boundary and so there is apparantly some leakage into the region where the theory predicts no-flow. It is conceivable that the collision mechanism at low density is not sufficient to prevent diffusion into the forbidden area. Alternatively, the Hall effect may reduce effective interaction near the body where the magnetic field is high and this reduced interaction may admit some flow. Finally, a no-flow region may be unstable. Or a combination of these effects may be present.

Smith, Schwimmer and Wu (Ref. 29) have extended their previous viscous, hypersonic, stagnation flow solution so that it is based on the natural parameters based on body radius and magnetic field. This involves the solution of a two point boundary value problem with second point unknown. The solution was accomplished through the use of normal quasilinearization wherein the non-linear equations are replaced by a sequence of systems of linear equations which are readily treated by the extensive theory of linear systems. Unfortunately, solutions at even moderate interaction parameter were not found because the linear system converged to an incorrect solution except for small S. The results they did obtain showed much larger shock stand-off than that predicted by Bush. Some of the difference can be attributed to an incorrect magnetic field boundary condition. The value used is consistant with an interaction parameter based on dipole

moment, such as in Bush's original notation, but they have used the reference magnetic field basis (as in the present work) and so their magnetic field is essentially everywhere twice as great as it should be. This would indicate that their plotted results could be corrected by multiplying the interaction parameter scale by 4 (since the square of the magnetic field is included in it). Wu has acknowledged that Bush's results were also plotted incorrectly.* The same correction factor applies to the curve attributed by Bush in that plot. The present author has repeated the computations (to be discussed later) and has found that the quasi-linearization scheme truly converges only for small S. Using a different scheme, the large difference in stand-off with that of Bush has disappeared leaving only a small expected effect due to viscosity. A comparison of these various computations is given later.

Bass and Anderson (Ref. 30) have applied an order of magnitude quasi one-dimensional analysis in order to estimate the MHD drag for hypersonic, blunt body flow. An effective duct length is involved. There is reasonable agreement with the experiments of Seeman (Ref. 31).

Seemann and Cambel (Ref. 32) and Nowak, Kranc, Porter, Yuen and Cambel (Ref. 33) have also made such estimates but in terms of the dimensionaless parameters. The computations involve integrating the Lorentz force on the fluid. These estimates generally turn out to be high because they fail to account for alteration of the flow. Improved methods of estimating the drag will be indicated later in this report.

---

* Porter, R. W. and A. B. Cambel, "Comment on 'Magnetohydrodynamic-Hypersonic Viscous and Inviscid Flow Near the Stagnation Point of a Blunt Body'", AIAA Journal, 4, 1966.

Smith, M. C., Schwimmer, H. S. and C. S. Wu, "Author's Reply", AIAA Journal 4, 1966.

CHAPTER II

FLOW REGIMES

2.1 Introduction

The purpose of this chapter is to evaluate and compare the flow regimes for flight magnetohydrodynamics and for simulation in the laboratory by means of hyperthermal plasma arc jet units.

When an entry vehicle enters an atmosphere, it is subjected first to a rarefied flow. It may have an electric charge accumulated on its surface depending on its past history and may experience electric drag (Ref. 34). The charged particles in the nose region will separate and produce a region of local charge non-neutrality called the plasma sheath. Passing into denser regions, a bow shock will form - the flow being continuum in nature but describable only with the full Navier - Stokes equations from the forward "surface" of the shock to the body, an incipient merged layer (Ref. 35). In this region, and at lower altitudes, the denser flow has a large momentum and reactive forces can arise due to interaction between the flow field and a magnetic field if a magnetic source is provided within the body. At still lower altitudes, the shock thickness is thin enough so that a viscous shock layer is formed behind a shock discontinuity. Finally, the flow in the shock layer becomes essentially inviscid except near the wall in the Prandtl boundary layer.

In this study, we are principally concerned with regions where the magnetogasdynamic effect is significant enough to be used to advantage. Thus, we expect a continuum theory to be applicable and neglect effects which are important only at extremely high altitudes. The extent of the regime of interest and the sub-regimes which occur at lower altitudes are

discussed in the rest of this chapter. First, however, we will briefly discuss differences that exist in laboratory simulation.

If photoionization is neglected (say below 80 km), the flight free stream is essentially a neutral gas and is shock heated into an ionized gas in the shock layer. On the other hand, in the laboratory the gas is pre-ionized due to heating in a thermal arc torch. A second difference arises from the flight free stream being essentially uniform and unbounded whereas the laboratory jet is non-uniform (but hopefully symmetric) and finite. Since magnetic field coils provide dipole-like fields at large distances and the field falls off rapidly in strength, the interaction in the pre-ionized region seems less important. Likewise, non-uniformity would appear less important if one had a small body so that the flow would be locally uniform near the interaction zone. So far, these presumptions have not been verified categorically. Other differences exist. For example, the type of gas, Mach number range, characteristic length, temperature and viscous effects differ:

In Flight	Laboratory
Air	Argon
$10 < M_\infty < 50$	$2 < M_\infty < 6$
$L \sim 10$ ft.	$L \sim 1$ in.
T_∞ low	T_∞ high
viscosity unimportant	viscosity important

Differences of this type are included in the discussion that follows.

2.2 Types of Regimes

Our description of the entry conditions was based on the dynamics of the flow. At various altitudes, the flow will have the various character-

istics mentioned and can be classified into aerodynamic regimes. Similarly, the thermodynamics of the flow undergoes changes and these may be classified into thermodynamic regimes. The introduction of magnetic sources leads to magnetogasdynamic regimes. While coupling of the phenomena occurs, this categorization is useful.

With respect to the aerodynamic regimes, we seek to answer on the basis of simple estimates the following questions: At what altitudes and laboratory conditions may the flow be considered continuum? When can the shock be treated as a thin discontinuity so that the Rankine-Hugoniot relations apply? At what conditions is the flow effectively viscous only very near the body surface (except in the shock itself) so that the Prandtl boundary layer applies? Finally, if a plasma sheath of local electric charge excess exists, is it merged into the aforementioned layers or is it a sublayer. To answer these questions we seek information with respect to:

1. The continuum flow regime characterized by the ratio of mean free path to the characteristic body dimension.
2. The Rankine-Hugoniot shock characterized by the ratio of shock thickness to the shock layer thickness.
3. The Prandtl boundary layer characterized by the ratio of boundary layer thickness to shock layer thickness.
4. The plasma sheath characterized by the ratio of the sheath thickness to boundary layer thickness.

Our approach is orientated toward conservative estimates of the consistancy type. For example, we will assume a Prandtl layer and determine when it becomes so large so as to invalidate the assumption.

The basic question under thermodynamic regimes is whether or not the flow is in chemical equilibrium. In magnetogasdynamic regimes the important factor is whether or not the flow is magnetically dominated. Since the principal interest of this work is aerodynamic like flow and the dynamics relating to drag, the aerodynamic regimes are discussed in more detail.

To formulate the analysis, let us define the flow conditions. For flight: Earth atmosphere, flight Mach number M_∞ from 8 - 50 and a hemisphere nose of 10 foot diameter with negligible afterbody. For the laboratory flow: argon plasma at free stream pressure p_∞ from 10^{-4} to 10^{-2} atmospheres and free stream gas temperature T_∞ from 1000 - 4000^{o}K, free stream Mach number 2 - 6 and a hemisphere body of 2 inch diameter. At this point we comment that higher Mach numbers are difficult to achieve in continuous plasma facilities, but that the important factor seems to be the shock layer enthalpy and density (Ref. 36) and these can be simulated.

2.3 Aerodynamic Regimes

The appropriate dimensionless parameter to determine whether the flow is continuum or rarefied is the free stream Knudsen number

$$Kn_\infty = \frac{\lambda_\infty}{D} \tag{2-1}$$

where λ_∞ is the free stream "mean free path" between collisions and D is the characteristic body dimension in the crosswise direction. When $Kn_\infty \ll 1$ there are many collisions of a typical particle in the nose region and the flow is expected to be continuum. Conversely, when

$Kn_\infty \gg 1$ the flow is rarefied. In between, transition and slip flow regimes exist (Ref. 37). Figure 2 shows the overlap of the Knudsen number values of flight and laboratory flows. For these estimates the model atmospheres of References 38, 39 and 40 were used for flight. For the argon plasma, we assumed that local thermodynamic equilibrium exists and used the real gas viscosity of Reference 41 to define an effective mean free path according to simple kinetic theory. The momentum averaged mean free path is (Ref. 42)

$$\bar{\lambda} = \frac{\eta}{\frac{5\pi}{32} \sum_i \rho_i \bar{V}_i} \tag{2-2}$$

where η is the viscosity, ρ_i the density of species i and $\bar{V}_i$ is the species mean molecular speed

$$\bar{V}_i = \sqrt{\frac{8RT_i}{\pi M_i}} \tag{2-3}$$

where the summation is over the heavy species. For a monotomic gas with the heavy particle temperatures about equal to the gas temperature (Ref. 42)

$$\bar{\lambda} = \frac{\eta}{\frac{5\pi}{32} \rho \sqrt{\frac{8RT}{\pi M}}} \tag{2-4}$$

For convenience, we have used the equilibrium density of Reference 44 which considers only the first degree of ionization without excitation.

Figure 2 suggests a flight continuum regime below 300 kilofeet and a laboratory continuum regime above 0.0005 atmospheres or lower depending on the temperature.

The Hugoniot shock assumption requires

$$Kn_s = \frac{\lambda_\infty}{\Delta} \ll 1 \tag{2-5}$$

where Δ is the shock stand-off distance. When the inequality holds, the shock thickness is thin with comparison to the shock layer and a discontinuity in the supersonic flow can be assumed. The shock thickness is approximated by λ_∞ since it is established in a few collisions. We can conservatively estimate

$$\Delta = .78\, \epsilon\, R_b \tag{2-6}$$

This is Seiff's correlation (Ref. 45) for high Reynolds number flow and is surprisingly accurate for moderate supersonic to hypersonic speeds. Viscous MHD flow will have a greater Δ. To make an order of magnitude estimate, the equilibrium values of the density ratio ϵ are used. For flight, the tables of Huber (Ref. 46) are convenient while for laboratory flow the method of Arave and Huseley (Ref. 44) is applicable. These assume a Hugonoit shock and so we are really demonstrating consistancy, as noted before.

The results, shown in Figure 3, indicate that a Hugoniot shock is present below about 250 kilofeet in flight. In the laboratory, a thickened shock must be expected. The thickening is due to the viscous and low density condition of the gas. The Hugoniot approximation appears less valid there, but since the situation is border-line and the alternative of considering incipient merged theory involves great difficulties, the assumption seems justified with forebearance.

The Prandtl boundary layer requires

$$\frac{\Delta_{b.l.}}{\Delta} \ll 1 \tag{2-7}$$

where $\Delta_{b.l.}$ is the boundary layer thickness. This can be estimated from

the solution for Hiemenz stagnation flow (Ref. 47) and the matching of the far flow to the shock pressure coefficient.

$$\frac{\Delta_{b.l.}}{\Delta} = 2.4\ Re_{\Delta}^{-.5} \tag{2-8}$$

Figure 4 was constructed using the equilibrium calculations as before. Once more, the flight situation appears better. The boundary layer would appear to be distinct below 250 kilofeet while viscosity seems important over much of the shock layer for some laboratory flow.

As mentioned earlier, the plasma sheath is a region near the body where charge separation can occur. The importance of the sheath depends on the extent of the sheath, the charge available for separation and the electrical bias of the body. A flight vehicle will float at a potential determined by its past history while a sting supported model will be grounded unless provisions are made. Whether the model or vehicle has a conducting or insulated surface may be an important effect but even this is complicated by the possibility of shorting out insulated areas through a highly conducting plasma sheath.

In the type of facility of interest here, the gas will experience a large potential near the electric arc of the torch. The potential will decrease away from the arc and probably reach a low level where models are normally inserted in the flow. However, because of the presence of supersonic flow, a bow shock is present and charge separation and an electrical potential may be generated at this surface. If the model is regarded as at ground potential and this potential is maintained with electrical contact with the facility as a whole, a sheath will exist to match the potential of the body to the flow.

In any case, the sheath acts as a region of potential gradient to match the body bias to the flow. A sheath would seem to be important only if such a bias exists. In this way, a grounded model may not experience any sheath effects so long as the plasma is also at ground potential (away from the electric arc) and charge separation is negligible at the shock.

Since the sheath is a wall phenomenon, it is of importance for heat transfer. Here the interest is in the outer flow and so it is sufficient to show that the sheath is small in order to neglect it. We mentioned in passing that it may be possible to maintain a potential across a shock in a highly ionized gas. This may occur naturally due to electron effects. A similar charge separation occurs with the shock analogous to a wall. The estimates therefore may have some applicability there too, although the high level of ionization required would probably remove the effect from the regime considered.

If the sheath is collisionless, analysis shows the sheath thickness is approximately (Ref. 48)

(collisionless) $$\Delta_s = \lambda_D \tag{2-9}$$

where λ_D is the Debye length

$$\lambda_D = \left(\frac{kT}{4\pi n_e e^2} \right)^{\frac{1}{2}} \tag{2-10}$$

where k is Boltzmann's constant, n_e is electron number density and e is the electron charge. The Debye length has several physical interpretations. Besides the results of analysis showing it to be the physical length over which a potential gradient can be maintained, it has microscopic significance as a measure of the range of inter particle forces

due to electric charge. If the sheath is collision dominated (Ref. 48)

(collisions) $\Delta_s = (\lambda_D/R_b)^{2/3}\ (Re)^{-1/6} R_b$ (2-11)

Thus, the sheath parameter is

(collisionless) $\Delta_s/\Delta_{bl} = 1/2\ \lambda_D/R_b\ Re^{1/2}/\epsilon$ (2-12)

(collisions) $\Delta_s/\Delta_{bl} = 1/2\ (\lambda_D/R_b)^{2/3} Re^{1/3}/\epsilon$ (2-13)

Since both ratios are about the same, we have employed Eq. (2-12) in Figure 4. The sheath is a very thin sub layer.

We conclude that the continuum, Hugoniot shock and boundary layer theories are adequate below 250 kft. (See also Ref. 49.) However, the assumptions hold up less well in the laboratory and so viscosity is included in some of the theory to follow. However, we do not consider the incipient merged layer.

2.4 Thermodynamic Regimes

Equilibrium flow generally exists below about 100 kft. (Ref. 51). It is substantially frozen above 300 kft. Nitrogen reaction slows equilibration (Refs. 36 and 52). However, a partially frozen gamma gives some correction and the average non-equilibrium profiles behind a normal shock (Ref. 52) do not differ too much from the equilibrium giving some justification for equilibrium estimates and the use of constant properties.

The laboratory situation is more complex even though use of a monotomic gas simplifies the thermodynamics of the mixture. The preionized gas may have a high level of ionization (though slightly ionized)

resulting in a lower effect "gamma". The lower temperature ratio would prolong relaxation. However, if the initial ionization is higher than the equilibrium value, a reduced rate may still be sufficient to bring the level to the equilibrium value. There is even the possibility of equilibrium occuring faster because of the presence of pre-ionization and the avalanche effect that follows. Equilibrium has been established for atmospheric argon plasmas at low electric field to pressure ratio (Ref. 54) but much remains to be done for shock layer flows.

The chemical equilibrium flow regime would appear to occur below 100 kilofeet and in high pressure laboratory flows. In other situations the kinetics are of possible importance. Fortunately, the thermodynamics are uncoupled from the dynamics if one makes the constant property assumption which is discussed in the next chapter. Non-equilibrium then enters in only when the dimensionless parameters are calculated.

2.5 Magnetogasdynamic Regimes

The results of Levy, Et. al. (Ref. 28), indicate that the shock layer will be magnetically supported when

$$\epsilon S_s \approx 1.6 \tag{2-14}$$

or in terms of the natural interaction parameter S when

$$S \gtrsim \frac{1.6}{\epsilon(1+\delta)} \left(\frac{B_o}{B_s}\right)^2 \tag{2-15}$$

where δ is recalled to be the nondimensional stand-off distance. The theory, reviewed in Section 1.2, indicates a limiting S_s exists and that this is approached at some finite interaction parameter S. If we assume an undistorted dipole field (Rem = 0) the condition is

$$S \geq \frac{1.6}{\epsilon}(1+\delta)^5 \tag{2-16}$$

Unfortunately, δ is an unknown function of S and increases rapidly with it at high interaction. Bush (Ref. 5) gives a table of S_s and δ for $\epsilon = 1/11$. The last value in the table is perhaps representative of the limit since solutions for an attached layer apparently could not be found beyond that point. In this way, we estimate

$$S^* \approx \frac{35}{\epsilon} \tag{2-17}$$

When $S > S^*$, the critical natural interaction parameter, the flow may be magnetically supported.

Since S contains the field strength, it is not possible to delineate the regimes as for the aerodynamic case. At any altitude magnetic support may be possible. Further (2-17) was based on theories not properly accounting for the effect of ϵ. Levy considered $\epsilon \to 0$ and Bush the single value of 1/11. Accordingly, we defer these estimates until a later chapter when the effect of ϵ is studied in detail.

As mentioned earlier, the magnetic effect is coupled with the flow and will certainly alter the values of the parameters of the estimates of regimes. This will occur in two ways.

First, for example, the shock stand-off distance is known to be greater for MHD flow. Thus, ratios such as $\Delta_{b.l.}/\Delta$ will become smaller and better justify a boundary layer assumption. Inspection of other parameters shows similar effects. Thus, our estimates may be conservative for MHD flow. Part of this may be negated within the coupling. For example, if the boundary layer grows as fast as the stand-off or

faster our suggestion would not hold true. Again we defer this discussion until the results of the theory are presented.

Second, the transport properties are effected. Even if the normal transport properties were constant in the layer, the magnetic field variation would cause the effective value to vary. In this investigation the effect on the fluid tensor conductivity is accounted for by using the electrodynamic equation including the Hall effect. When this theory is employed, the conductivity involved is the normal one and so the effect is properly accounted for.

Finally, the magnetogasdynamic effects may introduce problems with the boundary conditions. For example, a current sheet in the shock may invalidate the momentum Hugoniot relation neglecting MHD effects. Fortunately, this effect can occur only at high magnetic Reynolds number and the calculations of the following chapters indicate aerodynamic plasmas have low Rem. At low Rem, the magnetic field is little distorted by currents and the magnetic pressure is the same on both sides of the shock. Thus, the MHD effect cancels out for the case considered. Further, an infinitesimal sheet is practically impossible. Thus, if we assume that the gas dynamic discontinuity appears before a region of high current density we can use the regular Hugoniot relation and expect the effect to be largely accounted for.

A second problem occurs at the body when a sheath is present. A current boundary condition for an insulated body says the current normal to the surface vanishes. But a highly conducting sheath may give an insulated body the appearance of a conducting one with respect to the flow. Since the sheath is neglected in further development, this question cannot be answered within the scope of the present theory.

The fact that the estimates indicate the sheath is very thin suggests that it is at least partially collisionless. One would have to match an appropriate sheath theory to the solution for the outer flow. One might be able to decide whether the sheath acts in the way suggested above by considering a sheath that is backed by an insulated wall. The question is whether or not the sheath can sustain a current normal to its other surface. If so, the sheath will cause the body to appear electrically conducting.

CHAPTER III

EQUATIONS OF MAGNETOHYDRODYNAMICS

3.1 Basic Assumptions

The assumption of constant properties in the shock layer near the stagnation region allows great simplification of the problem at hand. By constant properties, we mean density, viscosity, electrical conductivity and any other thermophysical properties that may be involved. This simplification occurs in two ways. First, the number of dependent variables is reduced because these properties no longer vary but are fixed behind the bow shock and the Hugniot conditions allow their explicit determination. Second, the equations take on a simpler form and often can be reduced to ordinary differential equations (similarity). This characteristic is well known in the hypersonic flow literature (see the books by Hayes and Probstein (Ref. 35) and Truitt (Ref. 52)) and is considered in detail for the MHD problem in the next chapter.

The question immediately presents itself as to the validity of the constant property assumption. It should be emphasized that we are not suggesting that these properties (like density) are constant everywhere, but do not vary only in the region behind the bow shock (Figure 1) and not too far from the center line axis. In Figure 6, we show the ratio of stagnation point density to the value behind the shock as a function of the shock density ratio, a measure of Mach number. The calculations assumed a constant ratio of specific heats and constant molecular weight and are tabulated by Keenan and Kaye (Ref. 55). It is apparant that for $\epsilon \leq 1/4$ the variation of density

along the center stream line is less than 10%. Thus, the constant density assumption is reasonable, according to this criterion, for moderate supersonic to hypersonic speeds or for Mach numbers greater than about 3 depending on the gas. This criterion may be questioned since a constant gamma was employed under rather ideal circumstances (isentropic flow) and because the variation of the transport coefficients was not included. The first point is not critical because we are interested in the extent of compressibility and not the details of dissipation.

Table 2 shows the variation of these thermophysical coefficients, using real gas, equilibrium thermodynamics and isentropic flow. (Refs 41, 44, 46). The table contains the coefficients divided by density because it is convenient to divide out the density in order to form dimensionless groups in actual analyses. It appears that the properties can be assumed about constant along the center stream line from the shock to the stagnation point.

Figure 7 shows the variation in the lateral direction behind the bow shock which is assumed to be a circular arc. The variation is limited to about 10% to about 30^{o} off axis except for the laboratory conductivity. Toward the body, compression will tend to stabilize the values. This consideration suggests that the approximation may be useful to about 45^{o} or to the vicinity of the sonic line. After this line, compressibility will be important. It appears that the application of MHD forces moves the sonic line further from the stagnation point as suggested by Ericson and Maciulaitus (Ref. 27). As discussed earlier, most of the drag interaction occurs in the stagnation region and so we may feel reasonably confident in the constant property approach. This applies so

long as the flow is aerodynamic like and not magnetically supported. For the later, the large density variation approaching the no-flow region would invalidate the assumption. There is evidence that this approximation is valid up to the point of shock layer lift-off since theories for the present approximation and the magnetically supported layer have common features to their solution where the lift-off is believed to occur (Levy, Ref. 24). Thus, information as to when the flow is magnetically supported can be had by noting when the constant property system has no solution.

In addition to constant properties, we assume continuum flow and a Rankine-Hugoniot shock as discussed in Chapter II.

We consider steady flow. Therefore, the hypothetical flight vehicle cannot change speed or altitude too quickly. In the laboratory, the test time cannot be too short. The limitations for MHD flows should not be appreciably more severe than classical gasdynamic flows since electrodynamic phenomena propagate at high speeds.

The magnetic field will affect the transport phenomena in two ways. First of all, the collision cross-sections will be altered because of the presence of an electric field relative to the fluid. The kinetic theory of Chapman and Cowling (Ref. 42) shows that the distribution function will not be Maxwellian in this case. We neglect this effect when estimates of the transport coefficients are made here. However, the results of the present theory will be in terms of dimensionless groups and so this effect is not important except where applications are made of the theory.

A second effect occurs because the transport phenomena acquire tensor characteristics in the presence of a magnetic field. For example,

there will be currents generated at right angles to the local electric field due to the Hall effect. The transport of current, heat and momentum will tend to be reduced by a factor (Chapman and Cowling, Ref. 42)

$$\frac{1}{1 + C_H^2}$$

in the direction perpendicular to the magnetic field where C_H is the local Hall coefficient. We neglect this effect except on the current when we include the Hall effect.

We use the Newtonian pressure tensor, derived by Schlicting (Ref. 47) and neglect the gravity body force as is customary in most gas dynamic analyses (Prandtl and Tietjens Ref. 56).

We consider a quasi-neutral plasma where the electric body forces and convection currents are neglected in the momentum and current equations. The calculations of Schlüter (Ref. 57) show this to be a realistic assumption. However, as pointed out by Spitzer (Ref. 58), the excess charge density should not be set to zero in Gauss' law. This does not lead to an inconsistancy as this equation serves only to define the local excess charge density and is the only equation in which the excess charge density then occurs.

Relativistic effects are not included because the flow velocities of the present application are small compared with the speed of light.

Finally, we note that the derivation of the equations to follow from a microscopic theory would lead us too far afield and we refer to the references cited.

3.2 Continuity Equations

As in conventional steady hydrodynamics, conservation of mass requires (Cambel, Ref. 59)

$$\underset{\sim}{\nabla} \cdot \underset{\sim}{V} = 0 \tag{3-1}$$

where $\underset{\sim}{V}$ is fluid velocity and $\underset{\sim}{\nabla}$ the vector differential operator. In magnetohydrodynamics, for steady conditions, we have

$$\underset{\sim}{\nabla} \cdot \underset{\sim}{J} = 0 \tag{3-2}$$

where $\underset{\sim}{J}$ is current density.

3.3 Momentum Equation

Newton's second law is reflected in the Navier-Stokes equation for magneto-fluidmechanics (Cambel, Ref. 59)

$$\rho \frac{d\underset{\sim}{V}}{dt} = - \underset{\sim}{\nabla} p + \underset{\sim}{\nabla} \cdot \underset{\approx}{\tau} + \underset{\sim}{J} \times \underset{\sim}{B} \tag{3-3}$$

where ρ is density, p pressure, $\underset{\approx}{\tau}$ viscous stress tensor, $\underset{\sim}{B}$ magnetic field intensity and

$$\frac{d\underset{\sim}{V}}{dt} = \underset{\sim}{\nabla} \frac{V^2}{2} - \underset{\sim}{V} \times \underset{\sim}{\nabla} \times \underset{\sim}{V} \tag{3-4}$$

in invariant form (Ref. 47). The viscous stress tensor is (Ref. 47)

$$\underset{\sim}{\nabla} \cdot \underset{\approx}{\tau} = \eta \nabla^2 \underset{\sim}{V} \tag{3-5}$$

where η is viscosity.

Thus we obtain

$$\underset{\sim}{\nabla} \left(\frac{V^2}{2} + \frac{p}{\rho} \right) = \underset{\sim}{V} \times \underset{\sim}{\nabla} \times \underset{\sim}{V} + \frac{\eta}{\rho} \nabla^2 \underset{\sim}{V} + \frac{1}{\rho} \underset{\sim}{J} \times \underset{\sim}{B} \tag{3-6}$$

3.4 Ohm's Law

In its simplest form, Ohm's law is

$$\underset{\sim}{J} = \sigma \underset{\sim}{E}' \tag{3-7}$$

where $\underset{\sim}{E}'$ is the electric field relative to the fluid. This equation is inadequate in some cases and so we write

$$\underset{\sim}{J} = \underset{\approx}{\sigma} \cdot \underset{\sim}{E}' \tag{3-8}$$

where $\underset{\approx}{\sigma}$ is the tensor conductivity which is a function of the magnetic field intensity and includes the directional characteristics of phenomena like the Hall effect (Ref. 60). If we apply the correction of Section 3.1

$$\underset{\sim}{J} = \frac{\sigma}{1 + C_H^2} \underset{\sim}{E}' \tag{3-9}$$

where C_H is the Hall coefficient to be defined later. This approximation has been investigated by Levy (Ref. 4) who showed it to be incorrect to varying degrees depending on the flow parameters and geometry. His results, however, indicate it may be better to use Eq. (3-9) rather than not to include Hall effects at all. Since this involves a simple correction of σ, if we assume an average C_H, we do not consider it further explicitly in the theory that follows. Indeed, when we include the Hall effect exactly, Eq. (3-9) is unnecessary. The vector form of Ohm's Law that we now consider involves a linear combination of currents and so is equivalent to the tensor form Eq. (3-8).

Following Sears and Resler (Ref. 60) we consider a three fluid model of electrons e, ions i and neutrals a, with mass m_e, m_i and $m_a = m_i$ with electrons and ions of opposite charge e. That is, a

single degree of ionization is assumed. The simple kinetic theory (Cowling, Ref. 61) uses mean collision times τ_{ei}, τ_{ia} and τ_{ea} which are assumed to be known from a detailed solution involving the collision integrals. It is assumed that the particle drag forces are proportional to their relative velocities and that the light electrons have achieved an equilibrium terminal velocity and that the ion velocity is about that of the gas velocity. Dynamical equations for the electrons, ions and neutral gas can be written neglecting viscosity and thermoelectric effects and using the quasi-neutral approximation. These are combined to form Cowling's equation

$$
\begin{aligned}
& en_e \left(\underset{\sim}{E} + \underset{\sim}{V} \times \underset{\sim}{B}\right) + \left[1 - \left(1 + \frac{\omega_e \tau_{ea}}{2\omega_i \tau_{ia}}\right)^{-1} \left(1 + \frac{n_e}{n_a}\right)^{-1}\right] \underset{\sim}{\nabla} p_e = \\
& \left[(\omega_e \tau_{ea})^{-1} + \left(1 + \frac{\omega_e \tau_{ea}}{2\omega_i \tau_{ia}}\right)^{-1} (2\omega_i \tau_{ia})^{-1}\right] B\underset{\sim}{J} + \\
& \left[1 - 2\left(1 + \frac{n_e}{n_a}\right)^{-1} \left(1 + \frac{\omega_e \tau_{ea}}{2\omega_i \tau_{ia}}\right)^{-1}\right] \underset{\sim}{J} \times \underset{\sim}{B} + \\
& \left(1 + \frac{n_e}{n_a}\right)^{-2} \left[(\omega_e \tau_{ea})^{-1} + \left(\frac{\omega_i \tau_{ia}}{2}\right)^{-1}\right]^{-1} B\left[\underset{\sim}{\nabla} p_e \times \underset{\sim}{B} - \underset{\sim}{J} \times \underset{\sim}{B} \times \underset{\sim}{B}\right]
\end{aligned}
\tag{3-10}
$$

where n is number density, p_e is electron partial pressure and ω the cyclotron frequency

$$
\omega_e = \frac{eB}{m_e} \qquad \omega_i = \frac{eB}{m_i} \tag{3-11}
$$

Since $\omega_i/\omega_e \ll 1$ and writing the constant

$$
\omega' = \frac{e}{m} \tag{3-12}
$$

the cyclotron frequency per unit field strength, we get

$$n_e e \left(\underset{\sim}{E} + \underset{\sim}{V} \times \underset{\sim}{B}\right) + \underset{\sim}{\nabla} p_e = \left\{ \frac{1}{\omega_e'} \left(\frac{1}{\tau_{ei}} + \frac{1}{\tau_{ea}} \right) \underset{\sim}{J} + \underset{\sim}{J} \times \underset{\sim}{B} + \frac{2\omega_i' \tau_i}{\left(1 + \frac{n_e}{n_a}\right)^2} \cdot \left[\underset{\sim}{\nabla} p_e \times \underset{\sim}{B} - \underset{\sim}{J} \times \underset{\sim}{B} \times \underset{\sim}{B} \right] \right\} \tag{3-13}$$

Let

$$\tau_e = \left(\frac{1}{\tau_{ea}} + \frac{1}{\tau_{ei}} \right)^{-1} \tag{3-14}$$

the electron collision time and let

$$\alpha = \frac{n_e}{n_e + n_a} \tag{3-15}$$

be the degree of ionization and let

$$\sigma = \frac{e^2 n_e \tau_e}{m_e} \tag{3-16}$$

be the electrical conductivity and let

$$C_H' = \frac{e\tau_e}{m_e} \tag{3-17}$$

be the Hall coefficient per unit field strength. Let

$$C_i' = \frac{2e\,\tau_{ia}}{m_i} (1 - \alpha)^2 \tag{3-18}$$

be the ion slip coefficient per unit field strength. Ohm's law becomes

$$\underset{\sim}{J} = \sigma\left(\underset{\sim}{E} + \underset{\sim}{V} \times \underset{\sim}{B}\right) - C_H' \left[\underset{\sim}{J} \times \underset{\sim}{B} - \nabla p_e - C_i' \left(\underset{\sim}{J} \times \underset{\sim}{B} - \underset{\sim}{\nabla} p_e\right) \times \underset{\sim}{B}\right] \tag{3-19}$$

Now, Dalton's law of partial pressure shows $\underset{\sim}{\nabla} p_e = \frac{\alpha}{2} \underset{\sim}{\nabla} p$ if $\underset{\sim}{\nabla} \alpha = 0$ which we might infer from the constant property assumption. Thus, if α or $\underset{\sim}{\nabla} p$ is small, we expect that $\underset{\sim}{\nabla} p_e$ can be neglected. This is the case if

$$\underset{\sim}{\nabla} p_e = \frac{\alpha}{2} \underset{\sim}{\nabla} p \ll \underset{\sim}{J} \times \underset{\sim}{B}$$

or

$$\frac{\alpha}{4} \underset{\sim}{\nabla} \left(\frac{p}{\frac{\rho \bar{V}^2}{2}} \right) \ll \bar{S} \underset{\sim}{j} \times \underset{\sim}{b} \tag{3-20}$$

where

$$\bar{S} = \frac{\sigma \bar{B}^2 L}{\bar{\rho} \bar{V}} \tag{3-21}$$

where $\underset{\sim}{j}$ and $\underset{\sim}{b}$ are nondimensional. This relation will be satisfied for attached shock layers because pressure gradients are small. Thus, Ohm's law simplifies to

$$\underset{\sim}{J} = \sigma \left(\underset{\sim}{E} + \underset{\sim}{V} \times \underset{\sim}{B} \right) - C_H' \left[\underset{\sim}{J} \times \underset{\sim}{B} - C_i' \underset{\sim}{J} \times \underset{\sim}{B} \times \underset{\sim}{B} \right] \tag{3-22}$$

This equation has been derived by Demetriades (Ref. 62) who obtained it from the second approximation of the solution of the Boltzmann system. When this is done, the coefficients C_H', C_i' and σ are identified with integrals involving the details of the collisions. Because the free path theory by-passes these details it offers no information as to these values. In any case Eq. (3-22) is the appropriate macroscopic equation and we regard the coefficients as known. This equation can be simplified further by neglecting the last term due to ion slip due to the imperfection of coupling between ions and neutrals. This can be done when

$$C_i = C_i' \, \overline{B} \ll 1 \tag{3-23}$$

C_i' is given by Eq. (3-18). Letting

$$C_H = C_H' \, \overline{B} \tag{3-24}$$

where $\overline{B}$ is a reference magnetic field intensity, we find

$$C_i = \frac{2m_e}{m_i} \, (1 - \alpha)^2 \, \frac{\tau_{ia}}{\tau_e} \, C_H \tag{3-25}$$

This immediately suggests that the ion slip effect is much smaller than the Hall effect because of the ratio m_e/m_i. Further, as $\alpha \to 1$ or ionization increases, the coefficient decreases. The ratio τ_{ia}/τ_e can be written (Chapman and Cowling, Ref. 42)

$$\frac{\tau_{ia}}{\tau_e} = \frac{\frac{n_e}{n_a} + \left(\frac{A_{ea}}{A_{ei}}\right)^2}{\frac{1}{\sqrt{2}} \left(\frac{A_{ia}}{A_{ei}}\right)^2} \tag{3-26}$$

where A_{ij} is the collision cross-section. Typical values indicate (Cambel, Ref. 59)

$$\left(\frac{A_{ea}}{A_{ei}}\right)^2 = 0 \; (10^{-6})$$

Thus,

$$C_i \approx 2\sqrt{2} \, \frac{m_e}{m_i} \, (1 - \alpha)^2 \, \frac{n_e}{n_a} \left(\frac{A_{ei}}{A_{ia}}\right)^2 C_H \tag{3-27}$$

Finally, for both large and small ionization (De Vota, Ref. 63)

$$A_{ei} \approx A_{ia} \tag{3-28}$$

and so

$$C_i \approx 2\sqrt{2}\ \frac{m_e}{m_i}\ \alpha(1 - \alpha)\ C_H \tag{3-29}$$

Even for large Hall coefficient, C_i is very small. In the next chapter C_H is estimated to range to order 10 for 10,000 gauss field strength. Even for 100,000 gauss, ion slip would appear unimportant in the present application. Thus, the form of Ohm's law to be considered is

$$\underset{\sim}{J} = \sigma\ (\underset{\sim}{E} + \underset{\sim}{V} \times \underset{\sim}{B}) - C_H'\ \underset{\sim}{J} \times \underset{\sim}{B} \tag{3-30}$$

3.5 Maxwell Equations

The equations governing electromagnetic phenomena related to magnetofluidmechanics are summarized by Cambel (Ref. 59). For steady state media with constant permeability μ and permitivity ε

$$\underset{\sim}{\nabla} \cdot \underset{\sim}{E} = \rho_e/\varepsilon \tag{3-31}$$

$$\underset{\sim}{\nabla} \cdot \underset{\sim}{B} = 0 \tag{3-32}$$

$$\underset{\sim}{\nabla} \times \underset{\sim}{E} = 0 \tag{3-33}$$

$$\underset{\sim}{\nabla} \times \underset{\sim}{B} = \mu \underset{\sim}{J} \tag{3-34}$$

where ρ_e is excess charge density. For the gases of interest, which are non-magnetic, μ takes the value for a vacuum.

CHAPTER IV

ANALYSIS OF HIGH SPEED MAGNETOAERODYNAMICS

4.1 The Problem

The purpose of this investigation, as stated in Chapter I, is to give an account of magnetoaerodynamics for aerodynamic-like flow about a blunt body. In particular, the effect of magnetoaerodynamic forces on the body in a high speed environment such as exists in planetary entry or simulation of entry in the laboratory is of interest.

As a general problem, this is an immensely complicated undertaking. But almost immediately one can make certain assumptions so as to simplify and specialize the approach. We consider the nonlifting configuration of Figure 1, a hemisphere at zero angle-of-attack with a dipole field source at its nose center of curviture. We make the assumptions discussed in Chapter II: continuum flow, a Hugoniot shock and no plasma sheath effect on the outer flow. According to our estimates, these assumptions are valid below 250 kft. and for flight simulation with argon plasma at supersonic speeds above ambient pressures of 0.0005 atm. For the present, we include viscous effects since the estimates indicated their possible importance for laboratory flow.

At this point, one might begin a detailed computer analysis including the effects of chemically reacting flow in mixed regions of supersonic and subsonic flow adjacent to a catalytic body. This type of complete analysis has only recently been undertaken for conventional aerodynamic re-entry and after a decade of simpler analyses.

It seems reasonable to parallel this course of action in magnetoaerodynamics. As in conventional hypersonics (Ref. 8), we will use the constant property approximation discussed in Chapter III. Theory and experiment indicate that this approximation is valid for Mach numbers of about 3 and greater. It is expected that the corresponding MHD theory for aerodynamic like flow will be valid for moderate supersonic speeds and hypersonic flow as well.

The specialized boundary conditions for the equations are stated in the following section. When we assume a bow shock concentric with the body nose and that the dipole field source is located at the common center of curviture, a simple functional form of the solution is suggested for the stagnation region of interest. This form allows reduction to ordinary differential equations, a two point boundary value problem with the second point unknown, the shock location. The system is highly coupled and non-linear.

The remainder of the chapter deals with the formulation of the system of equations and the formulas for the magnetoaerodynamic coefficients of interest such as the shock stand-off distance and drag coefficients. The range of dimensionless groups that arise are estimated. In this way, the mathematical statement of the problem is completed. The solutions, analytic and numerical, are discussed in subsequent chapters.

4.2 Boundary Conditions

We consider axisymmetric flow without variation in the azimuthal or ϕ direction and postulate the existence of a bow shock.

Experiment (Ref. 64) indicates that the bow shock is nearly concentric with the nose for moderate supersonic speeds, and greater, up to near the body shoulder. As well, we assume a Rankine-Hugoniot shock as justified in Chapter II. The coordinate system is shown in Figure 8.

Uniform continuous flow requires that

$$- \rho_\infty V_\infty \cos\theta = \rho_1 V_{1_r}$$

where V_{1_r} is the radial component of velocity behind the shock. Thus,

$$V_{r_1} = - \epsilon V_\infty \cos\theta \qquad (4\text{-}1)$$

where ϵ is the shock density ratio. Tangentially,

$$V_{\theta_1} = V_\infty \sin\theta \qquad (4\text{-}2)$$

$$V_{\varphi_1} = 0 \qquad (4\text{-}3)$$

for initially parallel flow.

A momentum balance through the infinitesimal shock requires

$$p_\infty + \rho_\infty V_\infty^2 \cos^2\theta = p_1 + \rho_1 V_{r_1}^2$$

or using (4-1)

$$p_1 = p_\infty + (1-\epsilon)\, \rho_\infty V_\infty^2 \cos^2\theta \qquad (4\text{-}4)$$

At the body, to which we assume the shock layer to be adhered

$$V_{r_o} = 0 \tag{4-5}$$

For viscous flow, the no slip condition is

$$V_{\theta_o} = 0 \qquad (R_e \neq \infty) \tag{4-6}$$

$$V_{\varphi_o} = 0 \qquad (R_e \neq \infty) \tag{4-7}$$

being arbitrary for inviscid flow ($R_e = \infty$)

The electric boundary conditions are similar. For a nonconducting free stream

$$J_{r_1} = 0 \tag{4-8}$$

At an insulated body

$$J_{r_o} = 0 \tag{4-9}$$

while for a highly conducting body the potential is uniform and therefore

$$E_{\theta_o} = 0 \tag{4-10}$$

where $\underset{\sim}{E}$ is the electric field vector.

The magnetic field boundary condition is

$$B_r \ (r \to \infty) = B_\theta \ (r \to \infty) = B_\varphi \ (r \to \infty) = 0 \tag{4-11}$$

and

$$B_r \ (r \to o) = B_o \left(\frac{R_b}{r}\right)^3 \cos\theta \tag{4-12}$$

$$B_\theta \ (r \to o) = \frac{B_o}{2} \left(\frac{R_b}{r}\right)^3 \sin\theta \tag{4-13}$$

$$B_\varphi \ (r \to o) = 0 \tag{4-14}$$

That is, we assume that the source is that of a dipole (Ref. 65). At this point, we cannot state the general conditions referred to the shock or body because distortion of the magnetic field will be appreciable except for small magnetic Reynolds number. For the limit Rem = 0, a useful approximation, the field is undistorted as we shall see. For this special case

$$(\text{Rem} = 0) \quad \begin{cases} B_{r_1} = B_s \cos\theta \\ B_{\theta_1} = \dfrac{B_s}{2} \sin\theta \\ B_{\varphi_1} = 0 \end{cases} \tag{4-15}$$

or

$$(\text{Rem} = 0) \quad \begin{cases} B_{r_o} = B_o \cos\theta \\ B_{\theta_o} = \dfrac{B_o}{2} \sin\theta \\ B_{\varphi_o} = 0 \end{cases} \tag{4-16}$$

where B_s and B_o are reference magnetic fields related by

$$(\mathrm{Rem} = 0) \qquad \frac{B_s}{B_o} = \left(\frac{R_b}{R_s}\right)^3 \tag{4-17}$$

For the general case, $\mathrm{Rem} \neq 0$, the local value of magnetic field will not be that when no interaction is present, say B_s or B_o. The distortion will even be present within the body except for highly permeable bodies which we exclude. We seek a solution valid from body to shock

$$R_b \leq r \leq R_s$$

and the equations, (4-11) through (4-14) are external to that interval. We must match separate external solutions with this interval and its solution in order to define the correct boundary conditions. This is deferred until appropriate solutions become evident.

4.3 Functional Forms

Lighthill (Ref. 8) has shown that simple functional forms exist for the corresponding non-MHD problem relating to stagnation region flow. This approach was extended by Bush (Ref. 5) for the inviscid MHD problem without the Hall effect and later by Wu and co-workers (Refs. 26 and 29) to include viscosity. It was used by Levy (Ref. 4) to study the two dimensional subsonic flow with the Hall effect but without viscosity or deformation of the flow and magnetic fields. The form of similarity to be employed is rather well established and requires only generalization to the present problem.

The continuity equation can be written in spherical coordinates (Ref. 66). Without φ variation

$$\frac{1}{r} \frac{\partial}{\partial r}\left(r^2 V_r\right) + \frac{1}{r \sin\theta} \frac{\partial}{\partial \theta}\left(\sin\theta\, V_\theta\right) = 0 \qquad (4\text{-}18)$$

with boundary conditions (4-1) to (4-3) and (4-5) to (4-7) written for $V(r,\theta)$ as

$$\left.\begin{aligned} V_r\,(R_s, \theta) &= -\epsilon\, V_\infty \cos\theta \\ V_r\,(R_b, \theta) &= 0 \end{aligned}\right\} \qquad (4\text{-}19)$$

$$\left.\begin{aligned} V_\theta\,(R_s, \theta) &= V_\infty \sin\theta \\ V_\theta\,(R_b, \theta) &= 0 \qquad (Re \neq \infty) \end{aligned}\right\} \qquad (4\text{-}20)$$

$$\left.\begin{aligned} V_\varphi\,(R_s, \theta) &= 0 \\ V_\varphi\,(R_b, \theta) &= 0 \qquad (Re \neq \infty) \end{aligned}\right\} \qquad (4\text{-}21)$$

A simple functional form is suggested. The following satisfies the equation and boundary condition.

$$V_r = 2\epsilon\, V_\infty \frac{F(x)}{X^2} \cos\theta \qquad (4\text{-}22)$$

$$V_\theta = -\epsilon\, V_\infty \frac{F'(x)}{x} \sin\theta \qquad (4\text{-}23)$$

where x is the non-dimensional distance

$$x = \frac{r}{R_b} \tag{4-24}$$

We note that F(x) is non-dimensional and the scale factor ϵV_∞ corresponds to the value behind a normal shock. Equation (4-18) does not contain V_φ so its form can not be recognized from it.

The previous development is equivalent to introducing a stream function for the velocity in the meridian plane (r,θ) (Ref. 8).

$$\psi_v = - F(x) \sin^2\theta \tag{4-25}$$

which gives us the equation for the stream lines. It can be thought of as the first non-vanishing term of a power series expansion about the center stream line (Ref. 52). The velocities are obtained from differentiation of (4-25) and so follow a similar expansion. The first terms of which are given in (4-22) and (4-23). A direct expansion for V_φ with provision for $V_\varphi(r,\theta) = - V_\varphi(r,-\theta)$ gives the first term

$$V_\varphi = \epsilon V_\infty \frac{G(x)}{x} \sin\theta \tag{4-26}$$

where $\frac{G(x)}{x}$ was chosen for convenience in the manner of the previous case.

The magnetic field obeys an equation similar to that for velocity and (4-13) and (4-12) are boundary conditions that can be satisfied by

$$B_r = 2B_o \frac{M(x)}{x^2} \cos\theta \tag{4-27}$$

$$B_\theta = - B_o \frac{M'(x)}{x} \sin\theta \tag{4-28}$$

$$B_\varphi = B_o \frac{N(x)}{x} \sin\theta \tag{4-29}$$

with an analogous function for the flux lines

$$\psi_B = - M(x) \sin^2\theta \tag{4-30}$$

We note that M and N will have separate solutions for $x > \frac{R_s}{R_b}$, $R_s/R_b \geq x \geq 1$ and $x < 1$ and that the intermediate region boundary condition is obtained by matching. For the outer region with $\underset{\sim}{J} = 0$, (3-34) and the above functional forms give

$$- M'' + \frac{2M}{x^2} = 0 \tag{4-31}$$

for $x > R_s/R_b$. The solution is

$$M = \frac{C_1}{x} + C_2 x^2 \tag{4-32}$$

Since $\underset{\sim}{B}$ must vanish at infinity (4-14) we find that $C_2 = 0$. Thus

$$M = \frac{C_1}{x} \tag{4-33}$$

and so

$$B_r = 2B_o C_1 \left(\frac{R_b}{r}\right)^3 \cos\theta$$

$$B_\theta = B_o C_1 \left(\frac{R_b}{r}\right) \sin\theta \tag{4-34}$$

for $r > R_s$. We recognize (4-34) as dipole behavior. Thus the correct specification of the boundary condition for M in terms of a shock reference B_s is

$$B_r\ (R_s,\theta) = B_s \cos\theta$$
$$B_\theta\ (R_s,\theta) = \frac{B_s}{2} \sin\theta \qquad (4\text{-}35)$$

which was the condition assumed by Bush (Ref. 5). It is exact for the present approximation. A dipole source will appear as a dipole in the region forward of the shock. It will be altered only in magnitude according to the deformation that occurs behind the shock. Thus, the appropriate boundary condition for M in the interval is

$$M\left(\frac{R_s}{R_b}\right) = \frac{1}{2}\ \frac{B_s}{B_o} \qquad (4\text{-}36)$$
$$M'\left(\frac{R_s}{R_b}\right) = -\frac{1}{2}\ \frac{B_s}{B_o}$$

where B_o is the stagnation point field that would exist without field deformation (by definition). This is not a complete boundary condition since B_s is unknown. We must match the inner solution. Neglecting currents within the body (external to the source) again

$$M = \frac{C_1}{x} + C_2\, x^2 \qquad (4\text{-}37)$$

for $x < 1$. Let $\mathcal{C} = \frac{-C_2}{C_1}$ then

$$B_r = B_o \left(\frac{R_b}{r}\right)^3 2C_1 \left[1 - \mathcal{C} \left(\frac{r}{R_b}\right)^3\right] \cos\theta$$

$$B_\theta = \frac{B_o}{2} \left(\frac{R_b}{r}\right)^3 2C_1 \left[1 + 2\mathcal{C} \left(\frac{r}{R_b}\right)^3\right] \sin\theta \qquad (4\text{-}38)$$

which satisfies the other boundary condition (4-13). It is apparent from (4-13) that,

$$C_1 = 1/2$$

and so

$$B_r = B_o \left(\frac{R_b}{r}\right)^3 \cos\theta - B_o \mathcal{C} \cos\theta$$

$$B_\theta = \frac{B_o}{2} \left(\frac{R_b}{r}\right)^3 \sin\theta + B_o \mathcal{C} \sin\theta \qquad (4\text{-}39)$$

The actual stagnation point field strength can now be written in terms of the value that would exist without deformation.

$$B(R_b, \theta = o) = B_o (1 - \mathcal{C})$$

Along the body in general

$$B_r (R_b, \theta) = B_o (1 - \mathcal{C}) \cos\theta$$

$$B_\theta (R_b, \theta) = \frac{B_o}{2} (1 + 2\mathcal{C}) \sin\theta \qquad (4\text{-}40)$$

and so $\mathcal{C}$ is recognized as the fractional reduction of the stagnation field strength due to magnetic field deformation. The stress is such that the θ component is increased by a fraction $2\mathcal{C}$. This is due to the continuity of flux and the nature of a dipole with a factor 1/2 in (4-38). Clearly, (4-39) is not dipole behavior at the body surface. An assumption of dipole behavior at the surface, as was made by Smith, Schwimmer and Wu (Ref. 29),

corresponds to an actual dipole only for no field deformation. Such deformation leads to unphysical results, namely a higher magnetic field strength at the shock than at the body. This corresponds to having another magnetic source at infinity.

The constants $\mathcal{C}$ and B_o are found by matching the intermediate flow. Combining (4-27), (4-28) and (4-39) we find

$$M(1) = \frac{1}{2}\ (1 - \mathcal{C}\ )$$
$$M'(1) = -\frac{1}{2}\ (1 + 2\mathcal{C}\ ) \qquad (4\text{-}41)$$

Now, $\mathcal{C}$ is not known ahead of time. The complete boundary condition for M takes the form of 4 equations (4-36) and (4-34). We shall see that M is second order and requires only two. The extra two equations give the deformation fraction $\mathcal{C}$ and the shock reference B_s. If we wish to specify B_s in an "inverse" solution then B_o is determined instead.

The most important result of the matching process is that it is correct to specify the field as being dipole like at the shock but not at the body surface except for the limiting case of no field deformation in which case either reference is satisfactory.

Returning to the other functional forms, we note that the current obeys the same continuity equation as the velocity and magnetic field. The boundary conditions are also consistent with

$$J_r = 2\epsilon\ V_\infty\ \sigma_1\ B_o\ \frac{K(x)}{x^2}\ \cos\theta \qquad (4\text{-}42)$$

$$J_\theta = -\epsilon\ V_\infty\ \sigma_1\ B_o\ \frac{K'(x)}{x}\ \sin\theta \tag{4-43}$$

$$J_\varphi = \epsilon\ V_\infty\ \sigma_1\ B_o\ \frac{L(x)}{x}\ \sin\theta \tag{4-44}$$

$$\psi_J = -\ K(x)\ \sin^2\theta \tag{4-45}$$

where ψ_J is the current stream function in the meridian plane. The scale factors are motivated by $J \approx \sigma_1\ V_1\ B_o$ behind the shock with $V_1 = \epsilon\ V_\infty$.

The electric field is governed by $\underset{\sim}{\nabla} \times \underset{\sim}{E} = 0$. We can write the following for an azimuthal loop.

$$\int \underset{\sim}{\nabla} \times \underset{\sim}{E}\ da = 0$$

$$\oint \underset{\sim}{E} \cdot d\underset{\sim}{\ell} = 0$$

$$\int_o^{2\pi} E_\varphi\ (R,\theta) r\ \sin\theta d\varphi = 0$$

$$2\pi r\ E_\varphi\ (r,\theta)\ \sin\theta = 0$$

$$E_\varphi(r,\theta) = 0 \tag{4-46}$$

for arbitrary r and θ . Thus the azimuthal electric field vanishes for axisymmetry. The other components satisfy (3-34) which in spherical coordinates is

$$\frac{1}{r}\ \frac{\partial}{\partial r}\ (rE_\theta) - \frac{1}{r}\ \frac{\partial E_r}{\partial\theta} = 0 \tag{4-47}$$

which is satisfied by

$$E_r = \epsilon\ V_\infty\ B_o\ H'(x)\ \cos\theta$$

$$E_\theta = -\epsilon\ V_\infty\ B_o\ \frac{H(x)}{x}\ \sin\theta \qquad (4\text{-}48)$$

The quantity analogous to the stream function is the electric potential. Except for an arbitrary constant which depends on the body bias of voltage

$$\Phi = \epsilon\ V_\infty\ B_o\ R_b\ H(x)\ \cos\theta \qquad (4\text{-}49)$$

The functions have now been introduced and we write the boundary conditions in terms of them. For example, from (4-19)

$$V_r\ (R_s,\theta) = -\ \epsilon\ V_\infty\ \cos\theta$$

and from (4-22)

$$V_r\ (R_s,\theta) = 2\epsilon\ V_\infty\ \frac{F(x_s)}{x_s^2}\ \cos\theta$$

where $x_s = R_s/R_b$. These combine to give one of the F boundary conditions. The others follow.

$$F\ (X_s) = -\ X_s^2/2$$

$$F'\ (X_s) = -\ X_s/\epsilon$$

$$F\ (1) = 0$$

$$F'(1) = 0 \qquad (Re \neq \infty)$$

$$G\ (X_s) = 0$$

$$G\ (1) = 0 \qquad (Re \neq \infty)$$

$$K\ (X_s) = 0 \qquad (4\text{-}50)$$

$$K(1) = 0 \qquad \text{(insulated body)}$$

$$H(1) = 0 \qquad \text{(conducting body)}$$

$$M(X_s) = \frac{1}{2}\,\frac{B_s}{B_o} \qquad M(1) = \frac{1}{2}\,(1 - \mathcal{C})$$

$$M'(X_s) = -\frac{1}{2}\,\frac{B_s}{B_o} \qquad M'(1) = \frac{-1}{2}\,(1 + 2\mathcal{C})$$

$$C_p(X_s,\theta) = 2(1 - \epsilon)\cos^2\theta$$

where

$$C_p = \frac{p - p_\infty}{\frac{\rho_\infty V_\infty^2}{2}} \tag{4-51}$$

the pressure coefficient.

We note that the boundary conditions are split between the body $x = 1$ and shock $x = x_s$, a two point boundary value problem. It turns out there is one "extra" boundary condition which locates the shock or second point. The dimensionless shock stand-off distance is given by

$$\delta = \frac{R_s - R_b}{R_b} = x_s - 1 \tag{4-52}$$

which is added to the quantities sought.

The boundary conditions have been formulated and functional forms determined that satisfy these conditions and some of the partial differential equations, those of the continuity type. In the next section these functions are substituted into the remaining equations (3-6) and (3-34) and we show that indeed they are the correct forms. For small θ, the θ dependence divides

out and the equations involve only the functions F, G, etc. These are the ordinary difference equations which determine the functions and the solution of the problem at hand. The various scaling factors combine into dimensionless groups which we identify.

4.4 Ordinary Differential Equations

We start with Ampere's law because it is the simplest and results in a direct connection between certain functions. In spherical coordinates (Ref. 66), Eq. (3-34) is

$$\frac{1}{r \sin\theta} \frac{\partial}{\partial\theta} (B_\varphi \sin\theta) = J_r \mu \tag{4-53a}$$

$$-\frac{1}{r} \frac{\partial}{\partial r} (rB_\varphi) = J_\theta \mu \tag{4-53b}$$

$$\frac{1}{r} \frac{\partial}{\partial r} (rB_\theta) - \frac{1}{r} \frac{\partial B_r}{\partial\theta} = J_\varphi \mu \tag{4-53c}$$

where φ variation is omitted. Substituting Eqs. (4-27) to (4-29) and Eqs. (4-42) to (4-44) into Eq. (4-53)

$$\frac{B_o}{R_b} \frac{1}{x \sin\theta} \frac{\partial}{\partial\theta} \left(\frac{N}{x} \sin\theta \sin\theta\right) = 2\mu\varepsilon V_\infty B_o \sigma_1 \frac{K}{x^2} \cos\theta$$

$$-\frac{B_o}{R_b} \frac{1}{x} \frac{\partial}{\partial x} \left(x \frac{N}{x} \sin\theta\right) = -\mu\varepsilon V_\infty B_o \sigma_1 \frac{K'}{x} \sin\theta$$

$$\frac{B_o}{R_b} \frac{1}{x} \frac{\partial}{\partial x} \left[x\left(-\frac{M'}{x} \sin\theta\right)\right] - \frac{B_o}{R_b} \frac{1}{x} \frac{\partial}{\partial\theta} \left[2 \frac{M}{x^2} \cos\theta\right] =$$

$$\mu\varepsilon V_\infty B_o \sigma_1 \frac{L}{x} \sin\theta$$

Carrying out the indicated differentiation, the θ dependence divides out and we are left with

$$N = \mu\varepsilon\ V_\infty\ \sigma_1\ R_b\ K$$

$$N' = \mu\varepsilon\ V_\infty\ \sigma_1\ R_b\ K'$$

$$-\frac{M''}{x} + \frac{2M}{x^3} = \mu\varepsilon\ V_\infty\ \sigma_1\ R_b\ \frac{L}{x}$$

The first and second equations are degenerate. This is because we have already used $\underset{\sim}{\nabla} \cdot \underset{\sim}{J} = 0$ to find the functional forms and the latter is not an independent equation but is obtainable from Eq. (3-34). We note that x, N, M, L, K are dimensionless and so

$$\text{Rem} = \mu\varepsilon\ V_\infty\ \sigma_1\ R_b \tag{4-54}$$

is a dimensionless group, the magnetic Reynolds number. Some authors do not include the factor ε but since εV_∞ represents a shock layer velocity it is included here. The independent equations are

$$N = \text{Rem}\ K \tag{4-55}$$

$$M'' = \frac{2M}{x^2} - \text{Rem}\ L \tag{4-56}$$

Equations (4-29), (4-42) and (4-55) indicate that the azimuthal magnetic field and the radial current are directly related.

$$\frac{B_\varphi}{B_o} = 2\ \text{Rem}\ \frac{J_r}{\varepsilon V_\infty\ \sigma_1\ B_o}\ \frac{R_b}{r}\ \tan\theta \tag{4-57}$$

When one does not include the Hall effect J_r does not exist. Thus B_φ is an induced component requiring non-zero magnetic Reynolds number and the Hall effect. Once more, it is emphasized that

$$\text{Rem} = \mu\varepsilon\ V_\infty\ \sigma_1\ R_b = 0$$

is a mathematical limit which perhaps could be written more consisely

$$\text{Rem} \to 0$$

or

$$\text{Rem} \ll 1$$

We mean that the dimensionless group is very small and not that any single term is actually zero. Indeed, most of the terms will appear in other dimensionless groups where the combination may not be small.

It is noted that Eq. (4-56) reduces to the equation for dipole behavior (4-31) when Rem = 0. Thus, when we use this limiting case we are really neglecting distortion of the magnetic field. The distortion will be studied in what follows but the forementioned limit is a useful basis for comparison and as it turns out, a useful approximation.

Equation (4-55) allows one to replace N with K in subsequent equations reducing the unknowns by one. Another function that need not be considered further in the system is the excess charge density ρ_e which enters only in Eq. (3-31). Formally, we solve for it using Eq. (4-48).

$$\rho_e = \frac{\mathscr{e}}{r^2}\ \frac{\partial}{\partial r}\ (r^2\ E_r) + \frac{\mathscr{e}}{r \sin\theta}\ \frac{\partial}{\partial\theta}\ (\sin\theta\ E_\theta)$$

$$= \frac{\mathscr{e}\ \sigma_1\ \epsilon\ V_\infty\ B_o}{R_b}\ \frac{x^2\ H'' + 2\ x\ H' - 2H}{x^2}\ \cos\theta \qquad (4\text{-}58)$$

This quantity is not considered further since it is not connected with the dynamics or drag directly.

Ohm's law (3-30) is considered next. This contains $\underset{\sim}{J} \times \underset{\sim}{B}$ which is

$$\underset{\sim}{J} \times \underset{\sim}{B} = \hat{r}\,(J_\theta B_\varphi - J_\varphi B_\theta) + \hat{\theta}\,(J_\varphi B_r - J_r B_\varphi) +$$

$$\hat{\varphi}\,(J_r B_\theta - J_\theta B_r)$$

Using the functional forms of Eqs. (4-27) to (4-29) and (4-42) to (4-44) and (4-55)

$$\underset{\sim}{J} \times \underset{\sim}{B} = \sigma_1 \epsilon V_\infty B_o^2 \left[\hat{r}\,\frac{M'L - \mathrm{Rem}\,KK'}{x^2}\sin^2\theta + \right.$$

$$\hat{\theta}\,2\,\frac{ML - \mathrm{Rem}\,K^2}{x^3}\sin\theta\cos\theta + \qquad (4\text{-}59)$$

$$\left.\hat{\varphi}\,2\,\frac{MK' - M'K}{x^3}\sin\theta\cos\theta\right]$$

Similarly, the term

$$V \times B = \epsilon V_\infty B_o \left[\hat{r}\,\frac{M'G - \mathrm{Rem}\,KF'}{x^2}\sin^2\theta + \right.$$

$$\hat{\theta}\,2\,\frac{MG - \mathrm{Rem}\,KF}{x^3}\sin\theta\cos\theta + \qquad (4\text{-}60)$$

$$\left.\hat{\varphi}\,2\,\frac{MF' - M'F}{x^3}\sin\theta\cos\theta\right]$$

Using these relations and the functional forms for $\underset{\sim}{J}$ and $\underset{\sim}{E}$, (3-30) yields the three equations

$$\frac{2K}{x^2} \cos\theta = H' \cos\theta + \frac{M'G - \text{Rem } KF'}{x^2} - C_H' B_o \frac{M'L - \text{Rem } K'K}{x^2} \sin^2\theta \quad (4\text{-}61)$$

$$-\frac{K'}{x} \sin\theta = -\frac{H'}{x} \sin\theta + 2\frac{MG - \text{Rem } KF}{x^3} - 2C_H' B_o \frac{ML - \text{Rem } K^2}{x^3} \sin\theta \cos\theta$$

$$\frac{L}{x} \sin\theta = \frac{2}{x^3}(MF' - M'F) \sin\theta \cos\theta - 2C_H' B_o \frac{MK' - M'K}{x^3} \sin\theta \cos\theta$$

The dimensionless group

$$C_H = C_H' B_o \quad (4\text{-}62)$$

is recognized. C_H is the Hall coefficient and we recall that C_H' was the Hall coefficient per unit field strength. For small θ, which is the current approximation

$$\sin\theta = \theta - 0(\theta^3)$$
$$\cos\theta = 1 - \frac{\theta^2}{2} + 0(\theta^4) \quad (4\text{-}63)$$

At 45^o the errors are 10 and 2% respectively when $0(\theta^3)$ is neglected. The error decreases rapidly toward $\theta = 0$. Using Eq. (4-63) in (4-61) and retaining terms to order θ^2 we find that the θ dependence again divides out leaving

$$H' = \frac{2K}{x^2} \quad (4\text{-}64)$$

$$K' = H - 2\frac{MG - \text{Rem } KF}{x^2} + 2C_H \frac{ML - \text{Rem } K^2}{x^2} \quad (4\text{-}65)$$

$$L = 2\frac{MF' - M'F}{x^2} - 2C_H \frac{MK' - M'K}{x^2} \quad (4\text{-}66)$$

The equation for L may be regarded as an algebraic one to be coupled with the

differential system. These are the ordinary differential equations for the current.

The momentum equation contains several terms to be evaluated. The vorticity is

$$\underset{\sim}{\nabla} \times \underset{\sim}{V} = \hat{r}\ \frac{1}{r \sin\theta}\ \frac{\partial}{\partial\theta}(\sin\theta\ V_\varphi) + \hat{\theta}\ \frac{1}{r}\ \frac{\partial}{\partial r}(-r\ V_\varphi) + \hat{\varphi}\left[\frac{1}{r}\ \frac{\partial}{\partial r}(r\ V_\theta) - \frac{1}{r}\ \frac{\partial}{\partial\theta} V_r\right] \tag{4-67}$$

and using the functional forms of Eqs. (4-22), (4-23) and (4-26)

$$\underset{\sim}{\nabla} \times \underset{\sim}{V} = \frac{\epsilon\ V_\infty}{R_b}\left[\hat{r}\ \frac{2G}{x^2}\ \cos\theta - \hat{\theta}\ \frac{G'}{x}\ \sin\theta + \hat{\varphi}\ \frac{2F - x^2F''}{x^3}\ \sin\theta\right] \tag{4-68}$$

The acceleration term associated with it is

$$\underset{\sim}{\nabla} \times \underset{\sim}{V} \times \underset{\sim}{V} = \frac{\epsilon^2\ V_\infty^2}{R_b^2}\left[\hat{r}\ \frac{x^2\ G'G - F'(2F - x^2F'')}{x^4}\ \sin^2\theta + \hat{\theta}\ 2\ \frac{x^2G^2 - F(2F - x^2F'')}{x^5}\ \sin\theta\ \cos\theta + \hat{\varphi}\ 2\ \frac{F'G - FG'}{x^3}\ \sin\theta\ \cos\theta\right] \tag{4-69}$$

The viscous term is (Ref. 66)

$$\nabla^2 \underset{\sim}{V} = \hat{r}\left[\frac{1}{r^2}\ \frac{\partial}{\partial r}\left(r^2\ \frac{\partial V_r}{\partial r}\right) + \frac{1}{r^2 \sin\theta}\ \frac{\partial}{\partial\theta}\left(\sin\theta\ \frac{\partial\ V_r}{\partial\theta}\right) - \frac{2\ V_r}{r^2} - \frac{2}{r^2 \sin\theta}\ \frac{\partial}{\partial\theta}(\sin\theta\ V_\theta)\right] +$$

$$\hat{\theta}\left[\frac{1}{r^2}\frac{\partial}{\partial r}\left(r^2\frac{\partial V_\theta}{\partial r}\right)+\frac{1}{r^2\sin\theta}\frac{\partial}{\partial\theta}\left(\sin\theta\frac{\partial V_\theta}{\partial\theta}\right)-\frac{V_\theta}{r^2\sin^2\theta}+\frac{2}{r^2}\frac{\partial V_r}{\partial\theta}\right]+$$

$$\varphi\left[\frac{1}{r^2}\frac{\partial}{\partial r}\left(r^2\frac{\partial V_\varphi}{\partial r}\right)+\frac{1}{r^2\sin\theta}\cdot\frac{\partial}{\partial\theta}\left(\sin\theta\frac{\partial V_\varphi}{\partial\theta}\right)-\frac{V_\varphi}{r^2\sin^2\theta}\right]$$

Expanding with the functional forms

$$\nabla^2\underset{\sim}{V}=\frac{\epsilon V_\infty}{R_b^2}\left[\hat{r}\,2\frac{x^2F''-2F}{x^4}\cos\theta+\hat{\theta}\frac{-x^3F'''+2xF'-4F}{x^4}\sin\theta+\hat{\varphi}\frac{x^2G''-2G}{x^3}\sin\theta\right] \tag{4-70}$$

The dynamic pressure term is

$$\underset{\sim}{\nabla}\left(\frac{V^2}{2}+\frac{p}{\rho}\right)=\frac{1}{2}\underset{\sim}{\nabla}\left(V^2+\epsilon V_\infty^2 C_p\right)$$

where $\rho_{\infty/\epsilon}$ is the shock layer density and C_p the pressure coefficient of Eq. (4-51). The expanded form is

$$\frac{1}{2}\underset{\sim}{\nabla}\left(V^2+\epsilon V_\infty^2 C_p\right)=\hat{r}\left[\frac{1}{2}\frac{\epsilon^2 V_\infty^2}{R_b}\frac{\partial}{\partial x}\left(\frac{4F^2}{x^4}\cos^2\theta+\frac{F'^2}{x^2}\sin^2\theta+\frac{G^2}{x^2}\sin^2\theta+\frac{C_p}{\epsilon}\right)\right]$$

$$+\hat{\theta}\left[\frac{\epsilon^2 V_\infty^2}{R_b}\frac{1}{x}\frac{\partial}{\partial\theta}\left(\frac{4F^2}{x^4}\cos^2\theta+\frac{F'^2}{x^2}\sin^2\theta+\frac{G^2}{x^2}\sin^2\theta+\frac{C_p}{\epsilon}\right)\right] \tag{4-71}$$

There is no φ term here since $\frac{\partial}{\partial \varphi} = 0$. We now have all the terms for the momentum equation (3-6). The φ components add to give

$$0 = \frac{2\,\epsilon^2\,V_\infty^2}{R_b}\,\frac{F'G - G'F}{x^3}\sin\theta\cos\theta + \frac{\epsilon\,V_\infty\,\eta_1}{\rho_1\,R_b^2}\,\frac{x^2G'' - 2G}{x^3}\sin\theta \qquad (4\text{-}72)$$

$$+ 2\,\sigma_1\,\epsilon\,V_\infty\,B_o^2\,\frac{MK' - M'K}{x^3}\sin\theta\cos\theta$$

The scaling parameters combine to form dimensionless groups. Defining the Reynolds number as

$$Re = \frac{\rho_1\,V_1\,R_b}{\eta_1} = \frac{\rho_\infty\,V_\infty\,R_b}{\eta_1} \qquad (4\text{-}73)$$

and the interaction parameter as

$$S = \frac{\sigma_1\,B_o^2\,R_b}{\rho_1\,V_1} = \frac{\sigma_1\,B_o^2\,R_b}{\rho_\infty\,V_\infty} \qquad (4\text{-}74)$$

where $\epsilon = \frac{\rho_\infty}{\rho_1} = \frac{V_1}{V_\infty}$. As before, the θ dependence divides out for small θ.

$$2\,(F'G - G'F) + \frac{1}{Re}\,(x^2G'' - 2G) + 2S\,(MK' - M'K) = 0 \qquad (4\text{-}75)$$

This is the ordinary differential equation representing the φ momentum equation. The r and θ momentum equations add to

$$\frac{1}{2}\,\frac{\epsilon^2\,V_\infty^2}{R_b^2}\,\frac{\partial}{\partial x}\left(\frac{4F^2}{x^4}\cos^2\theta + \frac{F'^2}{x^2}\sin^2\theta + \frac{G^2}{x^2}\sin^2\theta + \frac{C_p}{\epsilon}\right) = \qquad (4\text{-}76)$$

$$\frac{x^2G'G - F'(2F - x^2F'')}{x^4}\sin^2\theta + \frac{2}{Re}\,\frac{x^2F'' - 2F}{x^4}\cos\theta +$$

$$2S\,\frac{M'L - Rem\,K'K}{x^2}\sin^2\theta$$

$$\frac{1}{2}\,\frac{\epsilon^2 V_\infty^2}{R_b^2}\,\frac{1}{x}\,\frac{\partial}{\partial\theta}\left(\frac{4F^2}{x^4}\cos^2\theta + \frac{F'^2}{x^2}\sin^2\theta + \frac{G^2}{x^2}\sin^2\theta + \frac{C_p}{\epsilon}\right) = \tag{4-77}$$

$$2\,\frac{x^2G^2 - F(2F - x^2F'')}{x^5}\sin\theta\cos\theta + \frac{1}{Re}\,\frac{-x^3F''' + 2xF' - 4F}{x^4}\sin\theta$$

$$+ 2S\,\frac{ML - Rem\,K^2}{x^3}\sin\theta\cos\theta$$

The pressure coefficient can be eliminated by cross-differentiation setting

$$\frac{\partial^2}{\partial x\,\partial\theta} = \frac{\partial^2}{\partial\theta\partial x}$$

Again for small θ the θ dependence divides out.

$$2F(x^3F''' - 2x^2F'' - 2xF' + 8F) + 2x^2G\,(xG' - 2G) -$$

$$\frac{x}{Re}\,(x^4F''' - 4x^2F'' + 8xF' - 8F) + \tag{4-78}$$

$$2Sx^2\left[M(xL' - 2L) + Rem\,K(2K - xK')\right] = 0$$

Having eliminated the pressure coefficient, we must convert the boundary condition (4-50) in terms of it. Substituting (4-50) in (4-76) evaluated at the shock $x = x_s$.

$$F''(x_s) + \frac{F'''(x_s)}{Re} - 2S\,\frac{M(x_s)L(x_s)}{x_s^2} = -\frac{1}{\epsilon^2} + 2\left(\frac{1}{\epsilon} - 1\right)\left(1 - \frac{1}{Re\,x_s}\right) \tag{4-79}$$

This is the so called vorticity boundary condition which replaces the pressure boundary condition in Eq. (4-50). We retain the viscous term instead of neglecting it as did Smith, Schwimmer and Wu (Ref. 29). Therefore, we do not assume a thin viscous boundary layer in the present formulation.

The differential equations are now complete. The equations and boundary conditions are summarized later. When this is done, it becomes evident that the boundary conditions are of sufficient order to satisfy the composite order of the system with one additional which gives the shock stand-off distance. First, however, we derive some auxiliary equations which give the aerodynamic and magnetoaerodynamic coefficients.

The equations derived so far reduce to those of Smith, Schwimmer and Wu (Ref. 29) when the Hall effect is excluded. When the viscous terms are omitted, the equations reduce to those of Bush (Ref. 5) if attention is paid to notation and the definition of dimensionless groups. Without the MHD effect, they reduce to those of Lighthill (Ref. 8).

4.5 Magnetoaerodynamic Coefficients

The coefficients relating to force and pressure are defined in this section.

The pressure coefficient has already been defined in equation (4-51) and is governed by equations (4-76) and (4-77). Of particular interest is the pressure coefficient on the body surface. Equation (4-77) may be integrated. To order θ

$$C_p(1,\theta) = C_{p_o} + \epsilon\theta^2 \left[G(1)^2 - F'(1)^2 - \frac{F'''(1)}{Re} + 2S \left[M(1)L(1) - Rem\ K(1)^2 \right] \right]$$

where C_{p_o} is the constant of integration, the stagnation pressure coefficient. This can be written

$$C_p(1,\theta) = C_{p_o} - \beta\theta^2 \qquad (4\text{-}80)$$

where $\mathcal{P}$ is the pressure relief function

$$\mathcal{P} = \epsilon\left[F'(1)^2 - G(1)^2 + \frac{F'''(1)}{Re} - 2S\left\{M(1)L(1) - Rem\ K(1)^2\right\}\right] \qquad (4\text{-}81)$$

The first two terms vanish for $Re \neq \infty$ (no slip) and the third vanishes for $Re = \infty$. The stagnation pressure coefficient

$$C_{p_o} = \frac{p_o - p_\infty}{\frac{\rho_\infty V_\infty^2}{2}} \qquad (4\text{-}82)$$

is obtained by integrating (4-76) along the stagnation stream line,

$$C_{p_o} = 2\left(1 - \frac{\epsilon}{2}\right) - \frac{4\epsilon}{Re}\int_1^{x_s} \frac{x^2F'' - 2F}{x^4}\,dx \qquad (4\text{-}83)$$

We note that the MHD forces have no effect on the inviscid stagnation pressure. At shock layer lift-off, not within the scope of the present theory, this pressure must essentially vanish and so there is a pronounced effect for magnetically supported shock layers. For the limiting inviscid hypersonic flow with $\epsilon = 0$ we have the Newtonian pressure coefficient $C_{p_o} = 2$.

We define a component of the total drag coefficient as

$$C_{D_i} = \frac{\text{Drag of component } i}{q_\infty \pi R_b^2} \qquad (4\text{-}84)$$

where

$$q_\infty = \frac{\rho_\infty V_\infty^2}{2} \qquad (4\text{-}85)$$

the dynamic pressure. The direction of the drag force is that of the free stream velocity.

One of the components is drag due to surface pressure (see Truitt, Ref. 52)

$$C_{D_p} = 2\int_o^{\pi/2} C_p(1,\theta) \sin\theta \cos\theta \, d\theta \tag{4-86}$$

The present theory is valid only in the stagnation region. We assume that the theory holds to some θ_L and that beyond the pressure coefficient is proportional to cos θ . This forces a zero value at the body shoulder.

$$C_{D_p} = \int_o^{\theta_L} 2(C_{p_o} - \beta \sin^2\theta)\sin\theta \cos\theta d\theta +$$

$$\int_{\theta_L}^{\pi/2} 2(C_{p_o} - \beta \sin^2\theta_L) \frac{\cos\theta}{\cos\theta_L} \sin\theta \cos\theta d\theta$$

where we have approximated $\theta \approx \sin\theta$ for $\theta < \theta_L$. Integrating

$$C_{D_p} = \frac{2}{3} C_{p_o} - (2\beta - \frac{C_{p_o}}{2}) \sin^2\theta_L + \frac{\beta}{3} \sin^4\theta_L \tag{4-87}$$

We must determine θ_L empirically. For $\epsilon = 1/11$, $\beta = 2.65$ (Bush, Ref. 5) and $C_{p_o} = 1.909$. Experiment (Ta Li, Ref. 67) indicates that $C_{D_p} = .93$. This corresponds to $\sin^2\theta_L = 1/3$ or $\theta_L = 35^o$. Using this value

$$C_{D_p} = \frac{1}{9} (7C_{p_o} - \frac{11}{6}\beta) \; ; \; \beta \leq 3C_{p_o} \tag{4-88}$$

We note that the pressure coefficient of Eq. (4-80) vanishes at about 35^o when $\beta = 3C_{p_o}$. Therefore, we will use Eq. (4-88) only when the coefficient in non-zero up to that point. This accounts for the inequality restriction in Eq. (4-88). The inequality may be violated in MHD flows of large induced pressure relief (Bush, Ref. 5). For the case of a vanishing pressure coefficient before $\theta = 35^o$ we cut off the integration at $C_p = 0$ and find

$$C_{D_p} = \frac{C_{p_o}^2}{2\mathcal{P}} \quad ; \quad \mathcal{P} > 3C_{p_o} \tag{4-89}$$

The base drag is not predicted by the present theory which is limited to the stagnation region. Base drag is due to suction accompanying a low pressure area behind a high speed vehicle. Newtonian theory predicts a zero base pressure. For a flat base

$$C_{D_B} = - C_{p_B} = \frac{P_\infty}{\frac{\rho_\infty V_\infty^2}{2}} = \frac{2}{\gamma_\infty M_\infty^2}$$

where γ_∞ is the free stream "gamma" based on the speed of sound and M_∞ is the flight or flow Mach number. For the lower supersonic speeds, Hoerner (Ref. 68) suggests

$$C_{p_B} = - \frac{2}{\gamma_\infty M_\infty^2} K$$

where K is a correction factor such that

$$\lim_{M_\infty \to \infty} K = 1$$

The data reported in Reference 68 suggest the simple relation

$$K = 1 - \frac{1}{M_\infty}$$

for $M_\infty > 2$. In the laboratory, the presence of a sting will reduce the base drag. For

$$\frac{D_s}{D} \leq .4$$

$$M_\infty > 2 \tag{4-90}$$

where D_s is the sting diameter, the base pressure is virtually uneffected by the presence of the sting (Hoerner, Ref. 68), a desirable state of affairs. Thus, we can correct the previous relation to read

$$C_{D_B} = \frac{2}{\gamma_\infty M_\infty^2} \left(1 - \frac{1}{M_\infty}\right)\left[1 - \left(\frac{D_s}{D}\right)^2\right] \tag{4-91}$$

which includes the effect of the sting.

Now if the sting is rigid and the pressure transducer is located at the body-sting bearing surface interface, we need not consider the sting further. If, however, the body and sting are connected with the force transducer aft of this system, we need to add the drag of the sting. This can be done by applying conventional aerodynamic estimates (Truitt, Ref. 52) depending on the sting configuration.

The base drag is normally a small percentage of the total drag particularly at high speeds. Even at moderate supersonic speeds it is generally less than 10% of the total drag. Therefore, its prediction is not too critical with respect to accuracy. The MHD interaction will affect this prediction but we neglect the effect here. This is reasonable here because the base drag would have to be increased by an order of magnitude to introduce substantial error.

The present theory uses the shock density ratio as a parameter rather than γ_∞ and M_∞. The following expression approximates Eq. (4-91)

$$C_{D_B} = \frac{2}{7}(6\epsilon - 1)\left(1 - \sqrt{6\epsilon - 1}\right) \quad ; \quad \epsilon > \frac{1}{6} \tag{4-92}$$

$$= 0 \quad ; \quad \epsilon \leq \frac{1}{6}$$

where we have dropped the sting correction entirely. Equation (4-91) with another term for sting drag, if present, is recommended for more precise correlation of experimental data.

Skin friction results in a positive stress in the θ direction on the body surface. This stress, divided by the dynamic pressure, is defined as the skin friction coefficient.

$$C_{F_\theta} = \frac{\eta_1}{q_\infty} \left(\frac{\partial V_\theta}{\partial r} \right)_{r = R_b}$$

$$= - \frac{2\epsilon}{Re} F''(1) \sin \theta \qquad (4\text{-}93)$$

Since there may also be flow in the azimuthal direction

$$C_{F_\varphi} = \frac{2\epsilon}{Re} G'(1) \sin \theta \qquad (4\text{-}94)$$

these quantities integrate to produce a viscous drag in the flow direction

$$C_{D_F} = 2 \int_o^{\pi/2} C_{F_\theta} \sin^2\theta \, d\theta \qquad (4\text{-}95)$$

and a rolling moment coefficient

$$C_{l_F} = 2 \int_o^{\pi/2} C_{F_\varphi} \sin^2\theta \, d\theta \qquad (4\text{-}96)$$

where

$$C_l = \frac{\text{Torque}}{q_\infty \pi R_b^2 \cdot R_b} \qquad (4\text{-}97)$$

being positive by convention when the torque is in the $+\varphi$ direction.

The reference moment arm is the body radius. Using the limiting $\theta_\angle$ ideal as with pressure

$$C_{D_F} = 2\int_o^{\theta_\angle} C_{F_\theta} \sin^2\theta d\theta \quad +2\int_{\theta_\angle}^{\pi/2} C_{F_\theta} \sin^2\theta d\theta$$

The stagnation theory of Fay and Riddel indicates (Hayes and Probstein, Ref. 50)

$$C_{F_\theta} \propto \frac{1.53}{\sqrt{Re}}$$

while flat plate theory (Schlicting, Ref. 47), more indicative of the flow away from the stagnation point, has

$$C_F \propto \frac{.332}{\sqrt{Re}}$$

For $\theta > \theta_\angle$ we use 1/5 of the value for C_F as suggested by the above proportionalities. Choosing $\theta_\angle = 45^o$, the integration gives

$$C_{D_F} = -\frac{4}{3}\frac{\epsilon}{Re} F''(1) \qquad (4\text{-}98)$$

Similarity, Equation (4-97) integrates to

$$C_{\ell_F} = \frac{4}{3}\frac{\epsilon}{Re} G'(1) \qquad (4\text{-}99)$$

The MHD or Lorentz drag is given by

$$C_{D_{MHD}} = -\int_{vol.} \underset{\sim}{J} \times \underset{\sim}{B} \frac{1}{q_\infty \pi R_b^2} \, d(vol.)$$

where the integration is over the region of interaction. For the present approximation, this extends from the body to the shock and from the stagnation stream line to some $\theta_\angle$. Using Eq. (4-59) for $\underset{\sim}{J} \times \underset{\sim}{B}$

$$C_{D_{MHD}} = - \frac{4}{R_b^2 \rho_\infty V_\infty^2} \int_o^{\theta_\angle} \int_{R_b}^{R_s} \left[(\underset{\sim}{J} \times \underset{\sim}{B})_r \cos\theta + (\underset{\sim}{J} \times \underset{\sim}{B})_\theta (-\sin\theta) \right] r^2 \sin\theta d\theta$$

$$= - \frac{S\epsilon}{4} \left[\frac{Rem}{2} K(1)^2 + \int_1^{x_s} (-M'L + \frac{2ML}{x} - \frac{2RemK^2}{x}) dx \right] \qquad (4\text{-}100)$$

with $\theta_\angle = 45^o$. This choice is rather arbitrary in the constant property approximation because one can argue for a corresponding value of the effective value of the electrical conductivity, presumably lowering as one extends $\theta_\angle$. Seemann (Ref. 32) has used $\theta_\angle = 30^o$ on the basis of sonic line considerations. Ericson and Maciulaitus (Ref. 27) argue for 60^o because of the possible movement of the sonic line with MHD interaction. Our choice of 45^o is intermediate and reflects a desire to use σ_1 for the effective conductivity because it is easy to estimate on the basis of the normal shock relations.

The force associated with Eq. (4-100) acts on the magnetic source and is transmitted to the vehicle through the structural elements. In the same manner, any Lorentz force in the φ direction causes a reactive torque on the magnet and its structure. Analogous to the Lorentz drag of Eq. (4-100) and the friction rolling moment coefficient of Eq. (4-96), the MHD rolling moment coefficient is

$$C_{\ell_{MHD}} = - \frac{S\epsilon}{2} \int_1^{x_s} MK' - M'K \, dx \qquad (4\text{-}101)$$

being positive in the $+\varphi$ direction (Figure 8).

The total drag coefficient sums to

$$C_D = C_{D_p} + C_{D_B} + C_{D_F} + C_{D_{MHD}} \tag{4-102}$$

and similarly for the total rolling moment coefficient

$$C_l = C_{l_F} + C_{l_{MHD}} \tag{4-103}$$

The actual drag and torque can be obtained from the coefficients by using their definitions of Eqs. (4-84) and (4.97). The rolling moment is a consequence of the Hall effect.

4.6 Dimensionless Parameters

The dimensionless parameters arose naturally in Section 4.4 as a combination of the scaling parameters for the dimensionless functions such as F, G, etc. Use of dimensionless parameters is important for several reasons. First of all, it is possible to formulate the problem in a minimum number of variable parameters, as is well known to the experimenter. We need do a minimum number of numerical calculations when they are used. Secondly, they defer the question of units to actual evaluation of the dimensional parameters and the solution does not depend on the system of units used. The dimensionless parameters may be evaluated independently and so a convenient system can be selected for each depending on the units used in tables, charts and equations in the literature.

We could have introduced the dimensionless parameters in Chapter III when the basic equations were first introduced. However, one is forced to choose a reference velocity, magnetic field, etc. in order to do this and the choice became more evident once the problem was more completely defined. Having a knowledge of the boundary conditions and the functional

forms we were able to choose scaling references so that the dimensionless functions, such as F, G, etc., would be of order unity. This is important numerically.

For a discussion of the significance of the dimensionless parameters and their interpretation in terms of ratios of force, etc., we refer to the book by Cambel (Ref. 59). The dimensionless parameters are summarized below

(shock density ratio) $$\epsilon = \rho_\infty / \rho_1 \qquad (1\text{-}30)$$

(Reynolds number) $$Re = \rho_\infty V_\infty R_b/\eta_1 \qquad (4\text{-}73)$$

(interaction parameter) $$S = \sigma_1 B_o^2 R_b/\rho_\infty V_\infty \qquad (4\text{-}74)$$

(magnetic Reynolds number) $$Rem = \mu\sigma_1 \epsilon V_\infty R_b \qquad (4\text{-}54)$$

(Hall coefficient) $$C_H = C_H' B_o \qquad (4\text{-}62)$$

$$= \frac{eB_o}{me} \tau_e \qquad (3\text{-}17)$$

Tables for normal shocks can be used to evaluate the dimensionless groups. These are readily available for flight conditions using real gas, equilibrium air. The data of Huber (Ref. 46) and Hansen (Ref. 69) are particularly suited for the flight conditions defined in Chapter II and were used to calculate the data of the charts of this investigation (Figures 9 through 18). For the argon plasma, equilibrium thermodynamics was employed. The data and formulas of Arave and Huseley (Ref. 44) were used.

The body radius was taken as 10 ft. for flight entry and 1 in. for the laboratory conditions. 10,000 gauss stagnation point field strength was used. Figures 9 through 18 can be corrected to apply to particular

values by noting the definition of the parameters and multiplying by an appropriate constant.

The Hall coefficients (Figures 17 and 18) were calculated by noting (Spitzer, Ref. 58),

$$\sigma = \frac{e^2}{n_e} \frac{\tau_e}{m_e}$$

so that

$$C_H = \frac{eB_o}{m_e} \tau_e = \frac{\sigma}{e n_e} B_o \qquad (4\text{-}104)$$

where σ and m_e were obtained from the references cited (Ref. 44 and 46). The speed of light appears in the denominator of the RHS of Eq. (4-104) if Gaussian units are used.

In order to give the reader a concise picture of the range of the parameters, we refer to Table 3. The range is rather extensive but narrowed if one takes into account that certain extremes are improbable. For example, one would probably not encounter very large Mach numbers at low altitudes or vice versa. We refer to the typical values of Table 3 for a more realistic estimate of conditions.

4.7 Summary

The mathematical problem has been defined. In order to solve the problem the following system must be solved.

$$x^2 M'' - 2M + \mathrm{Rem}\, x^2 L = 0 \qquad (4\text{-}56)$$

$$x^2 H' - 2K = 0 \qquad (4\text{-}64)$$

$$x^2(K' - H) + 2(MG - \text{Rem } KF) - 2C_H(ML - \text{Rem } K^2) = 0 \tag{4-65}$$

$$x^2L - 2(MF' - M'F) + 2C_H(MK' - M'K) = 0 \tag{4-66}$$

$$2F(x^3F''' - 2x^2F'' - 2xF' + 8F) + 2x^2G(xG' - 2G) -$$

$$\frac{x}{\text{Re}}(x^4F'''' - 4x^2F'' + 8xF' - 8F) +$$

$$2Sx^2[M(xL' - 2L) + \text{Rem } K(2K - xK')] = 0 \tag{4-78}$$

$$2(F'G - G'F) + \frac{1}{\text{Re}}(x^2G'' - 2G) + 2S(MK' - M'K) = 0 \tag{4-75}$$

over the range $1 \leq x \leq x_s$ with the boundary conditions of Eqs. (4-50) and (4-79)

$$F(1) = 0$$

$$F'(1) = 0 \qquad (\text{Re} \neq \infty)$$

$$G(1) = 0 \qquad (\text{Re} \neq \infty)$$

$$K(1) = 0 \qquad \text{(insulated body)}$$

$$H(1) = 0 \qquad \text{(conducting body)}$$

$$M(1) = \frac{1}{2}(1 - \mathcal{C})$$

$$M'(1) = -\frac{1}{2}(1 + 2\mathcal{C}) \tag{4-105}$$

at the body. At the shock

$$F(x_s) = -x_s^2/2$$

$$F'(x_s) = -x_s/\epsilon$$

$$F''(x_s) + \frac{F'''(x_s)}{\text{Re}} - 2S\frac{M(x_s)\,L(x_s)}{x_s^2} = -\frac{1}{\epsilon^2} + 2\left(\frac{1}{\epsilon} - 1\right)\left(1 - \frac{1}{\text{Re } x_s}\right)$$

$$G(x_s) = 0 \qquad (4\text{-}106)$$

$$K(x_s) = 0$$

$$M(x_s) = \frac{1}{2}\ \frac{B_s}{B_o}$$

$$M'(x_s) = -\frac{1}{2}\ \frac{B_s}{B_o}$$

We note that the order of the system in 2 in M of Eq. (4-56), 1 in H of Eq. (4-64), etc. The total order of the system is 2 + 1 + ... = 10. Six boundary conditions are specified at the body and 7 at the shock for a total of 13. The three "extra" conditions fix the values of x_s, B_s/B_o and $\mathcal{C}$ making the system determinant in terms of the 5 dimensionless parameters defined in Section 4.6. In this sense the problem is well posed and we presume, because of the physical nature of the problem, that only one solution exists. If the differential equations and boundary conditions are satisfied, we assume that we have the unique solution to the problem posed.

The magnetoaerodynamic coefficients are a function of the solution and are given explicitly as such in Section 4.5.

While the problem is well defined, the solution is quite difficult in the present form. Solutions are discussed in the next chapter. Special forms of the system are studied with attention to the effects of the dimensionless parameters one at a time. Some of these special forms are best handled if one considers the inverse problem where the dimensionless parameters are specified in terms of references at the shock rather than at the body. However, the present statement of the problem is complete and in terms of the natural parameters, that is, parameters that are normally known a priori.

The procedure of this investigation was to obtain solutions by the most convenient method available, often an inverse method, but to present the results in terms of the natural parameters of the problem (Section 4.6). The analytic and numerical procedures follow in the next chapter.

CHAPTER V

SOLUTIONS

5.1 Introduction

This chapter describes the methods of obtaining solutions to the mathematical problem formulated in Chapter IV and summarized in Section 4.7. Due to the complexity of the system to be solved, the methods will be primarily numerical. However, we start off with an analytical solution of the inviscid, non-MHD problem and show how this can be used to obtain a first approximation for the MHD drag.

The analytical solution also serves to introduce the inverse formulation. In many cases, it is more practical to base the dimensionless parameters on shock references. For example, the magnetic interaction parameter may be based on a reference magnetic field at the shock. One can often simplify or even eliminate the two point boundary value problem so that it is possible to integrate the system backwards from the shock to the body. The problem defined in the manner of Chapter IV requires the satisfaction of a number of boundary conditions at two points (the shock and the body) at once. One must solve the problem "simultaneously" rather than "march" either forward or backward to the second point. This is because not enough initial conditions are known at either single point. Formulation of the inverse problem allows one to fix enough initial conditions for direct integration in many special cases. The general problem is equally complicated in either formulation.

5.2 First Approximation

The MHD drag coefficient is given by Eq. (4-100). We consider inviscid flow without the Hall effect or magnetic field deformation. For this case the magnetic field is given by (Section 4.3)

$$M = \frac{x}{2} \tag{5-1}$$

Without the Hall effect, $C_H = 0$, the current function of Eq. (4-66) is

$$L = \frac{xF' + F}{x^4} \tag{5-2}$$

so that Eq. (4-100) is

$$C_{D_{MHD}} = -\frac{3}{8} S\epsilon \int_1^{x_s} \frac{xF' + F}{x^6}\, dx \tag{5-3}$$

We now study the case of small interaction (small S). In the limit S = 0 there is no characteristic length in the problem that either vanishes or diverges. The stand-off distance, boundary layer thickness, etc, simply approach their non-MHD values. This suggests that the problem can be handled as a regular perturbation in S (Van Dyke, Ref. 70). We expand

$$\begin{aligned} F &= F_o + SF_1 + S^2 F_2 + \dots \\ x_s &= x_{s_o} + Sx_{s_1} + S^2 x_{s_2} + \dots \end{aligned} \tag{5-4}$$

so that

$$C_{D_{MHD}} = \frac{-3}{8}\epsilon \left[S \int_1^{x_{s_o} + Sx_{s_1} + \dots} \frac{xF_o' + F_o}{x^6}\, dx + 0\,(S^2) \right]$$

$$= \frac{-3}{8}\epsilon \left[(x_{s_o} + Sx_{s_1} + \dots - 1) \int_o^1 \frac{xF_o' + F_o}{x^6}\, d(x-1) + 0(S^2) \right]$$

and to order S

$$C_{D_{MHD}} = -\frac{3}{8} S\epsilon \int_1^{x_s} \frac{xF_o' + F_o}{x^6} dx \tag{5-5}$$

We expand Eq. (4-78) in terms of the perturbation. For inviscid flow

$$2F(x^3F''' - 2x^2F'' - 2xF' + 8F) + S\frac{x^2F'' - xF' - 3F}{x^3} = 0$$

$$2F_o(x^3F_o''' - 2x^2F_o'' - 2xF_o' + 8F_o) + 0(S) = 0$$

so that F_o is given by

$$x^3F_o''' - 2x^2F_o'' - 2xF_o' + 8F_o \tag{5-6}$$

But this is just the equation for F without the MHD effect, the problem considered by Lighthill (Ref. 8). The boundary conditions can also be expanded in S. Those for zeroth order are those for the non-MHD flow

$$F_o(1) = 0$$

$$F_o(x_{s_o}) = -x_{s_o}^2/2$$

$$F_o'(x_{s_o}) = -x_{s_o}/\epsilon \tag{5-7}$$

$$F_o''(x_{s_o}) = -\frac{1}{\epsilon^2} + 2\left(\frac{1}{\epsilon} - 1\right)$$

where the stand-off distance is related to

$$\delta = x_{s_o} - 1 + 0(S)$$

but the problem is that x_{s_o}, the shock location, is not known ahead of

time. Thus, we cannot start an integration at x_{s_o} and integrate to the body, say numerically. We recall that

$$V_r = \frac{2F(x)}{x^2} \cos\theta \in V_\infty$$

$$V_\theta = -\frac{F'(x)}{x} \sin\theta \in V_\infty$$

where $x = r/R_b$. Instead, we could have defined

$$y = \frac{r}{R_s} \tag{5-8}$$

based on the shock radius, as yet unknown. And then let

$$V_r = \frac{2f(y)}{y^2} \cos\theta \in V_\infty$$

$$V_\theta = -\frac{f'(y)}{y} \sin\theta \in V_\infty \tag{5-9}$$

which results in the following replacement for Eq. (5-6) for first order in f

$$y^3 f_o''' - 2yf_o'' - 2yf_o' + 8f_o = 0 \tag{5-10}$$

with boundary conditions

$$f_o(y_b) = 0$$

$$f_o(1) = -\frac{1}{2}$$

$$f_o'(1) = -\frac{1}{\epsilon} \tag{5-11}$$

$$f_o''(1) = -\frac{1}{\epsilon^2} + 2\left(\frac{1}{\epsilon} - 1\right)$$

where the stand-off $\delta = \frac{R_s - R_b}{R_b}$ is

$$\delta = \frac{1}{y_b} - 1 \tag{5-12}$$

Contrary to Eq. (5-7), the set (5-11) does not contain the unknown shock position explicitly. Further Eq. (5-10) is third order and we have four boundary conditions in Eq. (5-11). While this was also true before, the present formulation has the shock position implicit in only one of the boundary conditions and the point of the condition is isolated from the three not containing it. This means that one can use the three as initial conditions for a backward integration from the shock to the body. One reaches the body when $f_o = 0$. And one can evaluate the shock standoff from Eq. (5-12) when this point is reached. This is an example of the inverse method. There is no problem numerically and the problem is said to be reduced to quadrature.

In this rather simple example, the solution of either formulation can be obtained analytically using the rather extensive linear theory. The three linearly independent solutions add to

$$f_o = a_1 y^4 + a_2 y^2 + \frac{a_3}{y} \tag{5-13}$$

or

$$F_o = b_1 x^4 + b_2 x^2 + \frac{b_3}{x} \tag{5-14}$$

The coefficients are determined by the boundary conditions of Eq. (5-7) or (5-11). For example,

$$b_1 = -\frac{(1-\epsilon)^2}{30\epsilon^2 x_s^2} \qquad b_2 = \frac{(1-4\epsilon)}{6\epsilon^2}$$

$$b_3 = 2(1-\epsilon)(1-6\epsilon) x_s \tag{5-15}$$

with x_{s_o} given in terms of the positive real root nearest and greater than unity of

$$2\,(1-\epsilon)\,(1-6\epsilon)\,x_{s_o}^5 - 5\,(1-4\epsilon)\,x_{s_o}^2 + 3\,(1-\epsilon)^2 = 0 \qquad (5\text{-}16)$$

The root can be found graphically, numerically or by special techniques but not in a general closed form owing to the high order of the polynomial. In this sense, the present solution is not completely analytical. We will refer to these results in the next chapter when the various effects are studied and compared. At this point we refer only to some empirical results that are obtained by using the solutions (5-14) and (5-16). When Eq. (5-14) is substituted in the expression for the MHD drag coefficient (5-5) and integrated one obtains a relation involving ϵ and x_{s_o} in a rather complicated way. This can not be written in closed form because of the nature of Eq. (5-16). However, numerical solutions of the simple algebraic problem indicate that

$$C_{D_{MHD}} = 0.0607\ S\epsilon \qquad (5\text{-}17)$$

with an error of less than 1% as compared with the numerical solution. The results correlate very well with $C_{D_{MHD}}/S\epsilon$ from $\epsilon = 1/2$ to $1/100$. A similar correlation for the shock stand-off is

$$\delta = .78\epsilon \qquad (5\text{-}18)$$

which is Seiff's correlation (Ref. 45). We note that Eq. (5-17) is correct to order S while Eq. (5-18) is only for zeroth order or for no MHD effect.

5.3 Inverse Formulation

The concept of the inverse solution was introduced in the last section. The reason for this approach is to allow specification of more boundary conditions at the shock than at the body. In some cases, it is possible to provide enough initial conditions for a single numerical integration from the shock to the body. This section concerns the inverse formulation in detail.

The original functional forms were introduced in Section 4.3. In conjunction with the non-MHD problem, we introduced an alternative form for the radial and polar velocities of Eq. (5-9) based on the shock reference of distance, namely the shock radius. Analogously, the shock reference field strength, B_s, can be used in place of B_o in the other functional forms as well. Thus

$$
\begin{aligned}
V_r &= 2\varepsilon\, V_\infty \frac{f(y)}{y^2} \cos\theta \\
V_\theta &= -\,\varepsilon\, V_\infty \frac{f'(y)}{y} \sin\theta \\
V_\varphi &= \varepsilon\, V_\infty \frac{g(y)}{y} \sin\theta \\
B_r &= 2B_s \frac{m(y)}{y^2} \cos\theta \\
B_\theta &= -\,B_s \frac{m'(y)}{y} \sin\theta \\
B_\varphi &= B_s \frac{n(y)}{y} \sin\theta
\end{aligned}
\qquad (5\text{-}19)
$$

$$J_r = 2\epsilon\, V_\infty\, \sigma_1\, B_s\, \frac{k(y)}{y^2} \cos\theta$$

$$J_\theta = -\,\epsilon\, V_\infty\, \sigma_1\, B_s\, \frac{k'(y)}{y} \sin\theta$$

$$J_\varphi = \epsilon\, V_\infty\, \sigma_1\, B_s\, \frac{\ell(y)}{y} \sin\theta$$

$$E_r = \epsilon\, V_\infty\, B_s\, h'(y) \cos\theta$$

$$E_\theta = -\,\epsilon\, V_\infty\, B_s\, \frac{h(y)}{y} \sin\theta$$

where $y = r/R_s$ and $y_b = R_b/R_s$ so that the boundary conditions corresponding to Eq. (4-105) are

$$f(1) = -\frac{1}{2}$$

$$f'(1) = -\frac{1}{\epsilon}$$

$$f''(1) + \frac{f'''(1)}{Re_s} - 2S_s\, m(1)\, \ell(1) = -\frac{1}{\epsilon^2} + 2\left(\frac{1}{\epsilon} - 1\right)\left(1 - \frac{1}{Re_s}\right) \qquad (5\text{-}20)$$

$$g(1) = 0$$

$$k(1) = 0$$

$$m(1) = \frac{1}{2}$$

$$m'(1) = -\frac{1}{2}$$

at the shock. At the body

$$f(y_b) = 0$$

$$f'(y_b) = 0 \qquad (Re_s \neq \infty)$$

$$g(y_b) = 0 \qquad (Re_s \neq \infty)$$

$$k(y_b) = 0 \qquad \text{(insulated body)}$$

$$h(y_b) = 0 \qquad \text{(conducting body)}$$

$$m(y_b) = \frac{1}{2}(1 - \mathcal{C})\frac{B_o}{B_s} \tag{5-21}$$

$$m'(y_b) = -\frac{1}{2}(1 + 2\mathcal{C})\frac{B_o}{B_s}$$

and the differential equations corresponding to Eqs. (4-56), (4-64), (4-65), (4-66) and (4-78) are

$$y^2 m'' - 2m + \mathrm{Rem}_s\, y^2 \ell = 0 \tag{5-22}$$

$$y^2 h' - 2k = 0 \tag{5-23}$$

$$y^2(k' - h) + 2(mg - \mathrm{Rem}\, kf) - 2C_{H_s}(m\ell - \mathrm{Rem}\, k^2) \tag{5-24}$$

$$y^2 \ell - 2(mf' - m'f) + 2C_{H_s}(mk' - m'k) = 0 \tag{5-25}$$

$$2f(y^3 f''' - 2y^2 f'' + 8yf' - 8f) + 2y^2 g(yg' - 2g) -$$

$$\frac{y}{\mathrm{Re}_s}(y^4 f'''' - 4y^2 f'' + 8yf' - 8f) + \tag{5-26}$$

$$2S_s y^2 [m(y\ell' - 2\ell) + \mathrm{Rem}_s k(2k - yk')] = 0$$

where the dimensionless groups analogous to those of Section 4.6 are defined as

$$\varepsilon = \rho_\infty / \rho_1 \qquad \text{(as before)} \tag{1-30}$$

$$Re_s = \rho_\infty V_\infty R_s/\eta_1 \tag{5-27}$$

$$S_s = \sigma_1 B_s^2 R_s/\rho_\infty V_\infty \tag{5-28}$$

$$Rem_s = \mu \sigma_1 \epsilon V_\infty R_s \tag{5-29}$$

$$C_H = C_H' B_s = \frac{e B_s}{me} \tau_e \tag{5-30}$$

We note that there are still as many boundary conditions at the shock as at the body and so there is no improvement for the general case. However, if one considers the inviscid problem without the Hall effect, the only boundary conditions remaining at the body are the first and last two of Eq. (5-21). We recall that there are three excess boundary conditions so these can be considered as the forementioned. Enough initial conditions are known at the shock. One can integrate directly backward to the body which is located when $f(y_b) = 0$. The last two equations of (5-21) define B_o/B_s and the field deformation $\mathcal{G}$. The MHD problem, including magnetic Reynolds number effects, but neglecting viscosity and the Hall effect is greatly simplified, being reduced to quadrature.

The magnetoaerodynamic coefficients can be written in terms of the inverse functions f, g, etc. The easiest way to do this is to note the relation between the old functions and the new.

$$F(x) = \left(\frac{R_s}{R_b}\right)^2 f(y)$$

$$G(x) = \frac{R_s}{R_b} g(y)$$

$$
\begin{aligned}
M(X) &= \left(\frac{R_s}{R_b}\right)^2 \frac{B_s}{B_o}\, m(y) \\
N(X) &= \frac{R_s}{R_b}\, \frac{B_s}{B_o}\, n(y) \\
K(X) &= \left(\frac{R_s}{R_b}\right)^2 \frac{B_s}{B_o}\, k(y) \\
L(X) &= \frac{R_s}{R_b}\, \frac{B_s}{B_o}\, \ell(y) \\
H(X) &= \frac{B_s}{B_o}\, h(y)
\end{aligned}
\tag{5-31}
$$

The relations between the dimensionless groups are

$$
\begin{aligned}
S &= \frac{R_b}{R_s} \left(\frac{B_o}{B_s}\right)^2 S_s \\
Re &= \frac{R_b}{R_s}\, Re_s \\
Rem &= \frac{R_b}{R_s}\, Rem_s \\
C_H &= \frac{B_o}{B_s}\, C_{H_s}
\end{aligned}
\tag{5-32}
$$

Once the solutions have been found in terms of S_s, Re_s, etc., they can be converted in terms of the natural parameters S, Re, etc. The latter are based on quantities that would normally be known.

5.4 Normal Quasi-Linearization

Normal quasi-linearization is an algorithm or procedure which lends itself to evaluating the nonlinear boundary value problem when the boundary

conditions are split between two or more points. In principle, it can be applied to the general problem concerned here and in either the direct or inverse form.

The first step in the procedure is to reduce the order of the equations to first order. The usual substitutions are made.

$$\begin{aligned} \mathbf{F}_1 &= F \\ \mathbf{F}_2 &= F' \\ \mathbf{F}_3 &= F'' \\ \mathbf{F}_4 &= F''' \quad (Re \neq \infty) \\ \mathbf{F}_5 &= G \\ \mathbf{F}_6 &= G' \quad (Re \neq \infty), \text{ etc.} \end{aligned} \tag{5-33}$$

One can write the system and the boundary conditions in terms of $\mathbf{F}_i$. The original equations are supplemented with equations like

$$\begin{aligned} \frac{d}{dx}\mathbf{F}_1 &= \mathbf{F}_2 \\ \frac{d}{dx}\mathbf{F}_2 &= \mathbf{F}_3 \text{ , etc.} \end{aligned} \tag{5-34}$$

and so the price of reducing the order of each equation is an increase in the number of equations. It is much better to work with the first order equations because they can be written in the standard form

$$\frac{d\mathbf{F}_i}{dx} = \mathbf{f}_i \quad (\mathbf{F}_1, \mathbf{F}_2, \ldots\ldots, x) \tag{5-35}$$

with boundary conditions for the two point problem in generalized form

$$\alpha_i\ (x_1,\ F_1,\ F_2,\ \ldots) = 0$$

$$\beta_i\ (x_2,\ F_1,\ F_2,\ \ldots) = 0 \qquad (5\text{-}36)$$

where there must be at least n equations (5-36) if there are n functions F_i. If there are unknown parameters, such as the value of x_2, there must be a corresponding number of additional boundary conditions.

So far, we have only put the system into a standard form convenient for most numerical analyses including the other methods to be discussed. In quasi-linearization, the original system (5-35) is replaced by a sequence of systems (Bellman and Kalaba, Ref. 71)

$$\frac{dF_i^{(k)}}{dx} = f_i\ (F_1^{(k-1)},\ F_2^{(k-1)} \ldots,\ x) + \sum_j \frac{\partial f_i\ (F_1^{(k-1)} \ldots, x)}{\partial F_j^{(k-1)}} \left(F_j^{(k)} - F_j^{(k-1)}\right) \qquad (5\text{-}37)$$

such that in the limit

$$\lim_{k \to \infty} F_i^{(k)} = F_i \qquad (5\text{-}38)$$

Each member of the sequence is required to satisfy the exact boundary conditions (5-36).

$$\alpha_i\ (x_1,\ F_1^{(k)},\ F_2^{(k)},\ \ldots) = 0$$

$$\beta_i\ (x_2,\ F_1^{(k)},\ F_2^{(k)},\ \ldots) = 0 \qquad (5\text{-}39)$$

A process that results in the boundary conditions being satisfied at each step of the process is called a <u>normal</u> process.

It can be shown (Bellman and Kalaba, Ref. 71) that if the interval

$$|x_2 - x_1| \leq \epsilon_x \tag{5-40}$$

is small enough, or if the initial guess $F_i^{(o)}$ is close enough

$$|F_i - F_i^{(o)}| \leq \epsilon_F^o \tag{5-41}$$

for

$$k \geq N$$

where for every specified error ϵ_F there exists an N such that for $k \geq N$, the sequence converges.

Unfortunately, while one has satisfied the boundary conditions one may not end up with a solution to the nonlinear equations (5-35). This means it is possible to converge to an incorrect solution. One can tell if this has occurred by seeing whether or not the solution satisfies the nonlinear equations.

The reasons for doing all of this is that the system (5-37) is linear in the current iteration in $F_i^{(k)}$. The very extensive theory of linear systems can be used to find the solution for each member of the sequence no matter how the boundary conditions are split. In linear theory the homogeneous solution given by the following

$$\frac{dF_i^{(k)}}{dx}H_j = \sum \frac{\partial f_i}{\partial F_j}^{(k-1)}(F_1^{(k-1)}, F_2^{(k-1)}, \ldots x)\ F_j^{(k)} \tag{5-42}$$

with boundary conditions

$$F_{i_{H_j}}^{(k)}(x_1) = \delta_{ij}$$

$$\delta_{ij} = 0 \qquad i \neq j$$
$$= 1 \qquad i = j \tag{5-43}$$

is added to the particular solution of (5-37) with boundary conditions

$$F_{i_p}^{(k)}(x_1) = 0 \tag{5-44}$$

so that the complete solution is

$$F_i^{(k)} = F_{i_p}^{(k)} + \sum_j C_j F_{j_{H_i}}^{(k)} \tag{5-45}$$

The constants C_j are determined by the boundary conditions of the complete problem. Equations (5-42) and (5-37) are integrated using (5-43) and (5-44) as initial conditions. After integrating to x_2, algebraic equations representing the boundary conditions (5-39) are solved for the constants in Eq. (5-45). This is a straight forward numerical problem.

In each iteration k, there is one system for the particular system and as many homogeneous systems as there are boundary conditions. The conditions (5-44) are such that the latter are linearly independent. It is possible to reduce the number of systems if some of the initial conditions are known explicitly. Assume the following are known

$$F_1^{(k)}(x_1)$$

$$F_2^{(k)}(x_1)$$

$$\vdots$$

$$F_q^{(k)}(x_1)$$

then set

$$F_{i_p}^{(k)}(x_1) = F_1^{(k)}(x_1) \qquad (5\text{-}46)$$
$$\vdots$$
$$F_{q_p}^{(k)}(x_1) = F_q^{(k)}(x_1)$$

Then there are q less homogeneous solutions with initial conditions

$$F_{i_{H_j}}^{(k)}(x_1) = \begin{cases} 0 & i = 1,q \\ \delta_{ij} & i = q+1,n \end{cases} \qquad j = 1,n-q \qquad (5\text{-}47)$$

where we have assumed n original functions F_i.

Since the boundary conditions were satisfied in the normal process, one must only check to see whether the solution actually satisfies the non-linear equations. This is done by evaluating Eq. (5-45) at $x = x_1$ and using these complete initial conditions to integrate the non-linear equations (5-35) forward to x_2. One then checks to see whether the boundary conditions are satisfied there. In some cases this will not occur and if convergence occurs it will be to an incorrect solution.

When the second point, x_2, is unknown as in the present application, the process must be modified slightly. Let

$$\xi = \frac{x - x_1}{x_2 - x_1} \qquad (5\text{-}48)$$

so that the quasi-linear system is

$$\frac{d}{d\xi} F_i^{(k)} = \Delta x^{(k-1)} f_i \left(F_1^{(k-1)}, F_2^{(k-1)} \ldots, \xi\right) +$$

$$\Delta x^{(k-1)} \sum_j \frac{\partial f_i}{\partial F_j^{(k-1)}} \left(F_1^{(k-1)} \ldots, \xi\right) : \qquad (5\text{-}49)$$

$$\left(F_j^{(k)} - F_j^{(k-1)}\right)$$

where

$$\Delta x^{(k-1)} = x_2^{(k-1)} - x_1 \qquad (5\text{-}50)$$

is the previous iteration of the interval. One must make an initial guess of $\Delta x^{(o)}$ as well as $F_i^{(o)}$. One can usually make a reasonable guess in terms of the boundary conditions and as solutions are found in terms of parameters, the previous solution can be used for the next value of the parameter. When convergence occurs, it occurs quadratically (Bellman and Kalaba, Ref. 71) in a few iterations (seldom more than five).

The quasi-linearization process was applied by Smith, Schwimmer and Wu (Ref. 29) for the current problem without the Hall effect. They apparently used slightly incorrect boundary conditions but this is immaterial for the present considerations. In Section 1.2 we noted that their interaction parameter could be multiplied by a constant to correct their plotted results. The fact that they specified the magnetic field boundary condition incorrectly at the body, as discussed in Section 4.3, has little consequence for low magnetic Reynolds number. Their results, to which we now refer, have been corrected in this way.

We refer to our Figure 19 for the shock stand-off distance that was found by Smith, Schwimmer and Wu (Ref. 29) compared with the results of

Bush (Ref. 5). Because of the large difference in these results (which would have been even larger had the forementioned correction not been applied), the computations of Bush and Smith, Schwimmer and Wu were repeated in the present investigation. We reproduced Bush's results using his inverse method showing them to be computationally correct. However, we could not reproduce the results of Smith, Schwimmer and Wu. Our calculation, using quasi-linearization (marked "quasi" in Figure 19) was somewhat closer to those of Bush but still too far off for the difference in Reynolds number. Further, we noted that the solution did not converge to the correct solution except for very small magnetic interaction (for zero interaction our result was identical with Smith, et al.). We suspect that the same thing happened in Smith's computation and that we both converged to different incorrect solutions probably owing to slight differences in the quasi-linearization schemes.

In order to find the correct solution, we applied a completely different method, discussed in the next section, and found good agreement with the results of Bush and that the solution obtained was indeed the correct solution. The solution is marked "extremal" in Figure 19. The difference is just what one would expect for the difference in Reynolds number. The results of Lykoudis (Ref. 19)have good agreement with those of Bush and the present theory.

Accordingly, we have abandoned the quasi-linearization method in favor of the extremal technique that follows. We refer the interested reader to the book by Bellman and Kalaba (Ref. 71) for more details of quasi-linearization. Orthonormalization of the homogeneous solutions is

particularly important in order to retain accuracy. This and methods to overcome machine storage problems are discussed in the book and were followed by the present author.

5.5 Extermal Algorithm

The basic problem of stellar structure in astrophysics is a two point boundary value problem where the boundary conditions are split between the center of the star and its edge (Schwarzchild, Ref. 72). The classical approach is to transform and simplify the equations so that all of the initial conditions are known except one. The last one is quessed and the system is integrated forward numerically. The error at the second point is noted and the process is repeated with a new guess. One continues the process by extrapolating and finally interpolating for the unknown initial condition. This can be done by sophisticated techniques such as the method of false position (Ref. 73). The number of iterations required is greater than that of quasi-linearization but convergence to the correct solution occurs when convergence occurs because the boundary conditions and non-linear equations have both been satisfied automatically.

The present system can not always be simplified so that only one initial condition has to be quessed. So we form a positive definite function of the error at the second point

$$Z^{(k)} = \sum_i \beta_i \left(F_1^{(k)}, F_2^{(k)}, \ldots, x \right)^2 \qquad (5\text{-}51)$$

We quess the unknown initial conditions and integrate forward evaluating the sum of the squares of the error in the boundary conditions of Eq. (5-36)

at each step of the integration. When we have a minimum of Z for the function of x we have located the "best" value of the unknown second point for the quessed initial conditions. The value of Z is the square of the errors in the boundary conditions at that point and for the present iteration and this value is noted. The initial conditions are then stepped in a systematic manner until we have minimized the value of Z at the second point. This represents convergence. It is convergence to the correct solution if Z can be made arbitrarily close to zero for then the boundary conditions to the non-linear problem are satisfied arbitrarily closely. Since the non-linear differential equations have been used all along they are automatically satisfied.

One can imagine the system of ordinary differential equations to be increased in dimension by the unknown initial conditions into a system of partial differential equations. The positive definite function of Eq. (5-51) is minimized with respect to the old and new independent variables. Sophisticated methods exist for such a minimalization (Kunz, Ref. 73) but the simplest method is to march about in the space continuing in the direction of decreasing Z.

Geometric arguments show that if one makes a close enough guess to the correct initial conditions that a solution is insured. Of course, in many cases the number of iterations is excessive making the method impractical. For example, in the viscid problem without Hall effect there are only two unknown initial conditions at the body $F''(1)$ and $F'''(1)$, and yet as many as 200 iterations were required in order to find a solution at an

interaction parameter of 50. The long time of computation prohibited going past a value of 100. However, the method is still superior to that of quasi-linearization which failed to converge to the correct solution except for very small interaction parameter. There is reason to believe that the viscous solution merges into the inviscid solution at moderate interaction. This phenomena is discussed in detail later.

5.6 Other Techniques

At least two other techniques exist for solving the two point problem. Picard's equation (Kunz, Ref. 73) is similar to the basic equation for quasi-linearization except the second term in Eq. (5-37) is neglected. Picard's method is based on a successive approximation so that the non-linear part is known from the previous iteration and linear analysis can be used. The second term in quasi-linearization gives a correction to the successive approximation similar to the slope-intercept techniques of the Newton-Raphson method for finding roots to algebraic equations. One would expect Picard's method to be less effective than quasi-linearization and so it was not applied in the present investigation.

Back and forth integration (Kunz, Ref. 73) involves guessing the unknown initial conditions and integrating forward to the second point and determined by the boundary conditions there. The known boundary conditions at the second point replace those calculated by the forward integration and the unknown ones are assumed to be those just calculated. A backward integration is performed to the first point. If the calculated conditions correspond to the known ones at that point within an acceptable error, convergence has occurred and to the correct solution. If not, the

process is repeated. Experimentation indicated that this technique to be inferior to the extremal method for the present application. It was not pursued further. The extremal method was used to obtain the results presented in the next chapter. We now discuss some of the details of the programs.

5.7 Computational Details

The equations of Section 4.7 were used for the viscous MHD solution. The direct formulation is superior to the inverse when there is the possibility of a boundary layers where functions change rapidly and are sensitive to errors that one might incur as one integrated into the layer. It is better to integrate out of the layer where the viscous effects are not important and errors in the higher order terms are less important. Also, one receives the solution as a function of the natural Reynolds number instead of the inverse one based on the shock radius. The results need not be cross plotted.

The Hall effect and deformation of the magnetic field was neglected. The functions G, K, H and N can be set arbitrarily to zero as they do not appear when the Hall effect is omitted (Smith, Schwimmer and Wu, Ref. 29). For Rem = 0,

$$M = \frac{1}{2x}$$

as we noted in Chapter III. Only a differential equation in F of Eq. (4-78) and an algebraic equation for L of Eq. (4-66) in terms of F remains. These are combined and the fourth order equation is written as four first order equations as shown in Section 5.4. There are two initial conditions known,

F(1) and F'(1). We guess F"(1) and F"'(1) and integrate forward until Eq. (5-51) is a minimum. F"(1) is stepped and the process is repeated until Z is a minimum with respect to both x anf F"(1). This process is repeated within steps of F"'(1) until a minimum is found with respect to all three. We required that $Z \leq 10^{-4}$ and all boundary conditions to be satisfied within 1%. The magnetoaerodynamic coefficients were calculated after each iteration in order to insure their convergence with the rest of the solution.

No special difficulties were encountered except the solutions required excess time, typically 10 minutes, for S greater than about 10 for a Reynolds number of 100. Fortunately, it became evident that the viscous solution was merging into the inviscid one at moderate interaction parameter.

The effect of non-zero magnetic Reynolds number was studied using the inverse formulation of Section 5.3 without the Hall effect or viscosity. This is essentially the problem treated by Bush (Ref. 5) where one is able to integrate directly from the shock to the body. With Re = ∞ and $C_H = 0$, there are a sufficient number of boundary conditions specified at y = 1 in Eq. (5-20). These constitute the initial conditions and the integration is performed backward until f(y) = 0 which locates the body.

The solution is in terms of the inverse parameters S_s and Rem_s and after obtaining it we solved for the natural variables S and Rem using Eq. (5-32). We intended to present the data versus S so the fact we had not complete control of this parameter did not matter. However, it is desirable to present the data as a family of solutions for various Rem. It is desirable to control the value of this parameter. We iterated

$$Rem_s^{(i)} = Rem\left(\frac{R_s}{R_b}\right)^{(i-1)} \tag{5-52}$$

and found convergence to the desired Rem within .1% within 3 or 4 iterations. The first guess is $Rem_s^{(1)} = Rem$.

The magnetoaerodynamic coefficients were calculated in each iteration to insure their convergence with the rest of the solution. For $Rem_s = Rem = 0$, only one integration is required.

The inverse method was also applied for the Hall effect study. Viscosity and magnetic field deformation were neglected. Thus

$$M = \frac{1}{2x}$$

$$\frac{1}{Re} = 0$$

in the equations of Section 5.3. The integration starts at the shock. The initial condition h(1) is quessed. Zero is a fair first guess and as one varies the parameters ϵ, C_{H_s} and S_s better quesses become apparent by extrapolation and interpolation of previous results. Using the guess h(1) the integration proceeds backward until

$$Z^{(i)} = f(y)^2 + k(y)^2 \qquad \text{(insulated body)}$$

$$= f(y)^2 + h(y)^2 \qquad \text{(conducting body)} \tag{5-53}$$

is a minimum. Another guess of h(1) is made and the procedure is repeated and the new value of $Z^{(i+1)}$ is compared to $Z^{(i)}$. If the new value is lower we continue to step in that direction. If not a step in the opposite sense is made. To speed the process, the initial steps are doubled until the minimum interval is located. This interval and sub-intervals that follow are halved until Z is sufficiently close to zero. Convergence

usually required less than 10 iterations. Again the magnetoaerodynamic coefficients were calculated at each iteration in order to insure their convergence by inspection.

The results were obtained in terms of S_s and C_{H_s} and the corresponding values of S and C_H were solved for after each solution. The results were cross-plotted in order to determine the variation in terms of C_H.

In all cases the integrations were performed numerically after writing the system as first order equations. A standard FORTRAN subroutine for Runge-Kutta integration of a coupled system of first order equations (Ref. 74) was employed. The subroutine allowed for a variable integration step which is altered internally so as to maintain a nominal absolute and per cent error of the integrated functions. We specified an absolute error of 10^{-10} and a relative error of .01% with an initial integration step of .001. The interval was increased or decreased automatically to insure the accuracy with maximum computation time.

The viscous solutions required from 2 to 10 minutes of time on the Northwestern University CDC 3400 high speed digital computer operating on the facility's SCOPE monitor system. The inviscid solutions that required no iteration required about .1 minute each. The magnetic Reynolds number computations increased this to .25 minutes, and the Hall effect results required about 1 minute of time each or less. The viscous solution required much more time because of the double iteration involved with two guesses of initial conditions required. Also, the integration intervals were necessarily small when the boundary layer was present.

The investigation used about 12 hours of computer time. Approximately half of that was used in developing the programs and the methods reported in this section.

CHAPTER VI

RESULTS AND CONCLUSIONS

6.1 Introduction

The results of the analytic and numerical computations are presented in this chapter. One of the principal aims of the investigation was to determine which effects are important for an account of MHD drag phenomena. The analyses were restricted to aerodynamic like flow with an attached shock layer but some information is presented which suggests when the solution can not be obtained beyond a certain value of magnetic interaction parameter when the attached layer is assumed.

While a procedure for obtaining a solution in terms of arbitrary values of the dimensionless groups ϵ, S, Re, Rem and C_H was described in Chapter V, practical considerations prohibited this course. The special cases indicate that it is not always necessary to consider all of the effects at once. The special cases demonstrated the magnetic interaction, the effect of ϵ and S, with viscosity, magnetic field deformation and the Hall effect considered separately. There is no reason to believe that the observations made here would be much different if all the effects were considered simultaneously. These observations will be summarized later in this chapter with regard to conclusions for an account of MHD drag in terms of the present theory and what assumptions should be made in improved theory.

The stand-off distance for the inviscid non-MHD theory as obtained from the solution of Section 5.2 is shown in Figure 20. The curve corresponds to that presented by Lighthill (Ref. 8). A comparison with experiments at moderate supersonic speeds (Kaattari, Ref. 64) and a correlation known to be valid for hypersonic speeds (Inouye, Ref. 45) is also shown. The agreement is very good over the entire range and improves at small density ratio ϵ which corresponds to high Mach numbers.

The important thing to note in Figure 20 is that the shock stand-off distance increases with ϵ. This means that the stand-off decreases with an increase in Mach number. Thus, a high Mach number flow will have a shock tightly wrapped about the body nose.

The aerodynamic coefficients for the same flow are shown in Figure 21. The total drag coefficient is compared with the data contained in Hoerner's book (Ref. 68) and the agreement is very good for ϵ less than about 1/3 or Mach numbers greater than about 2. The base drag is a small component of the total drag except for very low supersonic speeds. The present theory assumes that the base drag is unchanged with MHD interaction.

We note that the aerodynamic coefficients for small ϵ vary little with ϵ . This corresponds to the hypersonic approximation. Some laboratory flows will have ϵ as low as, say, 1/3 and so one must expect some Mach number dependence on the drag coefficient.

The stream lines and magnetic flux lines are shown in Figure 22. For the non-MHD case, neither are perturbed by the other. The qualitative picture in Figure 22 does not change with interaction, the predominant effect being an

increase in shock stand-off distance.

It can be seen that the magnetic field lines are nearly radial and the stream lines nearly parallel to the body in the shock layer. However, at large ϵ (low Mach number) the shock stand-off becomes large enough to violate this (hypersonic) approximation. One can imagine this in Figure 22 by noting how the field diverges from radial lines at large distances from the body.

The only variable in the inviscid non-MHD problem is the shock density ratio, a measure of the Mach number. The total drag varies little with the parameter for this case. Shock stand-off distance is proportional to ϵ .

6.2 Magnetic Interaction

Viscosity, magnetic field deformation and the Hall effect are neglected. The shock stand-off distance, shown in Figure 23, increases with the interaction parameter and the shock density ratio.

It can be noted that the density ratio ϵ has the main influence for small interaction parameter S whereas for large interaction both parameters are important. It is interesting to note that if one attempted to increase S by raising the Mach number in order to raise the conductivity by shock heating, one would lower the value of ϵ and perhaps not raise the stand-off distance as much as otherwise expected. However, if one raised S independently by increasing the magnetic field strength, the value of ϵ would be unaltered.

As expected, the MHD drag component increased with the interaction parameter (Figure 24). For low interaction ($S < 1$), the MHD component can be

closely approximated by Equation (5-17)

$$C_{D_{MHD}} = 0.0607\ S\epsilon \qquad (6\text{-}1)$$

At high interaction, this estimate tends to be inaccurate because the volume of interaction increases with the shock stand-off distance and non-linear effects acquire importance for large S.

The pressure drag coefficient is also shown in Figure 24. It tends to decrease with increasing interaction because the magnetic pressure begins to support the flow. For $S < 1$, one can neglect the reduction in pressure drag.

The total drag is shown in Figure 25. The decrease in pressure drag inhibits the increase in total drag. One can not neglect the alteration in pressure drag except at very low interaction. This is one reason that simple approximations tend to give high predictions. The total drag coefficient is independent of both S and ϵ for small interaction ($S < 1$). The drag itself depends on the dynamic pressure $\rho_\infty V_\infty^2/2$ which tends to increase with Mach number and ambient pressure. At increased interaction ($S > 1$) the dependence on ϵ is such that one can expect a greater drag coefficient for low Mach numbers at the same S. We should emphasize that the dynamic pressure drops with reduced Mach number and so the absolute drag would probably decrease (depending on how the other conditions, such as ambient pressure, changed).

Since the MHD component of drag is approximately linear in ϵ one can expect a greater relative increase (per cent increase) in drag with an increase in S in the laboratory than in flight at the same S. Viscous effects tend to

reduce this advantage as will be seen in the next section. Further, the estimates of Section 4.6 indicate that large values of S are easier to obtain in flight for the same field strengths.

The solutions were obtained with increasing interaction parameter until the boundary conditions could not be satisfied by starting with an interaction parameter S_s greater than a critical value. The variation of the shock interaction parameter with the natural parameter S is illustrated in Figure 26. Beyond the dashed line, no solution could be obtained consistent with the boundary conditions of the constant property attached shock layer. It was suggested in Chapter I that this may be associated with the onset of shock layer lift-off and magnetic support of the flow. Estimates for the range of S (Section 4.6) indicate that the critical value can probably be exceeded in flight at the higher altitudes with 10,000 gauss but the situation is at best borderline for the laboratory flows at the same field strength.

The results of this section are used as a basis for evaluating the effects of viscosity, magnetic field deformation and the Hall effect in the sections that follow.

6.3 Viscous Effects

We noted earlier that the viscous solution merges into the inviscid one at moderate interaction parameter. This is illustrated by the variation of the shock stand-off distance in Figure 27. The viscous layer has a larger shock stand-off. One can interpret this as a result of the boundary layer thickness being added to the stand-off distance for inviscid flow. Of course,

at low Reynolds number the boundary layer of the classical flow is not distinct but rather is merged into the outer layer. However, at large interaction the boundary layer becomes a distinct sub-layer. This is discussed later in this section. Figure 27 shows that an inviscid theory would predict a low value of shock stand-off but a high value of the relative or per cent increase with the interaction parameter S. We recall that the viscous effects were expected to be more important in the laboratory than in flight because of the lower Reynolds numbers in the laboratory.

The pressure and Lorentz drag coefficients (Figure 28) vary similarly to the inviscid values. Flow at low Reynolds number has a greater drag due to pressure. This is due to the reduction of pressure gradient along the body. The viscous forces tend to lower the velocity near the body and raise the pressure (consider Bernoulli's equation). Actually, the stagnation pressure reduces slightly because of viscous dissipation. This is a negligible effect here.

The Lorentz drag is virtually uneffected by the viscous effects. Apparently, the reduction of the MHD force in the axial direction due to a reduction in the velocity in $\underset{\sim}{J} \times \underset{\sim}{B} = \sigma \underset{\sim}{V} \times \underset{\sim}{B} \times \underset{\sim}{B}$ is enough to counteract the increase in the interaction volume with the increase in shock stand-off distance. One can approximate the Lorentz drag coefficient with Eq. (6-1) for $S < 1$.

Unfortunately, the inviscid theory can not properly account for the friction drag (Figure 29) which decreases with an increase in interaction parameter due to a reduction of the velocity gradient. The total drag (Figure 29) remains nearly constant over the range of low interaction owing to a decrease

in friction and pressure drag with an increase in Lorentz drag.

The total drag is greater for viscous flow but the relative increase with S is less. Thus an inviscid theory predicts too low of a total drag and too high of a per cent increase (neglecting other effects). This is more important in the laboratory where the Reynolds numbers are low. In flight, the Reynolds numbers are generally substantially greater than 10^3 and the results of Figure 29 show that the inviscid theory is sufficient for drag analysis.

We can make some observations from Figure 29 regarding the heat transfer coefficient. It is proportional to the skin friction coefficient if one assumes that Reynolds analogy is valid here. The friction drag coefficient involves the integral of the friction coefficient and is therefore proportional to the heat transfer coefficient. Since the friction drag decreases with the interaction parameter S, so must the heat transfer coefficient. The heat transfer coefficient should also decrease with an increase in Mach number (lower ε) according to the analogy and the results of Figure 29. In flight, the heat transfer itself would increase because of an increase in stagnation temperature. If the stagnation temperature is held constant in the laboratory by holding the arc power constant (and the flow rate and ambient pressure) the heat transfer should decrease with an increase in Mach number. The flight situation is different because the free stream velocity dominates the stagnation temperature.

At high interaction, S greater than about 50, viscosity can apparently be neglected in the drag analysis because of the merging of the solutions. This can be explained physically as follows.

At low Reynolds number, the entire shock layer is affected by viscosity and there is no distinct boundary layer. A typical velocity profile is shown in Figure 30. At high interaction, the flow is slowed principally near the body. Away from the body, the flow velocity must match the value forced at the shock boundary condition. This results in a deformed velocity profile and the creation of a distinctive layer near the body that looks like a boundary layer (Figure 30). At high interaction, the boundary layer approximation appears to be valid even for flow of low Reynolds number.

This suggests that the Reynolds number alone is no longer the appropriate parameter for determining whether the boundary layer exists. Since a large S makes the flow appear as though Re is large, a product of the two is suggested. This parameter would be large for either large Re or large S. Such a parameter is the Hartmann number

$$Ha = (Re\ S)^{1/2} \qquad (6\text{-}2)$$

This conclusion is not entirely surprising. Poiseuille flow has an inviscid profile at Ha = ∞ and the classical viscous one for Ha = 0 (Cambel, Ref. 59). Seeman and Cambel (Refs. 31 and 32) have interpreted their MHD blunt body experiments in terms of this parameter in addition to S. There seem to be theoretical grounds for doing this when viscous effects are important.

However, if one wishes to consider a wide range of conditions, often obtainable in a laboratory program, the Hartmann number should not replace the role of either the Reynolds number Re or the interaction parameter S except

possibly for heat transfer studies. The reason is that Re is the correct parameter for viscous non-MHD flow and the interaction parameter is the correct one for inviscid MHD flow. Thus S and Re are appropriate for the entire range including the extremes whereas the Hartmann number is appropriate only for viscous flow. Further, if one wishes to evaluate flight applications of MHD drag, the Hartmann number is not appropriate for a comparison.

In heat transfer studies, viscosity is always important and so one of the extreme cases is eliminated (the inviscid one). In this case, the parameters Re and Ha are appropriate instead of Re and S.

6.4 Magnetic Field Deformation

The magnetic field deformation was studied for the inviscid flow without the Hall effect. The shock stand-off distance is shown in Figure 31. A typical value of Rem is 10^{-2} with a practical limit of 10^{-1} (Table 3). However, very large values of Rem were considered in order to include the possibility of a seeded plasma. Perhaps even then, Rem = 1 would be a practical limit representing an order of magnitude increase in the electrical conductivity by seeding. The value of Rem = 10 was included because such large values are obtained in astrophysical situations and possibly some seeded plasmas.

We should note that the present definition of Rem includes the shock density ratio. Some authors do not include this parameter in the definition and so they appear to be dealing with a higher magnetic Reynolds number. The

factor ϵ reflects the shock layer velocity $V_1 = \epsilon V_\infty$.

For Rem less than .1, there appears to be no appreciable effect on the shock stand-off distance (Figure 31) or the total drag coefficient (Figure 32). However, both decrease with increasing Rem at constant S. That is, if one increased the conductivity in Rem and decreased the field squared B_o^2 in the magnetic pressure number such that the interaction parameter (the product of the magnetic Reynolds number and the magnetic pressure number) remained constant, the MHD interaction decreases. The reason for the effect seems to be the deformation of the magnetic field. The deformation is shown in Figure 33 for the moderate values of Rem and in Figure 34 for Rem = 10. The field lines are pushed towards the body with increasing magnetic Reynolds number. For infinite Rem they are actually wrapped about the body (Ref. 13 and 60).

The distortion causes the radial component of the field strength to decrease and the polar value to increase. The shock stand-off distance increases with magnetic interaction because the θ component of velocity is slowed and the flow rate remains the same as impressed by the supersonic free stream

$$\dot{m}\ (\theta) = 2\pi \int_{R_b}^{R_s} \rho_1\ V_\theta r \sin\theta\ dr$$

Thus, if V_θ is reduced, R_s increases in order to pass the flow. The local force in the direction that reduces V_θ is

$$J_\varphi\ B_r$$

neglecting the induced field in the azimuthal direction due to the Hall effect. The field distortion is such to reduce B_r and so the force that tends to reduce V_θ is reduced. The effect on the current

$$J_\varphi = (V_r B_\theta - V_\theta B_r)$$

tends to cancel out with an increase in B_θ and a decrease in B_r . The net effect is less shock stand-off at greater Rem and the same S.

The local fluid force associated with drag is in the axial direction

$$- J_\varphi B_r \sin\theta + J_\varphi B_\theta \cos\theta$$

The second term dominates when the flow is deformed. The analysis has shown that the value of B_θ tends to be increased by a factor $1 + 2\mathcal{C}$ while the value of B_r is reduced by the factor $1 - \mathcal{C}$. The polar field increases faster than the radial field decreases and the net effect is a somewhat greater local Lorentz force in the axial direction. This force integrates to give the total drag due to MHD forces. Because the interaction volume is substantially reduced with increasing Rem (decreasing shock stand-off), the total drag decreases.

Physically, it means that it is better to have a weakly conducting fluid with a high field strength than a highly conducting fluid and a low field strength. At least this occurs with the present geometry with the magnetic dipole axis alligned with the flow. In this case the deformation of the field is such to reduce the interaction. The factor $\mathcal{C}$ introduced in Section 4.3 gives the fractional decrease in the stagnation field strength which is radial in direction

here. The ratio of the stagnation point field strength to the value that would exist without magnetic field deformation, B_o, the value known ahead of time and used in S, is shown in Figure 35. For Rem less than .1 the effect is not very important. For Rem of 10, the stagnation field is reduced to about 1/4 of the original value B_o . This suggests a reduction in the magnetic pressure at the stagnation point due to deformation of the field with non-zero Rem.

These considerations suggest that seeding will not be as effective as otherwise thought. The magnetic Reynolds number would increase as well as S and so one would receive less an increase in interaction than if one increased S by increasing the magnetic field leaving Rem unchanged. It is also apparently more difficult to support the shock layer magnetically at greater Rem. The critical condition (Figure 36) occurs at a higher interaction parameter with increasing Rem.

6.5 Hall Effect

The Hall effect is different depending on whether the body is electrically conducting or insulated. The Hall currents for the two cases are shown in Figures 37 and 38. In the case of the insulated body, the currents can not penetrate the body. The currents must be opposite in sense near the shock as compared with near the body (Figure 38). In the case of the conducting body, the current is nearly normal to the body indicating that the currents must close by re-entering the body somewhere away from the stagnation region (Figure 37). We have sketched the probable closure pattern for the

region where the theory is invalid. If the conductivity of the expanded flow near the shoulder were high enough, the closure would be further aft. We do not suggest that there is no conduction beyond that point, but rather that the MHD forces are not great there.

In discussing the importance of the plasma sheath (Chapter II), we noted the possibility of an insulated body appearing as a conducting one because of the presence of a highly conducting sheath. One should not rule out the possibility of all bodies appearing as conducting ones as viewed from the flow. The Hall currents for a conducting body are radial near the body and parallel to the shock near the shock. This is the type of information that is useful in approximate analyses.

The shock stand-off distance is shown in Figure 39. There is a very great effect for $C_H = 10$ which could be attained in flight and laboratory conditions with 10,000 gauss field strength. The stand-off increases only slowly until an interaction parameter of about a hundred is reached. At very large interaction parameter, as may be encountered in flight, the Hall effect seems less important. It should be noted that an increase in the interaction parameter by increasing the field strength will cause a linear increase in the Hall coefficient whereas the interaction parameter increases by the square. One would not follow a single curve of C_H = constant. However, the theory indicates a definite lower value of stand-off with the Hall effect present and that a conducting body has a larger stand-off than an insulated one under similar conditions.

At great interaction, the stand-off tends to approach the value without the Hall effect in the sense that if one extended the curves without Hall effect beyond the critical condition (where solutions were not obtained) they would merge with the solution with $C_H = 10$. The reason for the merging of solutions is not known. It also occurs with the total drag coefficient (Figure 40). We can only speculate on this behavior. At large interaction a large portion of the shock layer flow is further from the stagnation point. Because the magnetic field is reduced relative to the stagnation point, the local Hall coefficient is much lower than the reference (stagnation) value. The effective Hall coefficient may be considerably reduced. This high level of interaction is probably not obtainable in the laboratory. Also, the present theory is not valid when the onset of magnetic support occurs. It is likely that a magnetically supported shock layer will behave electrically as though an insulated body were present. This depends on the conductivity of the no-flow region and possibility of its having a breakdown voltage for arcing, all unknown factors. The phenomena of the Hall effect of large interaction flow requires study through an analysis that is valid when the magnetic forces dominate.

The Hall effect for aerodynamic-like flow is such to reduce the drag appreciably. The theory indicates that the conducting body will have a greater drag than an insulated one. The reduction of both drag and stand-off with the Hall effect suggests an effective lowering of the conductivity as

described in Chapter III

$$\sigma \text{ eff} = \sigma \frac{1}{1 + (C_H' B)^2} \tag{6-3}$$

where C_H' is the Hall coefficient per unit field strength. Levy (Ref. 4) has shown that this is not completely acceptable because of the induced electric fields. The present theory shows that it makes a difference whether the body is conducting or insulated. The fact that there is a difference shows these electric fields are important. A conducting body has a zero polar electric field. Thus an assumption such as (6-3) is probably better for a conducting body. As we have already noted from Figure 40, the drag is less when the Hall effect is important. In addition, an insulated body has a lower drag than a conducting one. Our estimates of the dimensionless groups indicate that the Hall coefficient is less than one for low interaction parameter flow ($S < 10$). It is probably reasonable to neglect the Hall effect under this condition. However, larger values are obtainable under some conditions. This is the case with the experimental work with which the theory is compared later in the chapter.

The Hall effect tends to increase the magnetic interaction required for the critical condition associated with magnetic support. However, the results shown in Figure 41 indicate that the magnetic support may still occur. In the case of a conducting body, the interaction parameter is not altered greatly at the shock with the Hall effect. This may make a conducting body easier to treat by approximate theoretical means.

The rolling moment coefficient, due to a Lorentz force in the azimuthal direction is shown in Figure 42. The reversal of the Hall currents for an insulated body has a cancelling effect on the integrated values of $(\underset{\sim}{J} \times \underset{\sim}{B})_{\varphi}$. In the case of the conducting body, these currents are in the φ direction (Figure 37) where for an insulated body they are in the $-\varphi$ direction near the body and in the φ direction near the shock. The field is greater near the body and so the $-\varphi$ currents contribute more. Because, the integrated forces are opposite in sense, the rolling moment that occurs as a result of the torque of the forces is opposite for the two types of bodies.

A reversal of polarity of the magnetic field would cause the torque to reverse in sign.

The large rolling moment coefficient for a conducting body with $C_H = 10$ is apparent in Figure 42. A Hall coefficient of this order is expected under some flight and laboratory conditions. Later, we shall present estimates of the torque predicted.

The conducting body appears to have a larger moment because of the uniform sense of $(\underset{\sim}{J} \times \underset{\sim}{B})_{\varphi}$, as noted above. While the rolling moment coefficient reaches a maximum as a function of S, we once more point out that one would normally not operate along a curve of constant Hall coefficient. The effect is greater, for a conducting body, with larger ϵ . This is traced to the larger interaction volume of large ϵ flow (larger stand-off distance) when all other quantities are kept the same.

In the case of an insulated body there is a cross-over point as to the dependence on ϵ . This is probably due to the nature of the cancelling of the $(\underset{\sim}{J} \times \underset{\sim}{B})_{\varphi}$ forces described above.

We can summarize the comparison of the insulated and conducting bodies by saying the Hall effect is stronger for an insulated body. Because the Hall effect reduces the MHD effect, the conducting body will have a greater shock stand-off, drag and, probably, less heat transfer than the comparable insulated body. These considerations indicate that a conducting body is preferable for utilizing the MHD effect.

6.6 Summary

The numerical results indicate that it is necessary to include viscosity in the analysis only for small interaction unless, of course, one is interested in phenomena at the wall such as heat transfer which was not studied in the present investigation. Even for moderate interaction parameter as low as 50 the viscous solution appears to be almost completely merged into the inviscid one (Figures 27-29). This was explained physically on the basis of a developed boundary layer (Figure 30) and the influence of the Hartmann number.

Under flight conditions, the Reynolds number is quite high (Table 3) and so it seems reasonable to neglect viscosity entirely. In the laboratory, where the Reynolds number is low, it is necessary to include the viscous effect at least for the flow without MHD interaction. If one used the inviscid theory to predict per cent increase in drag one would predict too high

of an increase because the non-MHD drag would have been predicted too low.

This suggests an approximate way to predict the drag. The viscous effect should be included for the non-MHD flow but neglected for $S > 0$. There will be some error for small S but the difficulties associated with the viscous MHD solution are eliminated. Consider a plot of drag versus interaction parameter as sketched in Figure 43. Near $S = 0$, the MHD interaction is neglected and so the horizontal line shows no increase. For moderate and large interaction parameter the inviscid theory is used. Under flight conditions, only the inviscid theory is necessary.

The results indicate that it is entirely realistic to neglect magnetic field deformation at least for unseeded flows with $Rem \leq .1$. Thus, one can set $Rem = 0$ and use the undeformed magnetic field pattern as a known function. The deformation due to interaction (Figure 33) is less than the usual difference in actual field patterns and ideal ones such as a dipole (see Reference 33 for an example of the latter). Thus, it would be more desirable to use an actual field pattern than to include deformation of an ideal field. Use of actual field patterns may or may not be feasible depending on the type of analysis.

The Hall effect has an appreciable effect on the solution (Figures 39 and 40) and should be included for good results. The effect is to reduce the shock stand-off, drag, etc. The reduction is greater for an insulated body. Thus, a conducting body has a larger drag, shock stand-off, etc. The Hall effect introduces a rolling moment which is stronger for a conducting body.

6.7 Prospects for Magnetoaerodynamics

The numerical data allows one to evaluate the possible application of the MHD effect for entry vehicles at least within the scope of the present theory for aerodynamic-like flows.

The total drag coefficient without MHD effect is about unity for high speed flight with $\epsilon = 1/20$ (Figure 21). According to Figure 40, the total drag is increased 100% for an interaction parameter of 10^3 and increased 250% for S = 4000. Slightly beyond, magnetic support is apparently in onset. Thus, 250% increase in drag is about maximum for flight with an attached shock layer. Figure 13 shows the interaction parameter for 10,000 gauss and we use this data to see what stagnation point field is required for the forementioned increase in drag.

At 250 kilofeet, a value of 6300 gauss is indicated for the 250% increase in drag and the onset of magnetic support. A 100% increase in drag would occur at half that strength.

At 200 kilofeet, 20,000 gauss is required for the 250% increase and half for the 100% increase in drag.

At 150 kilofeet, the requirement increases to 90,000 gauss for a 250% increase in drag.

These figures were based on Mach 20 and a Hall coefficient of 10. Higher Mach numbers and lower Hall coefficients would reduce the required fields. It is apparent that very large field strengths are required at the lower altitudes. However, one should be able to produce an appreciable effect above 200 kilofeet with 5 to 10 kilogauss. The increase in drag

at high altitudes would be welcome for entry control.

Let us consider the torque produced by the Hall effect on a conducting body. The rolling moment coefficient is shown in Figure 42. For $\epsilon = 1/20$ and $C_H = 10$, the coefficient is about .5 for an interaction parameter greater than 100. The controlling factor is the Hall coefficient but previous calculations show this parameter is obtainable as well as the interaction parameter of 100 or so. The actual torque would be

$$\text{Torque} = .5\, q_\infty\, \pi R_b^2 \cdot R_b$$

At 250 kilofeet and Mach 30 the torque is about 45,000 ft - lb_f for a 10 ft radius body.

The direction of the torque could be reversed by reversing the polarity of the magnetic field providing the vehicle with roll control as well as drag. Unmanned vehicles such as ballistic missiles could use the resulting spin for stabilization. However, it may be an undesirable effect for manned vehicles as in the case of Gemini 8. It may be possible to mount the magnet on bearings so that the torque is not transmitted to the body proper except by viscous stress of the rotating fluid. The magnet would then spin free of the rest of the vehicle. S. Kranc, of this laboratory, has suggested placing a conductor near the rotating magnet so that the relative motion would result in field lines being cut and power produced in a homo-polar electric generator (Ref. 75). The power from the generator might be used to power the magnet, auxiliary equipment

for long range communications of deep space probes or electronic warfare with ballistic missiles.

At 3600 rpm and 90% efficiency, the 45,000 ft - lb_f would produce

$$45{,}000 \times \frac{3600}{60} \times 2\pi \times \frac{1}{737} \times .9$$

or about 20 kilowatts of power. The principal requirement for the torque is in the Hall coefficient since the torque is relatively constant for $S > 100$, as shown in Figure 42. In order to produce the Hall coefficient used in the example, one would need about 2,000 gauss at Mach 30 and 250 kilofeet or 20,000 gauss at Mach 20 and 150 kilofeet. Thus the torque feature appears about as feasible as the drag effect.

The present theory did not account for a spinning magnetic source. There will be an additional electric field induced in the fluid due to the relative rotation (just as in the homo-polar generator). This should oppose the Hall currents and reduce the effect to some degree. The amount depends on how fast the magnet rotates relative to the fluid. The system would essentially be "loaded" and as in the case of MHD power generators, one must consider the characteristics of the external load to which the fluid magnetic system is coupled. This is beyond the scope of the present investigation.

It appears as though the prospects for magnetoaerodynamics are good and warrant further investigation.

6.8 Comparison with Experiment

In Section 5.2, we showed good agreement between the present theory and experiment for the non-MHD problem. The experimental data was for air at high Reynolds number as obtained in conventional wind tunnels where there is no problem of an incipient merged layer and so the data shown in Figures 20 and 21 tend to verify only the general approach and not the neglect of the merged layer.

Below 250 kilofeet of altitude, the merged layer is not present either and so the experiments seem to justify the application of the theory for flight. Unfortunately, the MHD effect must be tested in an adverse environment. Conventional wind tunnels do not provide the enthalpy to produce appreciable electrical conductivity and magnetic interaction parameter. Shock tubes do not provide the test time for force measurements.

The experimental group of the Gas Dynamics Laboratory has employed their thermal arc plasma facility to study the phenomena in a high total-enthalpic, supersonic environment. The facility is described in Reference 33. Argon is arc heated and expanded to supersonic speeds and low pressure provided by a vacuum tank and pump system. Shock stand-off distance is measured photo-optically by means of windows in the tank and the photographs are analyzed with a microdensitometer. Such a trace of measured intensity is shown in Figure 44 (Ref. 33). The operating conditions are given in the appendix. The Reynolds number is quite low and the shock thickness quite high as estimated in Chapter II. Thus there is a considerable difficulty in locating the shock boundaries. Further, the intensity is believed to be largely stimulated by electrons affected forward of the shock. However, the theoretical position of the shock, assumed infinitesimal in thickness, is shown in Figure 44 to be

in the region of increase in intensity which one would normally suspect to be associated with the shock front.

The location of the shock front can be determined by various graphical techniques and when per cent increase in shock stand-off is considered, much of the difference in the techniques seems to be cancelled out. The data of Figure 45 (Ref. 33) shows a comparison between theory and experiment on this basis. The theory is quite high as compared with experiment. Part of this must be attributed to the theory which does not include a thick shock and an incipient merged layer but part is probably also due to the use of photographic intensity as a measure of the shock front as mentioned above. Spectroscopic diagnostics, in progress by the experimental group, should help deliniate the shock structure. Finally, direct measurement of quantities appearing in the dimensionless groups or used in their evaluation should be an improvement over the estimates used here. The appendix describes the method used here.

Theoretical and experimental values of drag are shown in Figure 46. The viscous theory seems to give best results here. The theory seems to be low by a fairly constant amount which suggests that perhaps our estimates of the dynamic pressure for the flow conditions were low (Appendix). We estimate that non-equilibrium can alter the dynamic pressure by about 25%. In Figure 47, we show the per cent increase in drag which eliminates this dependence. In this case the agreement is much better and shows the theory including the Hall effect (but neglecting viscosity) to be superior to the viscous theory (neglecting the Hall effect). The excellent agreement with the Hall effect theory is probably fortuitous because at low interaction parameter the viscous

effects are theoretically important (Section 7.1). The influence of non-equilibrium and non-uniformity of the flow make it difficult to accurately estimate the interaction parameter. Recent diagnostics show that our estimate of S is low. If one uses these diagnostics, there is better agreement with the viscous theory and values even fall below it at high interaction showing the influence of the Hall effect. The diagnostics of S are in a preliminary stage and so are not reported here.

The simple theory using the first approximation for the MHD drag Eq. (5-17) and neglecting the Hall effect, viscosity and pressure alteration is shown to give high results in Figure 47 as expected. At very large magnetic interaction one might subtract off the viscous and pressure drags owing to their theoretical reduction. One would use Eq. (5-17) or an improved relation similar to it for a better estimate of the drag by simple means. The pressure and viscous drags would be neglected at high interaction parameter. Current experiments are at not high enough interaction parameter to verify this suggestion, however.

NOMENCLATURE

A	collision cross-section
B	magnetic field intensity
C_D	drag coefficient - drag/$q_\infty \pi R_b^2$
C_i	ion slip coefficient
C_F	skin friction coefficient
C_H	Hall coefficient
C_l	rolling moment coefficient - torque/$q_\infty \pi R_b^3$
C_p	pressure coefficient
$\mathcal{C}$	fraction for magnetic field reduction
D	diameter
E	electric field intensity
e	electron charge
ϵ	permitivity
F	velocity function
f	inverse velocity function
F_i	dependent first order variable i
f_i	dF_i/dx
G	azimuthal velocity function
g	inverse azimuthal velocity function
H	electric field function
h	inverse electric field function

J current density

K Hall current function

k inverse Hall current function

L azimuthal current function

ℓ inverse azimuthal current function

M molecular weight, Mach number, magnetic field function

m inverse magnetic field function

N azimuthal magnetic field function

n inverse azimuthal magnetic function, polytropic exponent and number density

p pressure

q_∞ dynamic pressure $\rho_\infty V_\infty^2/2$

R radius, gas constant

r radial coordinate

Re Reynolds number $-\rho_\infty V_\infty R_b/\eta_1$

Re_s shock Reynolds number $-\rho_\infty V_\infty R_s/\eta_1$

Rem magnetic Reynolds number $-\mu \sigma_1 \epsilon V_\infty R_b$

Rem_s shock magnetic Reynolds number $-\mu \epsilon \sigma_1 V_\infty R_s$

S interaction parameter $-\sigma_1 B_o^2 R_b/\rho_\infty V_\infty$

S_s shock interaction parameter $-\sigma_1 B_s^2 R_s/\rho_\infty V_\infty$

T absolute temperature

t time

V velocity

$\mathcal{V}$ volume

x	r/R_b
x_s	R_s/R_b
y	r/R_s
y_b	R_b/R_s

Greek

α degree of ionization

γ specific heat ratio, gamma based on speed of sound

δ dimensionless shock stand-off distance $(R_s - R_b)/R_b$

Δ absolute shock stand-off distance $R_s - R_b$

Δ_s plasma sheath thickness

Δ_{bl} boundary layer thickness

β magnetic pressure number $B_o^2/\mu \rho_\infty V_\infty^2$

ϵ shock density ratio ρ_∞/ρ_1

λ mean free path

ρ density

ρ_e excess charge density

η viscosity

ν kinematic viscosity

ψ_B flux function (constant for a flux line)

ψ_J current function (constant for current path line)

ψ_V stream function (constant for stream line)

Φ electric potential

θ polar coordinate

φ	azimuthal coordinate	
τ	collision time	
ω	cyclotron frequency eB/m	
ξ	dimensionless distance	$(x-1)/\delta$
σ	electrical conductivity	

SUBSCRIPTS

1	shock layer (behind a normal shock)
∞	free stream
b	body
B	base
e	electron
b.l.	boundary layer
F	friction
i	species i
MHD	magnetohydrodynamic
r	radial
s	shock
p	pressure
o	stagnation point
θ	polar
φ	azimuthal

APPENDIX

ESTIMATES OF LABORATORY CONDITIONS

Consider a comparison between theory and experiment. It is necessary to determine the dimensionless groups S, ϵ, etc. Conditions may be specified as follows:

Argon plasma (arc generated)

p_∞ = .00041 atmospheres

M_∞ = 2.75

$\dot{m}$ = .165 lbm/min (flow rate)

$\dot{P}$ = 960 amp at 25 v = 24 kw (gross power)

The charts of this report allow one to estimate the dimensionless groups as a function of p_∞, M_∞ and T_∞ and so we must estimate the latter. We regard the latter to be the gas temperature.

Assume that an energy balance showed that the net power to the gas was 11 kw (46% efficiency). The stagnation enthalpy would be

$$h_o = \frac{11 \text{ kw}}{.165 \text{ lbm/min}} = 3700 \text{ Btu/lbm}$$

We assume equilibrium in the arc chamber and one atmosphere pressure there and use the data h(T,p) of Arave and Huseley (Ref. 44) to find

$$T_o = 10{,}900 \ ^oK$$

The ratio of T_o/T_∞ is approximated by the familiar formula

$$T_o/T_\infty = 1 + \frac{\gamma - 1}{2} M^2_\infty \qquad \text{(A-1)}$$

The value of γ for the arc chamber is 1.2 (equilibrium) and for the expanded flow would be near 1.67 if equilibrium were maintained. We use the intermediate value of 1.4 and find

$$T_\infty = 4400\ ^oK$$

Thus, p_∞, T_∞, and M_∞ have been specified. From Figure 10

$$\epsilon = 1/5 \qquad \text{(A-2)}$$

and from Figure 12

$$Re = 0(100) \qquad \text{(A-3)}$$

The interaction parameter for 10,000 gauss and a 1 inch radius body is 350 (Figure 14). The actual interaction parameter is

$$S = 350\ (B_o/10^4\ \text{gauss})^2\ \ (R_b/1\ \text{inch}) \qquad \text{(A-4)}$$

The magnetic Reynolds number is less than .1 (Figure 16) and according to Section 6.6 we set Rem = 0.

$$Rem = 0 \qquad \text{(A-5)}$$

The Hall coefficient, given by Figure 18, is

$$C_H = 10\ (B_o/10^4\ \text{gauss}) \qquad \text{(A-6)}$$

The dimensionless parameters are now given by (A-2) to (A-6) and they can be used to obtain the theoretical results.

For the non-MHD case we include viscosity and find (Figure 27)

$$\delta = \frac{\Delta}{R_b} = .175 \qquad (B_o = 0) \tag{A-7}$$

From Figure 29 we find the total drag to be

$$C_D = 1.48 \qquad (B_o = 0) \tag{A-8}$$

(A-7) can be multiplied by the body radius to give the actual stand-off. To get the actual drag

$$\begin{aligned} \text{Drag} &= \pi R_b^2 \; q_\infty \; C_D \\ &= \pi R_b^2 \; \frac{\rho_\infty V_\infty^2}{2} \; C_D \\ &= \pi R_b^2 \; \gamma_\infty \frac{P_\infty M_\infty^2}{2} \; C_D \end{aligned} \tag{A-9}$$

And for a 3/4 inch radius body

$$\text{Drag} = 30.6 \; C_D \quad \text{(grams force)} \tag{A-10}$$

Equation (A-10) can be used with (A-8) to find

$$\text{Drag} = 45.2 \text{ grams force} \qquad (B_o = 0)$$

Equation (A-9) can also be used for the MHD case where the appropriate drag coefficient is used.

At low interaction parameter ($S < 50$) one should use the viscous theory for shock stand-off and drag (Figures 27 and 29).

At high interaction parameter, one should use the calculations including the Hall effect (Figures 39 and 40).

It may be desirable to consider both especially with moderate interaction parameter. If known values of the quantities estimated are available they should be used. For example, a measured value of electrical conductivity could be used in place of the equilibrium one inferred in Figure 14.

BLOCK DIAGRAMS FOR THE COMPUTER PROGRAMS

There are three programs for the viscous, magnetic Reynolds number and Hall effects, respectively. The case where none of these effects is included can be obtained by using either of the last two programs in which case no iteration is required.

Input data generally consists of the appropriate dimensionless groups, initial guesses of boundary conditions, specification of the initial fractional step of the initial guesses, a minimum step or tolerance as a fraction, maximum number of iterations, etc.

The programs integrate the differential equations using the initial conditions and a Runge-Kutta subroutine with variable integration step and an error control of 10^{-10} and 10^{-4}% on the solution functions. The RMS error in the second point boundary conditions are calculated. If this is within 1% and the step of the initial conditions have been varied according to the specified tolerance, the solution is complete and the functions and the flow observables (magnetoaerodynamic coefficients, shock stand-off, etc.) are printed out. If not, the initial conditions are varied so as to make the RMS error a minimum. If the error increases for a given step, a step of half the interval is made of opposite sense and these steps are repeated until the error again increases upon which the process is repeated until the RMS error and initial condition tolerance are acceptable. At each step, the observables are printed out in order to determine convergence by observation. In the case of the viscous program, two such initial conditions must be varied and this

is done by minimizing with respect to one for each step of the other.

In the case of the magnetic Reynolds number program the values of

$$Rem_s^{(i)} = Rem\ (1 + \delta^{(i-1)})$$

are repeated until $Rem^{(i)}$ is within a tolerance and the error is acceptable. The value of $\delta^{(o)}$ is taken as zero.

BLOCK DIAGRAM FOR VISCOUS EFFECTS PROGRAM

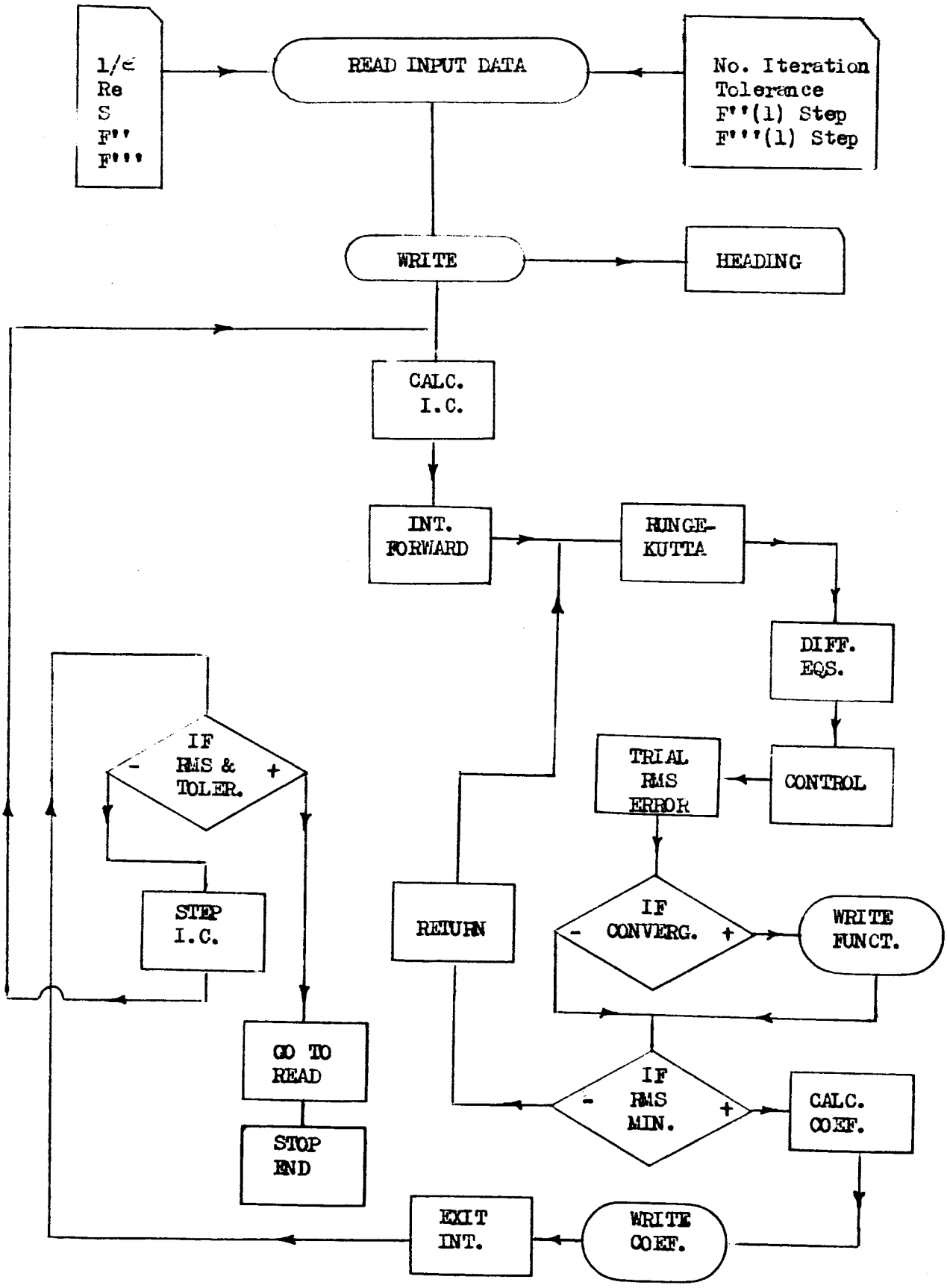

BLOCK DIAGRAM FOR Rem PROGRAM

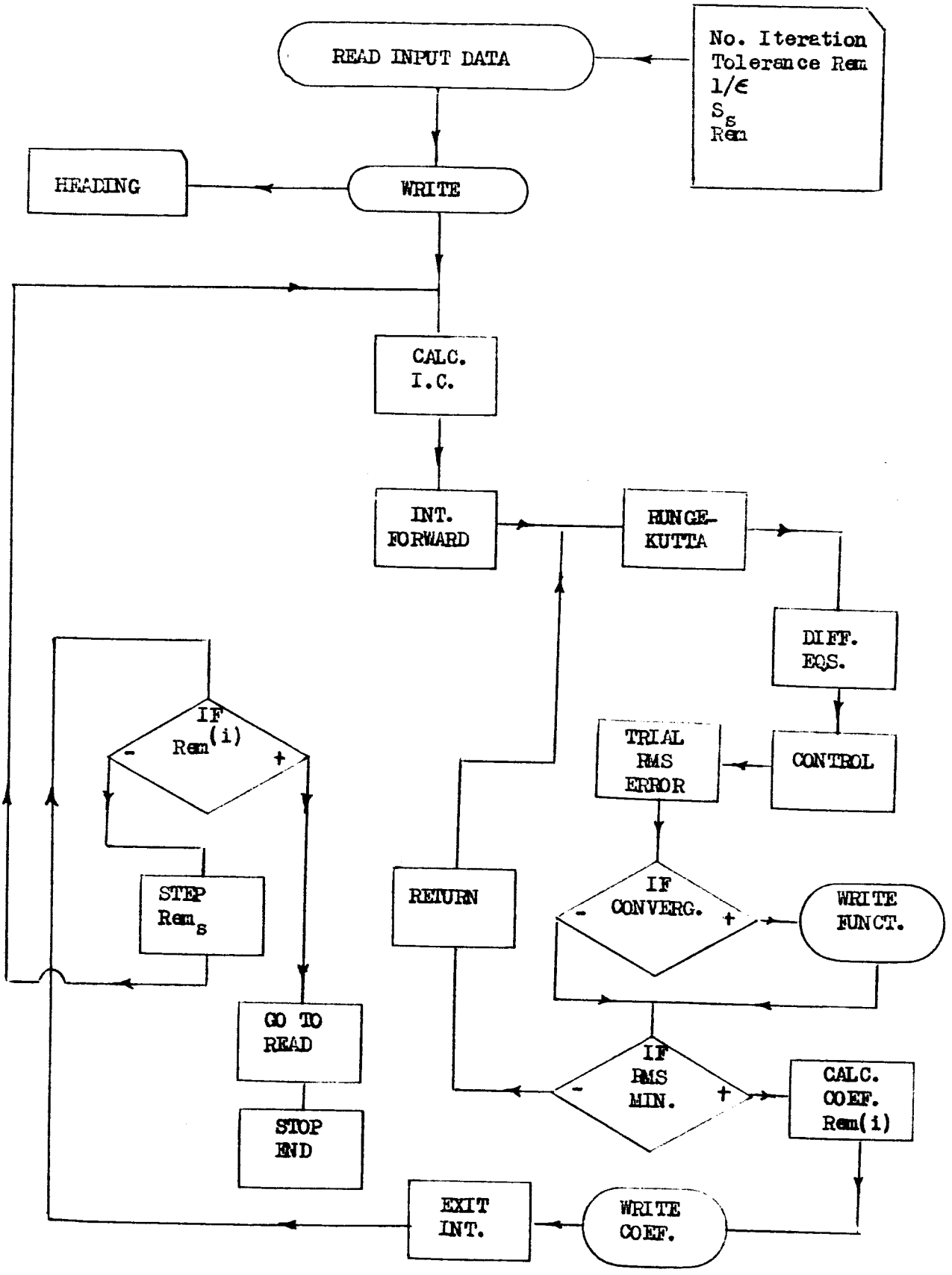

BLOCK DIAGRAM FOR HALL EFFECT PROGRAM

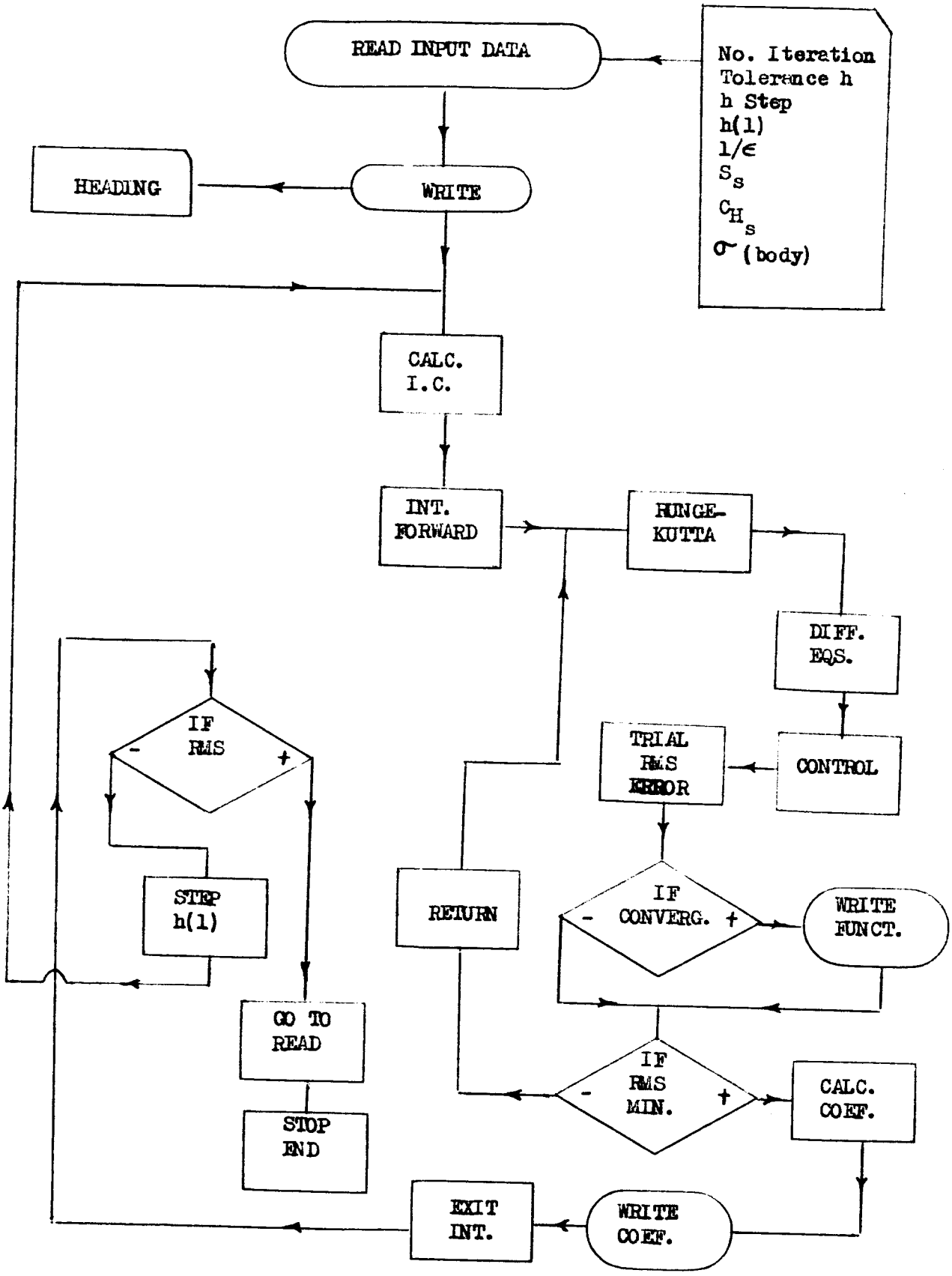

B I B L I O G R A P H Y

1. Kantrowitz, A. R., "A Survey of Physical Phenomena Occurring in Flight at Extreme Speeds", Proceedings of the Conference on High Speed Aeronautics, p. 335, Edited by A. Ferri, N. J. Hoff and P. A. Libby, Polytechnic Institute of Brooklyn, 1955.

2. Resler, E. L., Jr., and W. R. Sears, "The Prospects of Magnetoaerodynamics", Journal of Aeronautical Sciences,26, p. 235, April, 1958.

3. Wood, G. P., "The Electric Drag Forces on a Satellite in Earth's Upper Atmosphere", Proceedings of the NASA -University Conference on the Science and Technology of Space Exploration, 2, p. 337, NASA SP-11, November, 1962.

4. Levy, R. H., "A Simple MHD Flow with Hall Effect", AIAA Journal, 1, p. 698-699, March, 1963.

5. Bush, W. B., "Magnetohydrodynamic - Hypersonic Flow Past a Blunt Body", Journal of the Aero/Space Sciences, 25, p. 685-690, 728, November, 1958.

6. Bush, W. B., "A Note of Magnetohydrodynamic Hypersonic Flow Past a Blunt Body", Journal of the Aero/Space Sciences, 26, p. 536-537, August, 1959.

7. Kemp, N. H., "On Hypersonic Blunt Body Flows with a Magnetic Field", Journal of the Aero/Space Sciences, 25, p. 405-407, June, 1958.

8. Lighthill, M. J., "Dynamics of a Dissociating Gas, Part I, Equilibrium Flow", Journal of Fluid Mechanics, 2, p. 28-31, January, 1957.

9. Freeman, N. C., "On the Flow Past a Sphere at Hypersonic Speed with a Magnetic Field", Journal of the Aero/Space Sciences, 26, p.670-672, Oct., 1959.

10. Lighthill, M. J., "A Technique for Rendering Approximate Solutions for Physical Problems Uniformly Valid", Philosophical Magazine, 40, p. 1179-1201, December, 1949.

11. Kemp, N. H., "Author's Reply", Journal of the Aero/Space Sciences, 26, p. 672, October, 1959.

12. Meyer, R. C., "Magnetohydrodynamics and Aerodynamic Heating", ARS Journal, 29, p. 187-192, March, 1959.

B I B L I O G R A P H Y

13. Ladyskenskii, M. D., "Flow Problems in Magnetohydrodynamics", Journal of Applied Mathematics and Mechanics, 23, p. 419-427, February, 1959.

14. Ladyskenskii, M. D., "Hypersonic Flow Past a Body in Magnetohydrodynamics", Journal of Applied Mathematics and Mechanics, 23, p. 1427-1443, May, 1959.

15. Yen, K. T., "Incompressible Wedge Flows of an Electrically Conducting Viscous Fluid in the Presence of a Magnetic Field", Journal of the Aero/-Space Sciences, 27, p.74-75, January, 1960.

16. Ludford, G.S.S., and J. D. Murray, "On the Flow of a Conducting Fluid Past a Magnetized Sphere", Journal of Fluid Mechanics, 7, B, p. 516-528, 1960.

17. Wu, C. S., "Hypersonic Viscous Flow Near the Stagnation Point in the Presence of a Magnetic Field", Journal of the Aero/Space Sciences, 27, p. 882-893, 950, December, 1960.

18. Meyer, R. X., "MHD and Its Application to Propulsion and Re-entry", Xth Internati onal Astronautical Congress, Vol. 1, Springer-Verlog, Wein, p. 33-41, 1960.

19. Lykoudis, P. S., "The Newtonian Approximation in Magnetic Hypersonic Stagnation Point Flow", Journal of the Aero/Space Sciences, 28, p. 541-546, July, 1960.

20. Lykoudis, P. S., "The Matching of the Viscid and Inviscid Regions for the Stagnation Magnetic Flow", Journal of the Aero/Space Sciences, 26, p.315-317, May, 1959.

21. Pai, S. I., and E. T. Kornowski, "Stagnation Point Flow of Magnetized Blunt Body in Hypersonic Flow", Engineering Aspects of Magnetohydrodynamics, Edited by C. Mannal and N. Mathur, Columbia University Press, New York 1962.

22. Andrade, C. A., "Magnetogasdynamic Shock Layer Flow", Engineering Aspects of Magnetohydrodynamics, Edited by C. Mannal and N. Mathur, Columbia University Press, New York, 1962.

23. Power, G. and A. Turnbridge, "Flow of a Conducting Liquid Past a Magnetized Cylinder", Applied Scientific Research Journal, 9, B, p. 383-392, 1962.

24. Levy, R. H. and H. E. Petschek, "Magnetohydrodynamically Supported Hypersonic Shock Layers", The Physics of Fluids, 6, p. 946-961, July, 1963.

B I B L I O G R A P H Y

25. Locke, E., Petshek, H. E., and P. H. Rose, "Experiments with Magnetically Supported Shock Layers", NASA CR-58823, August, 1964.

26. Smith, M. C. and C. S. Wu, "Magnetohydrodynamic Hypersonic Viscous Flow Past a Blunt Body", AIAA Journal, 2, p. 963-965, May, 1964.

27. Ericson, W. B., and A. Maciulaitus, "Investigation of Magnetohydrodynamic Flight Control", Journal of Spacecraft and Rockets, 1, p. 283-289, May, 1964.

28. Levy, R. H., Gierasch, P. J. and D. B. Henderson, "Hypersonic Magnetohydrodynamics with or without a Blunt Body", AIAA Journal, 2, p. 2091-2099, December, 1964.

29. Smith, M. C., Schwimmer, H. S., and C. S. Wu, "Magnetohydrodynamic-Viscous and Inviscid Flow Near the Stagnation Point of a Blunt Body", AIAA Journal, 3, p. 1365-1367, July, 1965.

30. Bass, R. R., and T.P. Anderson, "Lorentz Drag: An Engineering Approximation", Journal of Spacecraft, 2, p. 810-812, September-October, 1965.

31. Seemann, G. R., "Experimental Aspects of Magnetoaerodynamic Drag", Ph.D. Dissertation in Mechanical Engineering and Astronautical Sciences, Northwestern University, Evanston, August, 1963.

32. Seemann, G. R., and A. B. Cambel, "Observations Concerning Magnetoaerodynamic Drag and Shock Stand-off Distance", Proceedings of the National Academy of Sciences, 55, p. 457-465, March, 1966.

33. Nowak, R. J., Kranc, S., Porter, R. W., Yuen, M. C., and A. B. Cambel, "Magnetoaerodynamic Re-Entry", AIAA paper, 66-161, March, 1966.

34. Wood, G. P., "The Electric Drag Forces on a Satellite in the Earth's Upper Atmosphere", Proceedings of the NASA University Conference on the Science and Technology of Space Exploration, Vol. 2, NASA SP-11, p. 337, November, 1962.

35. Hayes, W. D., and R. F. Probstein, Hypersonic Flow Theory, Academic Press, New York, 1959.

36. Stollery, J. L., "Real Gas Effects on Shock Tube Performance at High Shock Strength", Royal Aircraft Establishment Technical Note AERO-2413, Nov., 1957.

37. Schaaf, S. A. and P. L. Chambré, Flow of Rarefied Gases, Princeton University Press, Princeton, 1961.

B I B L I O G R A P H Y

38. Anon., Handbook of Supersonic Aerodynamics, Vol. 1, NAVORD Rept. 1488, 1950.

39. Anon., U. S. Standard Atmosphere, 1962, U. S. Committee on Extension to the Standard Atmosphere, December 1962.

40. Warfield, C. N., "Tentative Tables for the Properties of the Upper Atmosphere", NACA TN 1200, 1947.

41. Pindroh, A. L., "Transport Properties of Argon in Ionization Equilibrium", Boeing Document D2-11253, August, 1961.

42. Chapman, S. and T. G. Cowling, The Mathematical Theory of Non-Uniform Gases, Cambridge at the University Press, 1960.

43. Lochte-Holtgreven, W., "Production and Measurement of High Temperatures", Reports on Progress in Physics, 21, The Physical Society, London, 1958.

44. Arave, R. J., and O. A. Huseley, "Aerothermodynamic Properties of High Temperature Argon", Boeing Document D2-11238, February, 1962.

45. Inouye, M., "Shock Stand-Off Distance for Equilibrium Flow Around Hemispheres Obtained From Numerical Calculations", AIAA Journal, 3, p. 172-173, January, 1965.

46. Huber, P. W., "Hypersonic Shock-Heated Parameters for Velocities to 46,000 Feet per Second and Altitudes to 323,000 Feet", NASA TR R-163, 1963.

47. Schlicting, H., Boundary Layer Theory, McGraw-Hill, New York, 1960.

48. Tonks, L., "Plasma Physics", Foundations of Future Electronics, Edited by D. B. Langmuir and W. D. Hershberger, McGraw-Hill, New York, 1961.

49. Su, C. H., "Compressible Plasma Flow over a Biased Body", AIAA Journal, 3, p. 842-848, May, 1965.

50. Probstein, R. F., "Shock Wave and Flow Field Development in Hypersonic Re-Entry", ARS Journal, 31, p. 185-194, February, 1961.

51. Bortner, M. H., "Chemical Kinetics in a Re-entry Flow Field", GE Space Sciences Laboratory Report R63SD63, August, 1963.

52. Truitt, R. W., Hypersonic Aerodynamics, Ronald Press, New York, 1959.

53. Meyer, F., Kressner, W. K. H. and J. R. Steffey, "Nonequilibrium Plasma Characteristics in a Hypersonic One-Diemnsional Flow", AIAA Journal, 1, p. 1198, May, 1963.

54. Knopp, C.F., "The Spectroscopic Measurement of Temperatures in Transparent Argon Plasmas", Journal of Quantitative Spectroscopy and Radiative Transfer, 2, p. 297-299, July/September, 1962.

B I B L I O G R A P H Y

55. Keenan, J. H., and J. Kaye, Gas Tables, Wiley, New York, 1948.

56. Prandtl, L. and O. G. Tietjens, Fundamentals of Hydro- and Aeromechanics, Dover, New York, 1957.

57. Schluter, A., "Dynamik des Plasmas I, Grundgleicheigen, Plasma in Gekreuzten Feldern", Zeitschrift für Naturforshung, 5a, p. 72-78, May, 1950.

58. Spitzer, L., Jr., Physics of Fully Ionized Gases, Interscience, New Yor, 1962.

59. Cambel, A. B., Plasma Physics and Magnetohydrodynamics, McGraw-Hill, New York, 1963.

60. Sears, W. R., and E. L. Resler, Jr., "Magneto-Aerodynamic Flow Past Bodies", Advances in Applied Mechanics, p. 1-67, Academic Press, New York, 1964.

61. Cowling, T. G., Magnetohydrodynamics, Interscience, New York, 1957.

62. Demetriades, S. T. and G. S. Argyropoulis, "Ohm's Law in Multicomponent Non-Isothermal Plasmas with Temperature and Pressure Gradients", STD Research Corp., Report STD-65-12, September, 1965.

63. De Voto, R. S., "Transport Properties of Partially Ionized Monotomic Gases", AIAA paper 65-540, July, 1965.

64. Kaattari, G. E., "Shock Envelopes of Blunt Bodies at Large Angles of Attack", NASA TN D-1980, December, 1963.

65. Jackson, J. D., Classical Electrodynamics, Wiley, New York, 1962.

66. Morse, R. M. and H. Feshbach, Methods of Theoretical Physics, Part I, McGraw-Hill, New York, 1953.

67. Li, T., "Arc-Tangent Fits for Pressure and Pressure Drag Coefficients of Axisymmetric Blunt Bodies at All Speeds", Journal of Aero/Space Sciences, 27, p. 309-310, April, 1960.

68. Hoerner, S. F., Fluid-Dynamic Drag, published by the author at 148 Busteed Drive, Midland Park, N. J., 1958.

69. Hansen, C. F., "Approximations for the Thermodynamic and Transport Properties of High Temperature Air", NASA TN 4150, March, 1958.

70. Van Dyke, M., Perturbation Methods in Fluid Mechanics, Academic, New York, 1964.

B I B L I O G R A P H Y

71. Bellman, R. E., and R. E. Kalaba, Quasilinearization and Nonlinear Boundary-Value Problems, Elsevier, New York, 1965.

72. Schwarzschild, M., Structure and Evaluation of the Stars, Princeton, Princeton, N. J., 1958.

73. Kunz, K. S., Numerical Analysis, McGraw-Hill, New York, 1957.

74. Staff of the Computer Center, "RKS3 - Library No. SD 1171", NU 0027, Vogelback Computer Center, Northwestern University, Evanston, Ill., June,1965.

75. Alfven, H., Cosmical Electrodynamics, Oxford University Press, 1950.

76. Crocco, l., "A Suggestion for the Numerical Solution of the Steady Navier-Stokes Equations", AIAA Journal, 3, p. 1824-1832, October, 1965.

77. Bochavesky, I. O. and E. L. Rubin, "A Direct Method for Computation of Nonequilibrium Flows with Detached Shock Waves", AIAA Journal, 4, p. 600-607, April, 1966.

TABLE I

SURVEY OF LITERATURE

REFERENCE	M_∞	COMPRESSIBLE	Re	S	Rem	BODY	MAGNET	SOLUTION	STAND OFF	DRAG
6. BUSH 1958	$\gg 1$	NO	∞	ARB.	ARB.	STAG. PT.	DIPOLE	SIMILAR NUMERICAL	YES	NO
7. KEMP 1958	$\gg 1$	NO	∞	SMALL	0	STAG. PT.	RADIAL FIELD	EXPANSION	YES	NO
9. FREEMAN 1959	$\gg 1$	NO	∞	SMALL	0	STAG. POINT	RADIAL FIELD	EXPANSION	YES	NO
11. KEMP 1959	$\gg 1$	NO	∞	SMALL	0	STAG. PT.	RADIAL FIELD	NUMERICAL	YES	NO
20. LYKOUDIS 1959	$\gg 1$	NO	ARB.	ARB.	0	STAG. PT.	RADIAL FIELD	ANALYTICAL	NO	NO
12. R.C. MEYER 1959	$\gg 1$	NO	ARB.	ARB.	0	STAG. PT.	SIMILAR	SIMILAR NUMERICAL	NO	NO
13. LODYZHENSKII F. '59	<1	NO	∞	ARB.	∞	B. LAYER	ARB.	ANALYTICAL	NO	NO
14. LODYZHENSKII M. '59	$\gg 1$	YES	∞	ARB.	SMALL	WEDGE CONE	$\perp$ SURFACE	ANALYTICAL	ATTACHED SHOCK	NO
15. YEN. 1960	<1	NO	ARB.	ARB.	ARB.	WEDGE	SIMILAR	SIMILAR	NO	NO
16. LUDFORD 1960	<1	NO	∞	SMALL	SMALL	SPHERE	DIPOLE	EXPANSION	NO	YES
17. WU 1960	$\gg 1$	NO	ARB.	SMALL	SMALL	CYLINDER SPHERE	DIPOLE	SIMILAR	NO	NO
18. R.X.MEYER 1960	$\gg 1$	YES	∞	SMALL	SMALL	CONE	SIMILAR	SIMILAR	NO	NO
19. LYKOUDIS 1961	$\gg 1$	NO	∞	SMALL	0	STAG. PT.	CONST. FIELD	ANALYTICAL	YES	NO
21. PAI 1962	$\gg 1$	NO	∞	ARB.	ARB.	STAG. POINT	POWER LAW	SIMILAR NUMERICAL	YES	NO
22. ANDRADE 1962	> 1	YES	∞	$\gg 1$	∞	INVERSE	SIMILAR	SIMILAR	NO	NO
23. POWER 1962	<1	NO	∞	SMALL	SMALL	CYLINDER	2d DIPOLE	EXPANSION	NO	YES
24. LEVY 1963	$\gg 1$	YES	∞	ARB.	ARB.	CYLINDER	WIRE	ANALYTICAL	YES	NO
26. SMITH 1964 29. 1965	$\gg 1$	NO	ARB.	ARB.	ARB.	STAG. PT.	DIPOLE	SIMILAR NUMERICAL	YES	NO
27. ERICSON 1964	$\gg 1$	NO	∞	ARB.	ARB.	STAG. PT.	DIPOLE	NUMERICAL	BUSH	LIFT
28. LEVY 1964	$\gg 1$	YES	∞	$\gg 1$	0	WITH or WITHOUT	DIPOLE	ANALYTICAL NUMERICAL	YES	NO

TABLE 2

VARIATION OF DENSITY AND TRANSPORT COEFFICIENTS

	FLIGHT	ARGON PLASMA
	M_∞ = 24 200 kft.	M_∞ = 3.5 $p_\infty = 10^{-3}$ atm. T_∞ = 2000 ^oK
DENSITY ρ_o/ρ_1	1.03	1.16
VISCOSITY ν_o/ν_1	.972	.893
CONDUCTIVITY $\frac{\sigma_o/\sigma_1}{\rho_o/\rho_1}$		
(EQUILIBRIUM)	1.10	1.40
(FROZEN)	.995	1.01

NOTE: 1. Based on real gas and equilibrium thermodynamics except for the "frozen" conductivity where the free stream gamma was used.

2. "o" is the stagnation value and "1" the value behind a normal shock.

3. ν is kinematic viscosity η/ρ .

TABLE 3

SUMMARY OF THE RANGE OF PARAMETERS

(Equilibrium Flow)

	FLIGHT		ARGON PLASMA	
	RANGE	TYPICAL[1]	RANGE	TYPICAL[2]
ϵ	1/10 - 1/20	1/20	1/3 - 1/20	1/5
Re	10^2 - 10^7	10^3	10 - 10^3	10^2
S	10^{-2} - 10^6	10^5	10^2 - 10^3	10^2
Rem	10^{-7} - 10^{-1}	10^{-2}	10^{-5} - 10^{-1}	10^{-2}
C_H	10^{-1} - 10^4	10	10^{-2} - 10^4	10

1. Conditions: R = 10 ft., M_∞ = 30, 250 kilofeet altitude.

2. Conditions: R = 1 in., M_∞ = 3, p_∞ = 10^{-3} atm., T_∞ = 4000 ^oK.

Note: Based on 10,000 gauss stagnation point field strength.

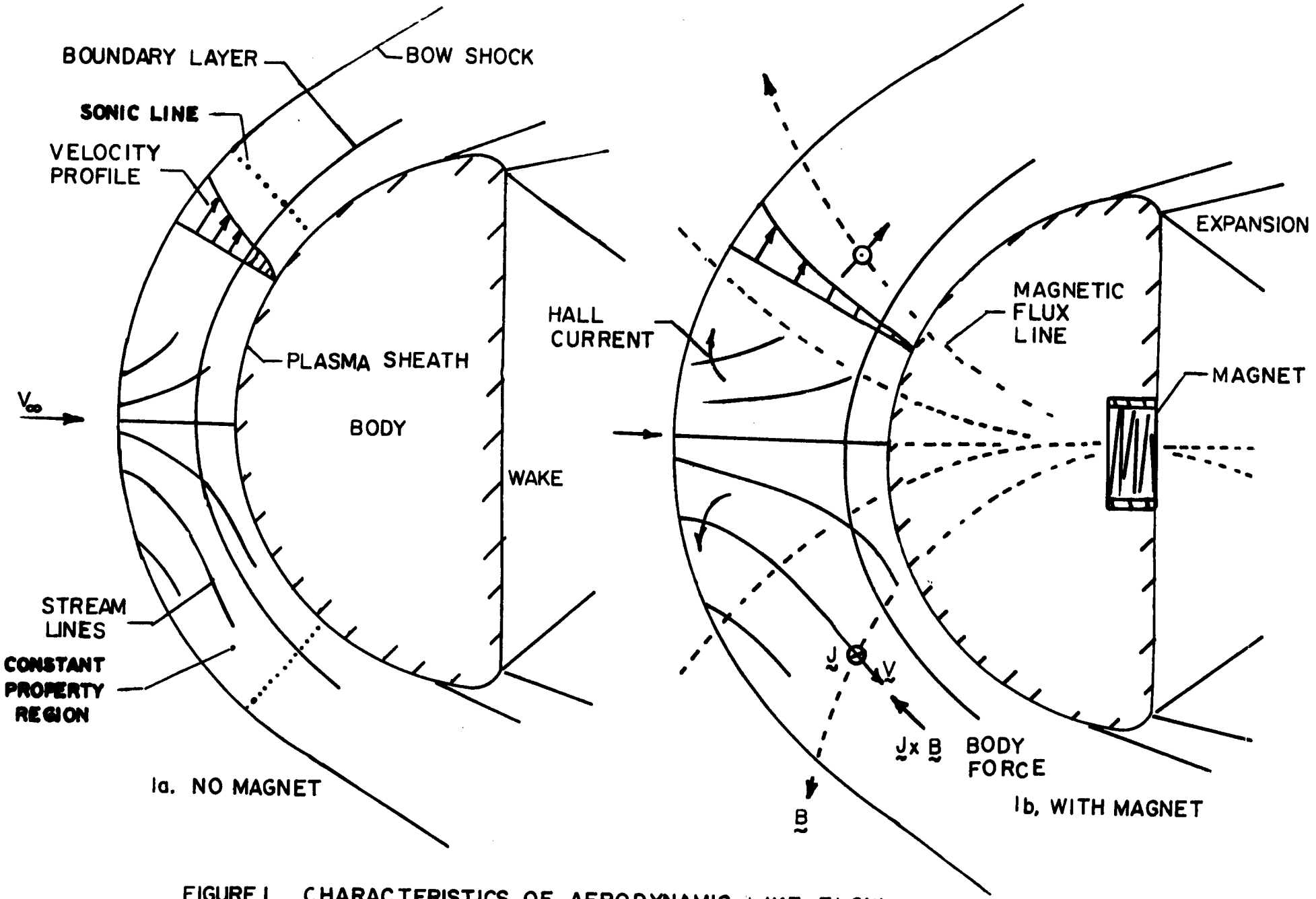

FIGURE I. CHARACTERISTICS OF AERODYNAMIC LIKE FLOW

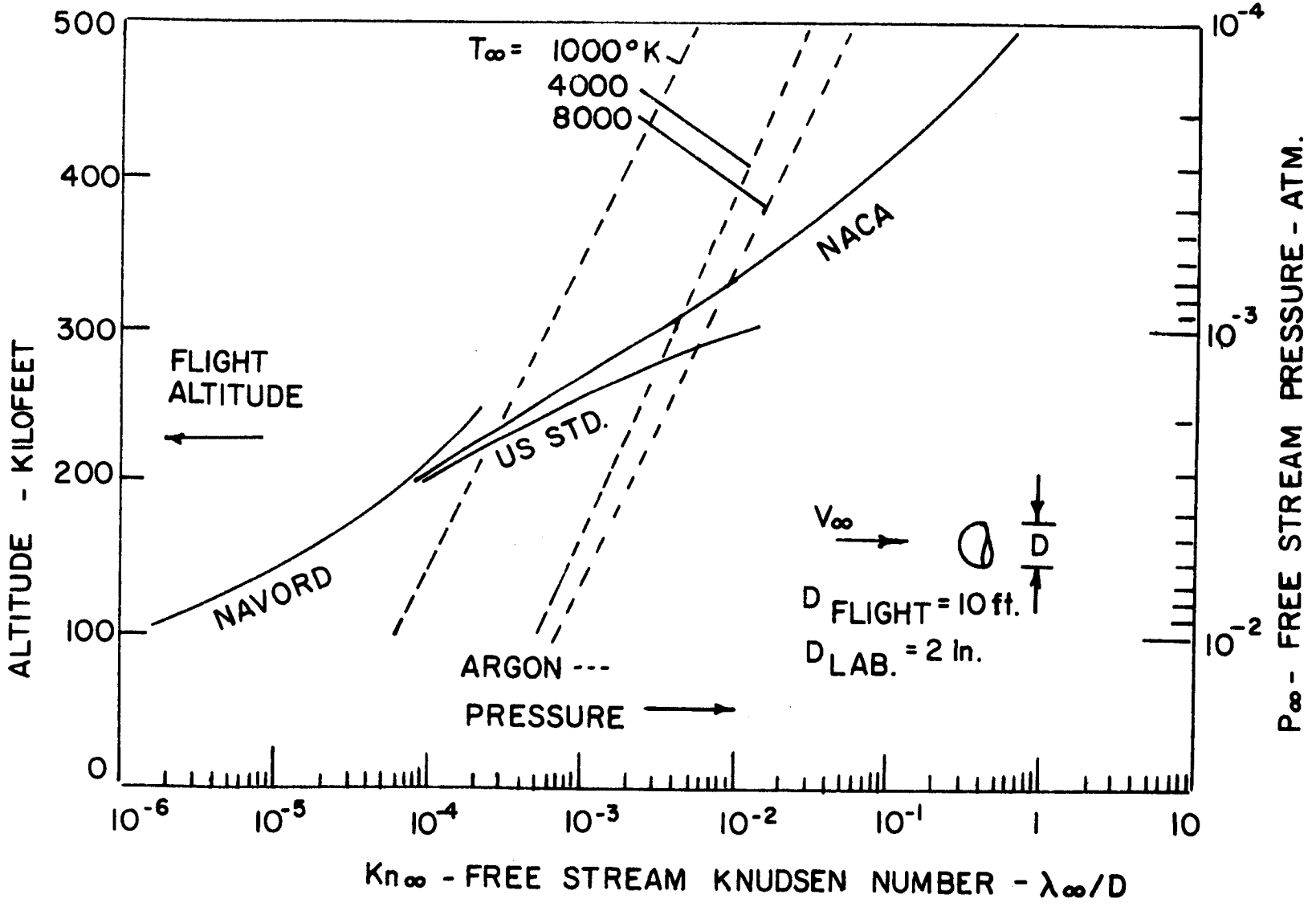

FIGURE 2. FREE STREAM KNUDSEN NUMBERS

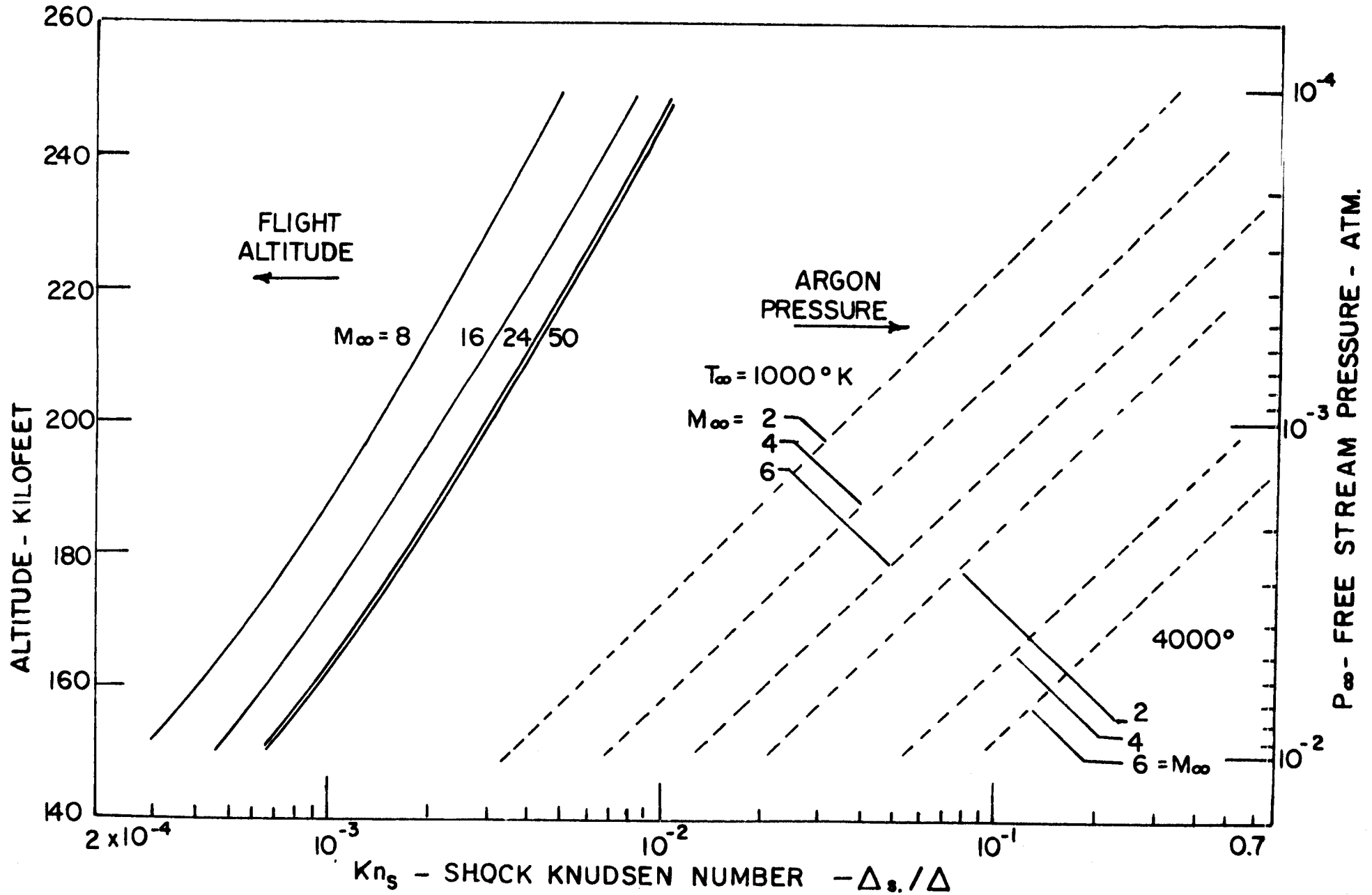

FIGURE 3. SHOCK KNUDSEN NUMBERS

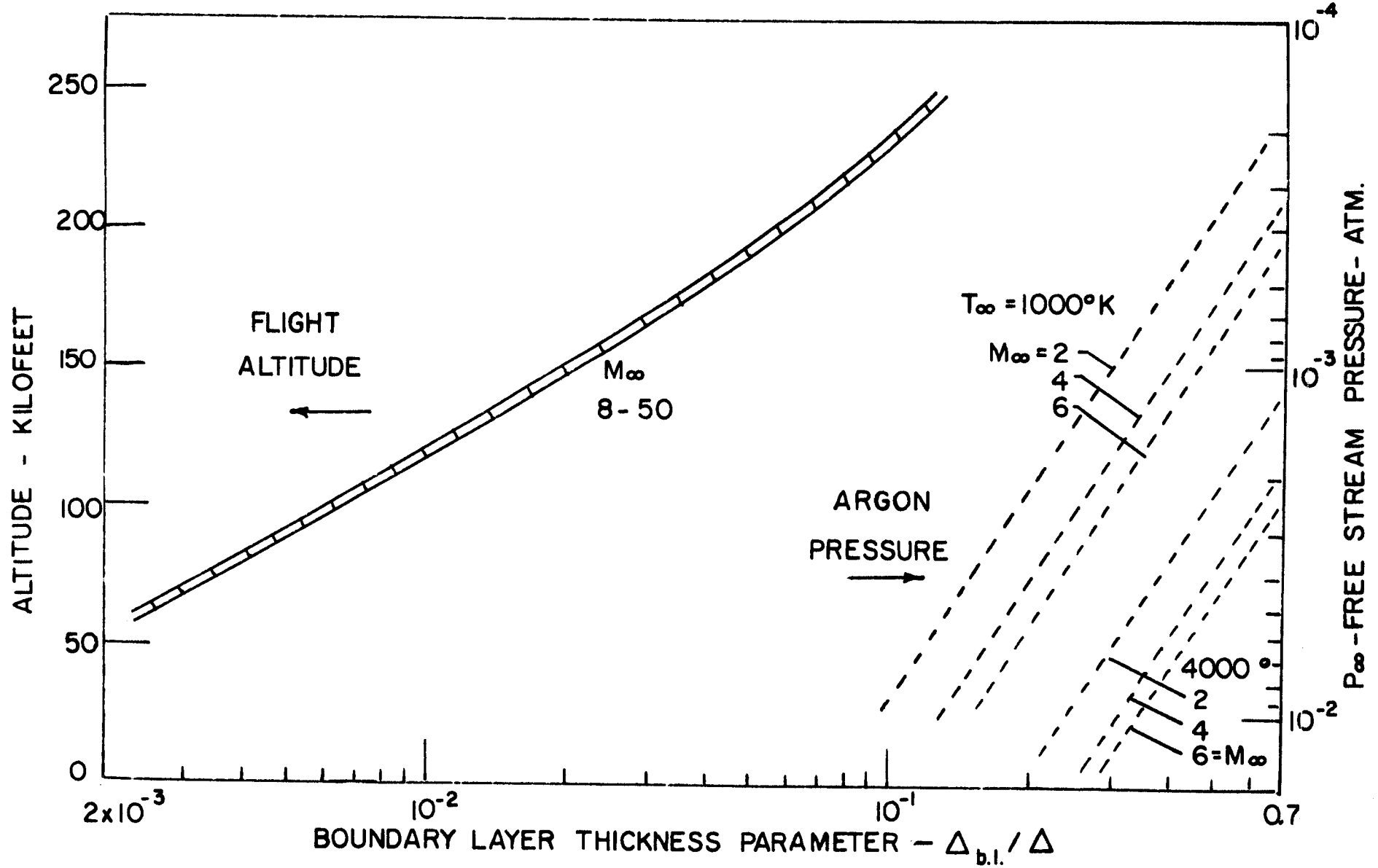

FIGURE 4. BOUNDARY LAYER THICKNESS PARAMETERS

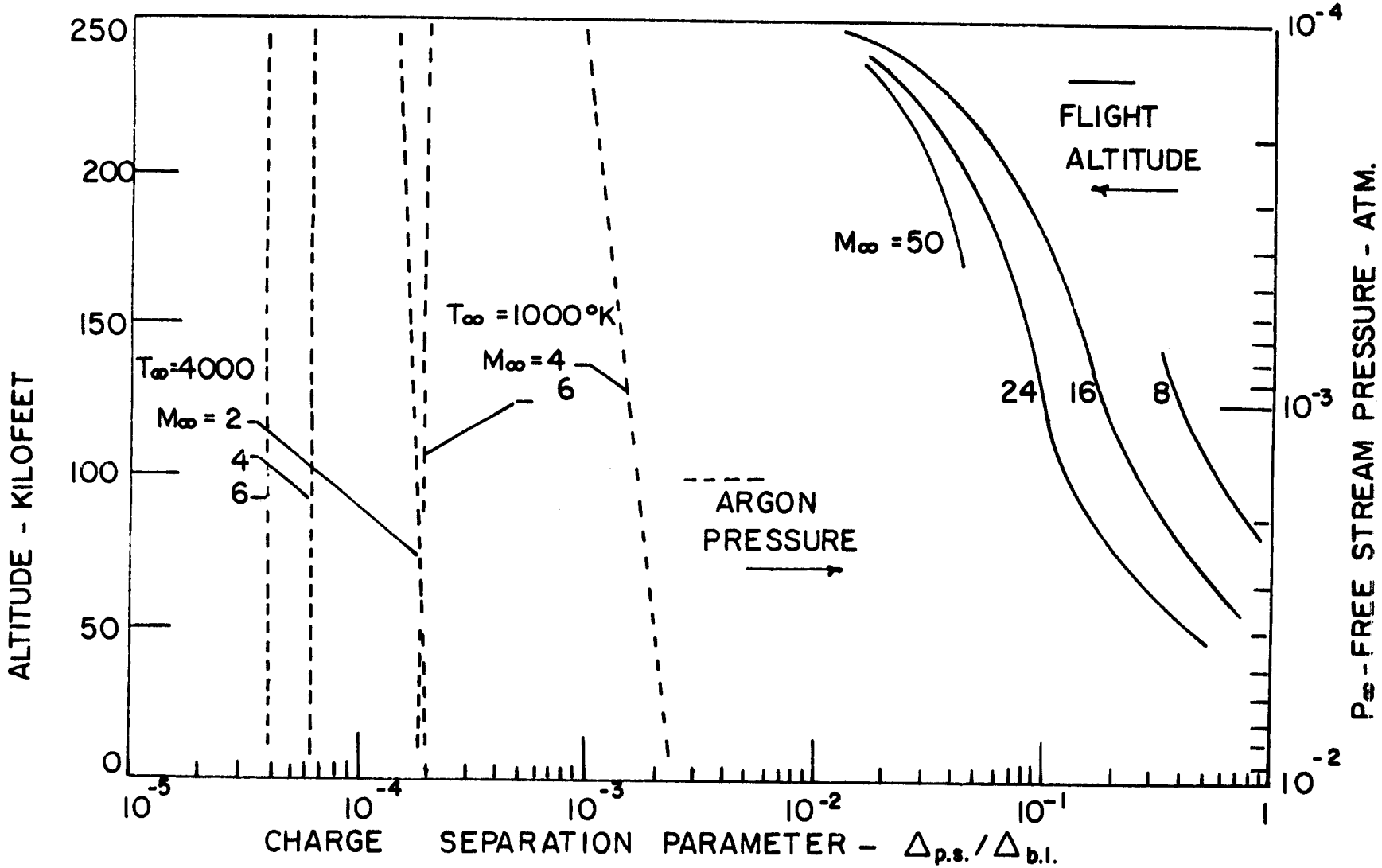

FIGURE 5. PLASMA SHEATH PARAMETERS

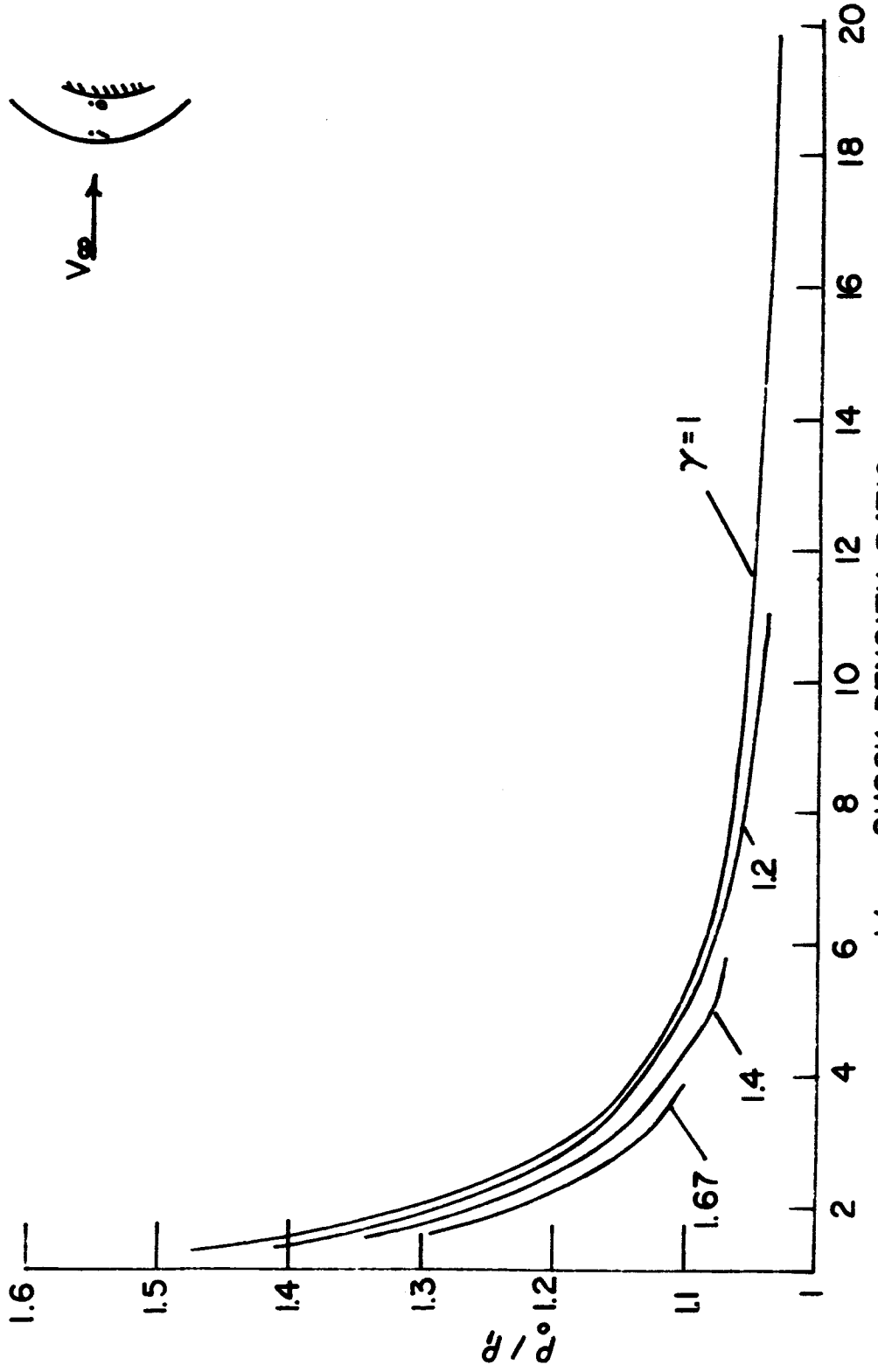

FIGURE 6. VARIATION OF DENSITY IN THE SHOCK LAYER

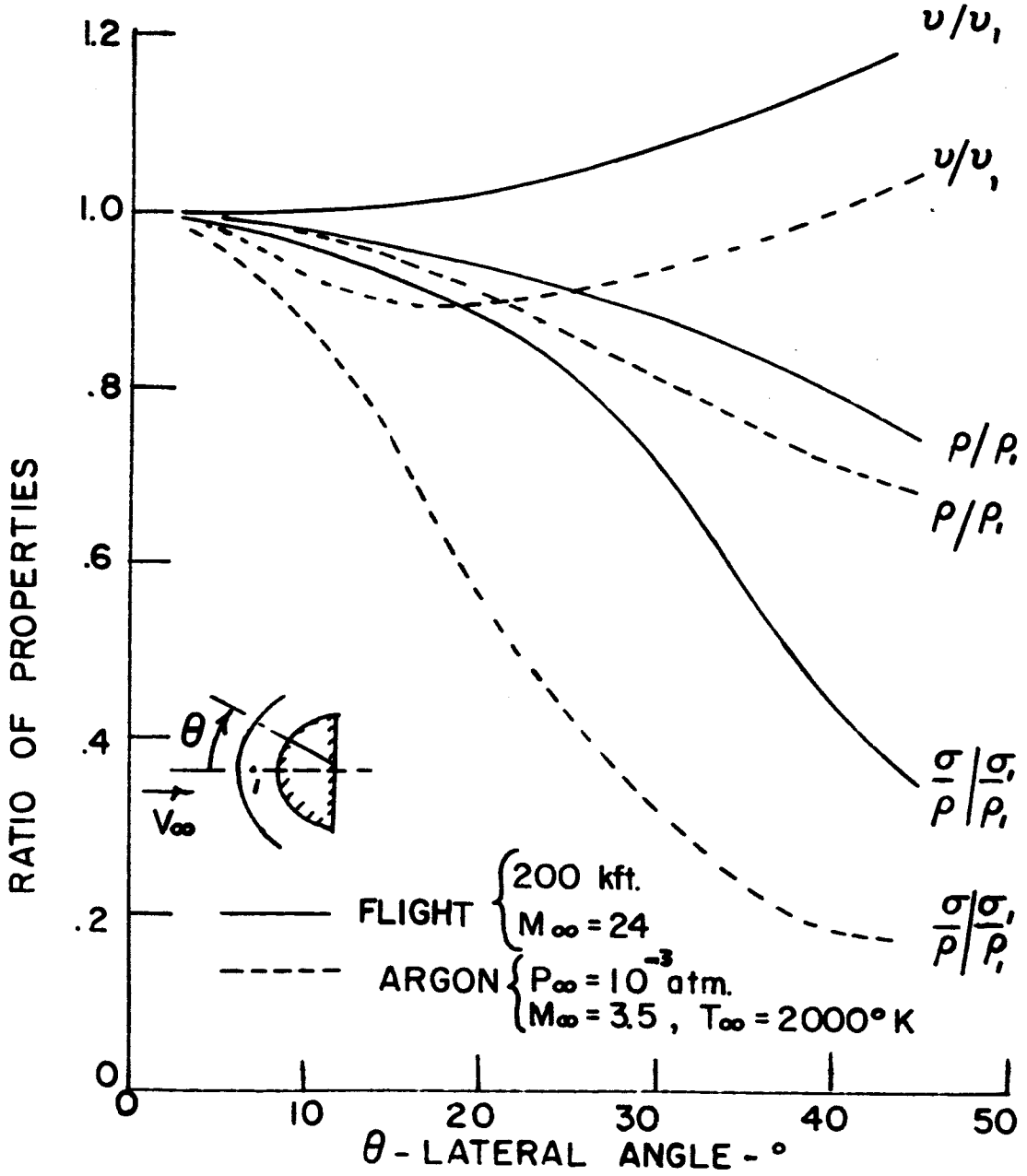

FIGURE 7. LATERAL VARIATION OF DENSITY AND TRANSPORT COEFFICICIENTS

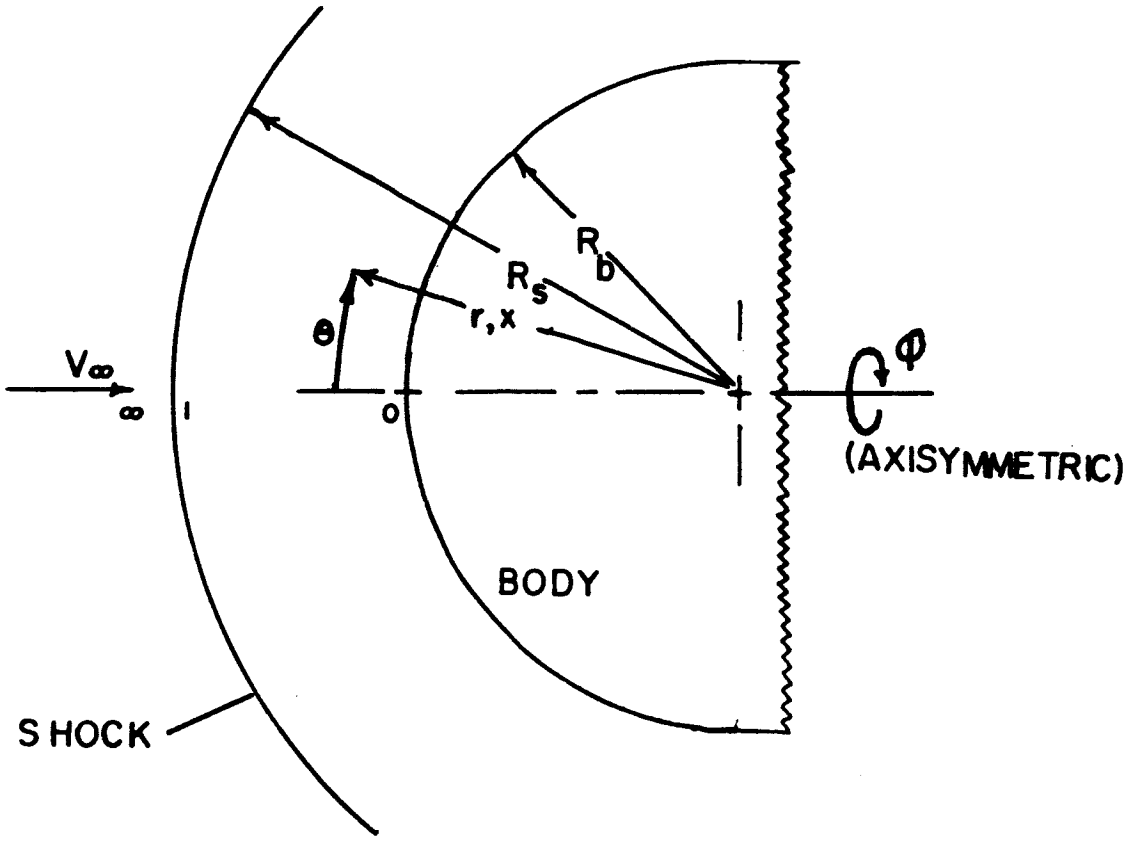

FIGURE 8. GEOMETRY & COORDINATE SYSTEM

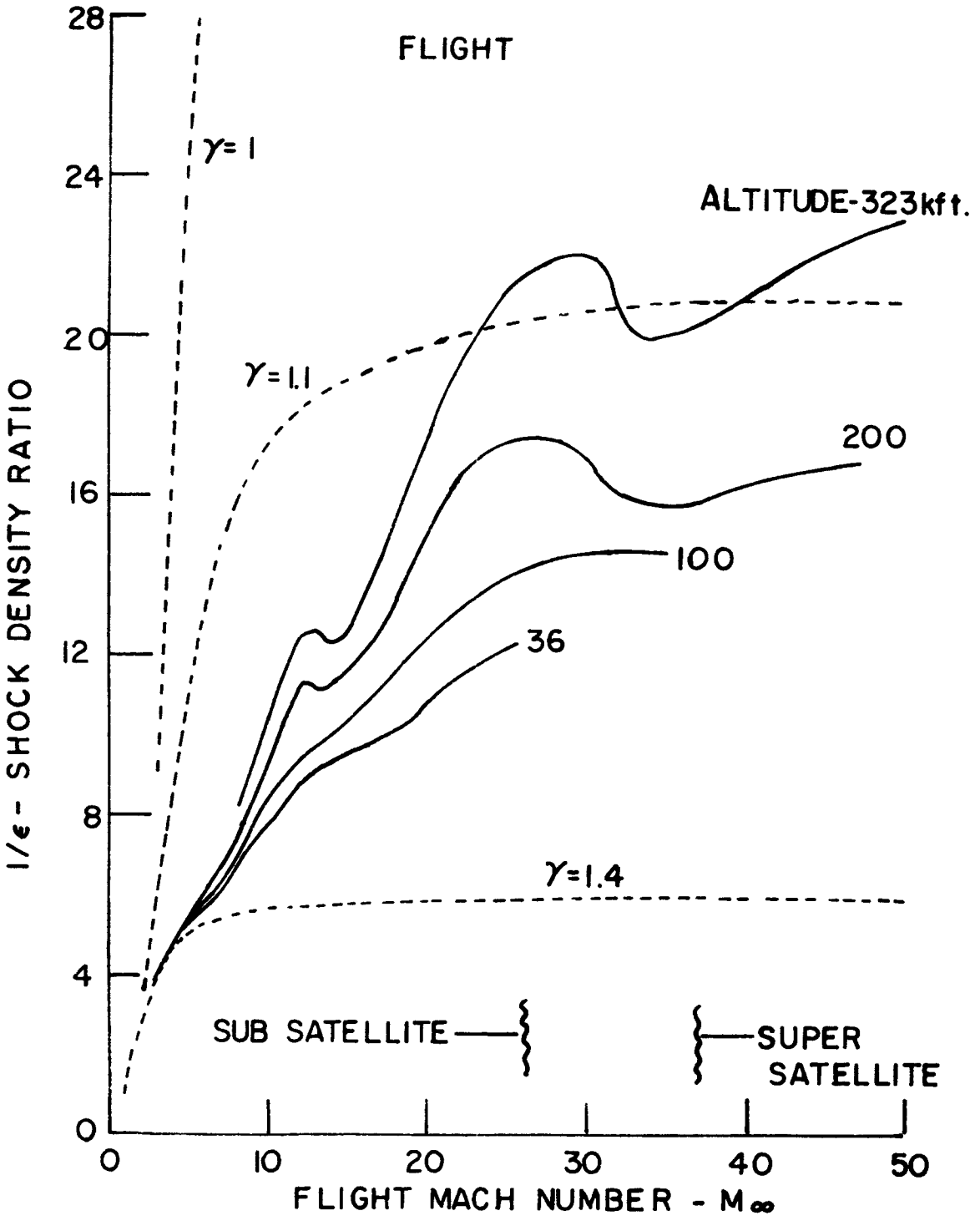

FIGURE 9. SHOCK DENSITY RATIO - EARTH ENTRY

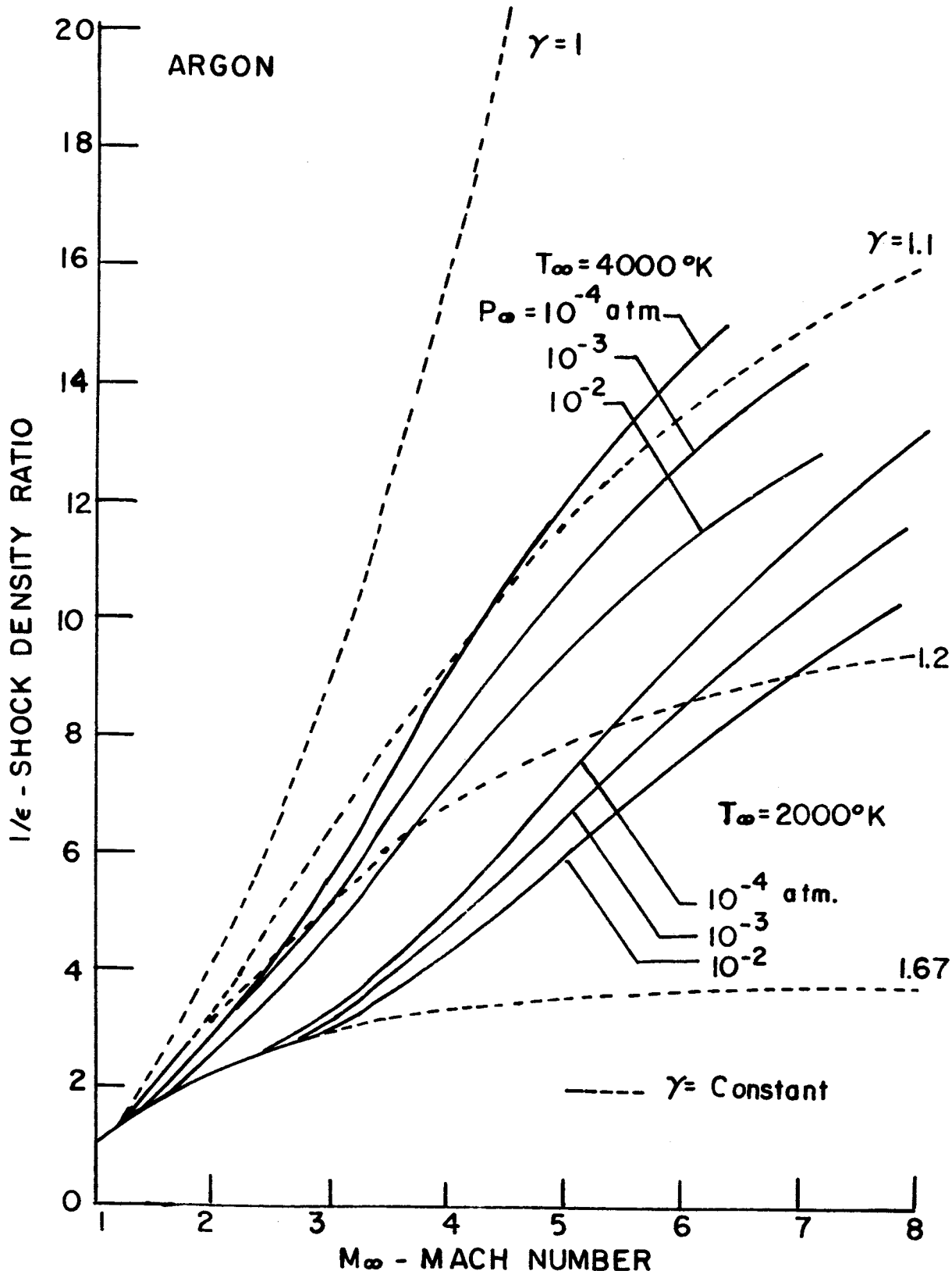

FIGURE 10. SHOCK DENSITY RATIO - ARGON PLASMA

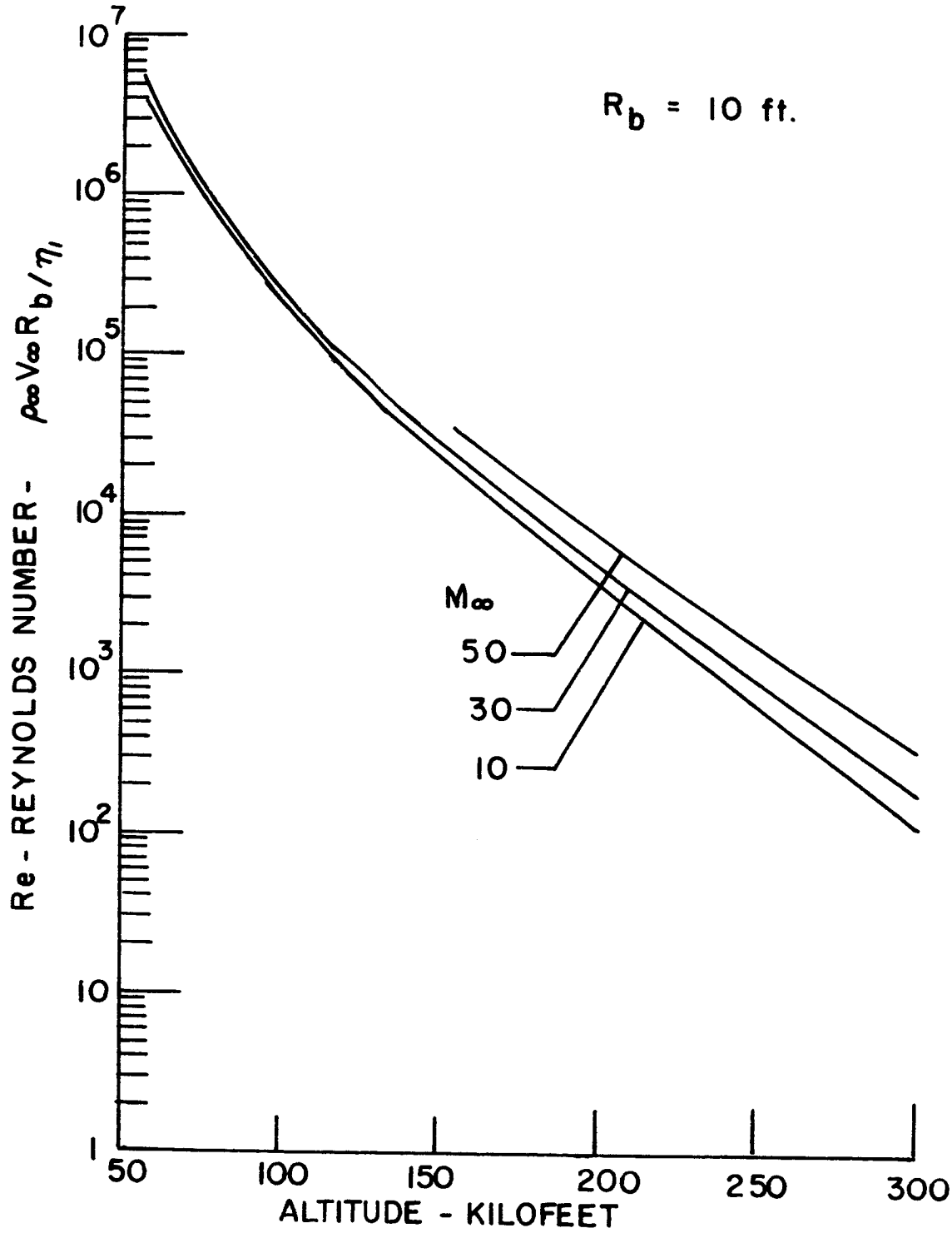

FIGURE 11. REYNOLDS NUMBER - ENTRY FLIGHT

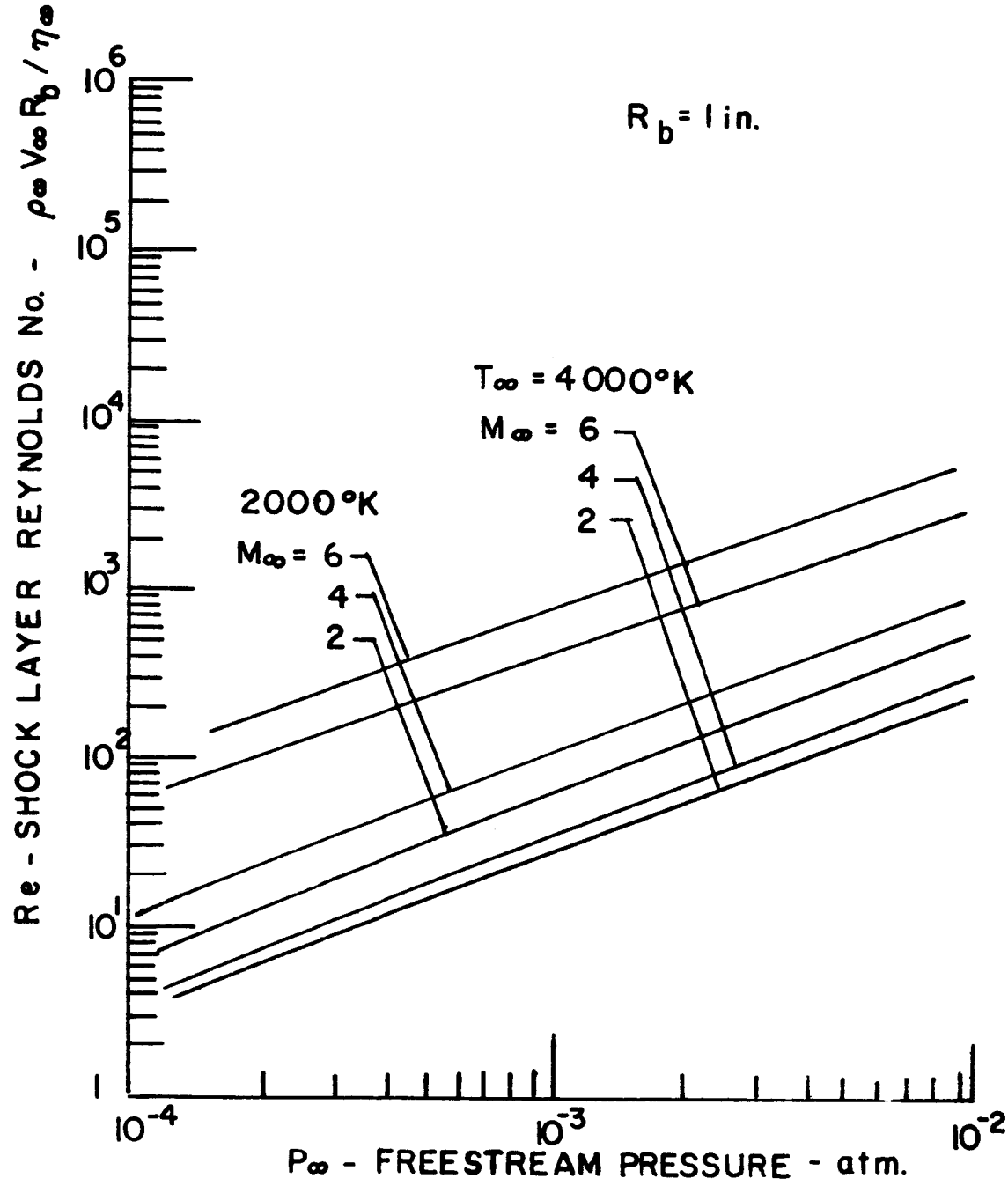

FIGURE 12. REYNOLDS NUMBER - ARGON PLASMA

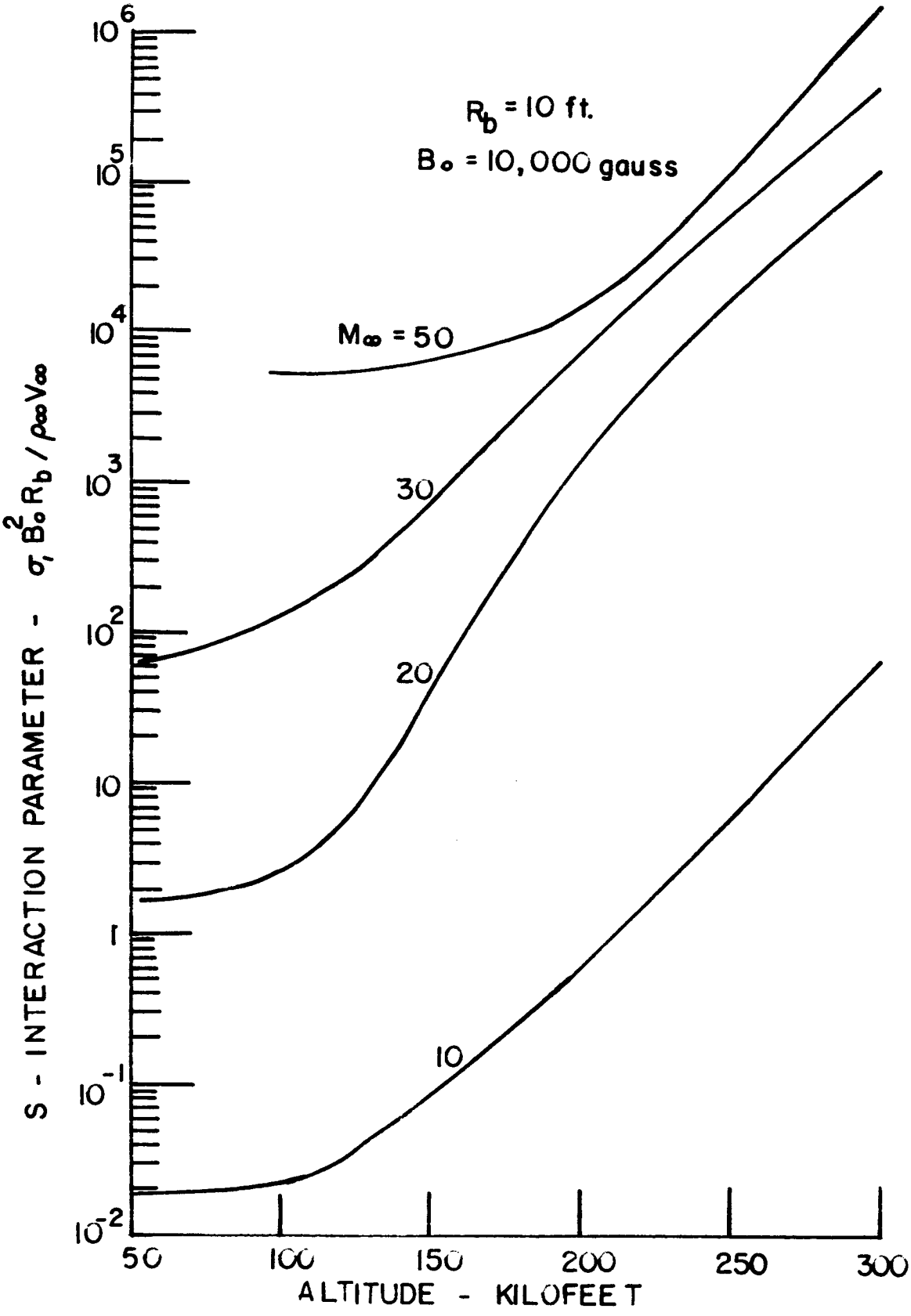

FIGURE 13. INTERACTION PARAMETER - ENTRY FLIGHT

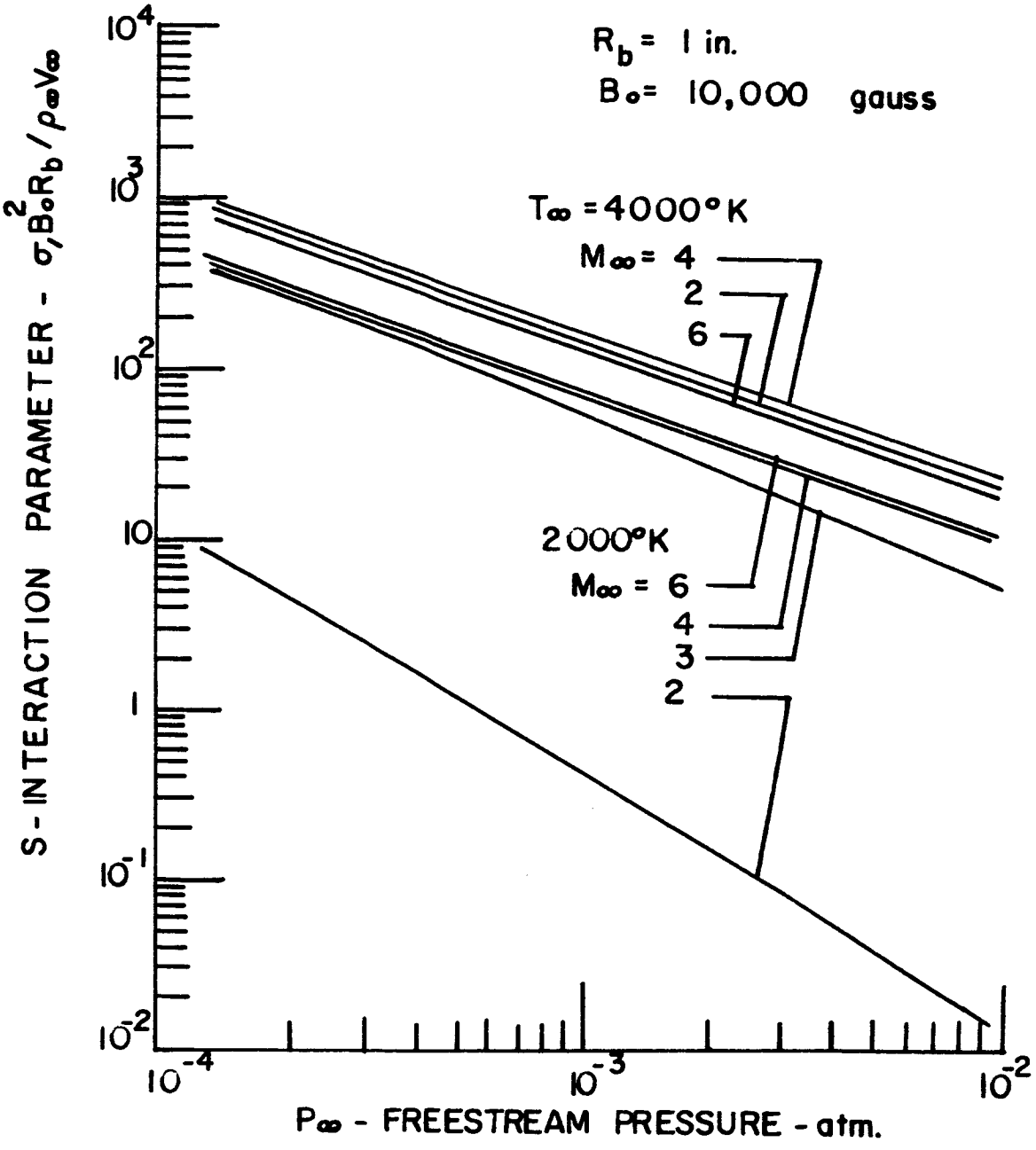

FIGURE 14. INTERACTION PARAMETER - ARGON PLASMA

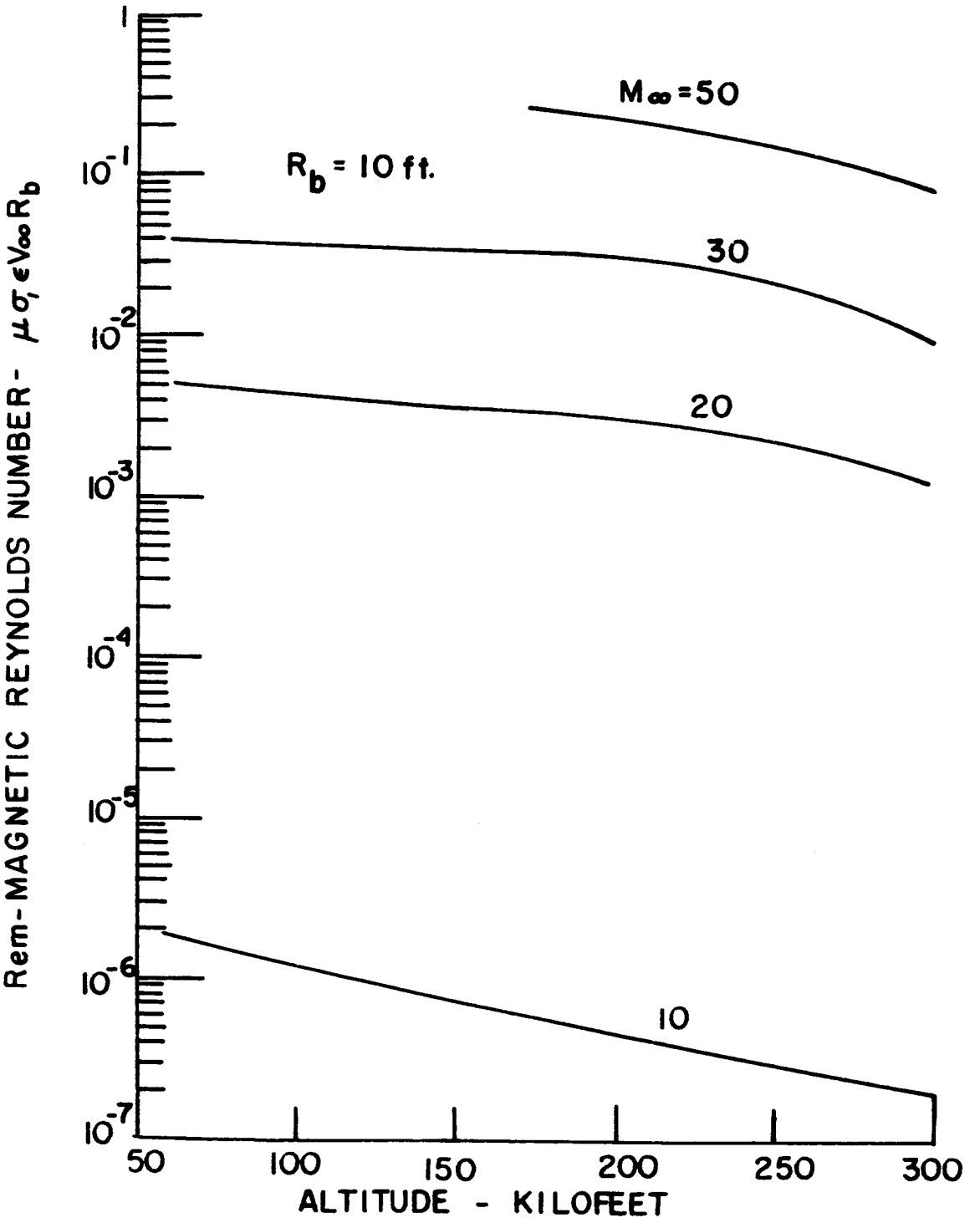

FIGURE 15. MAGNETIC REYNOLDS NUMBER - ENTRY FLIGHT

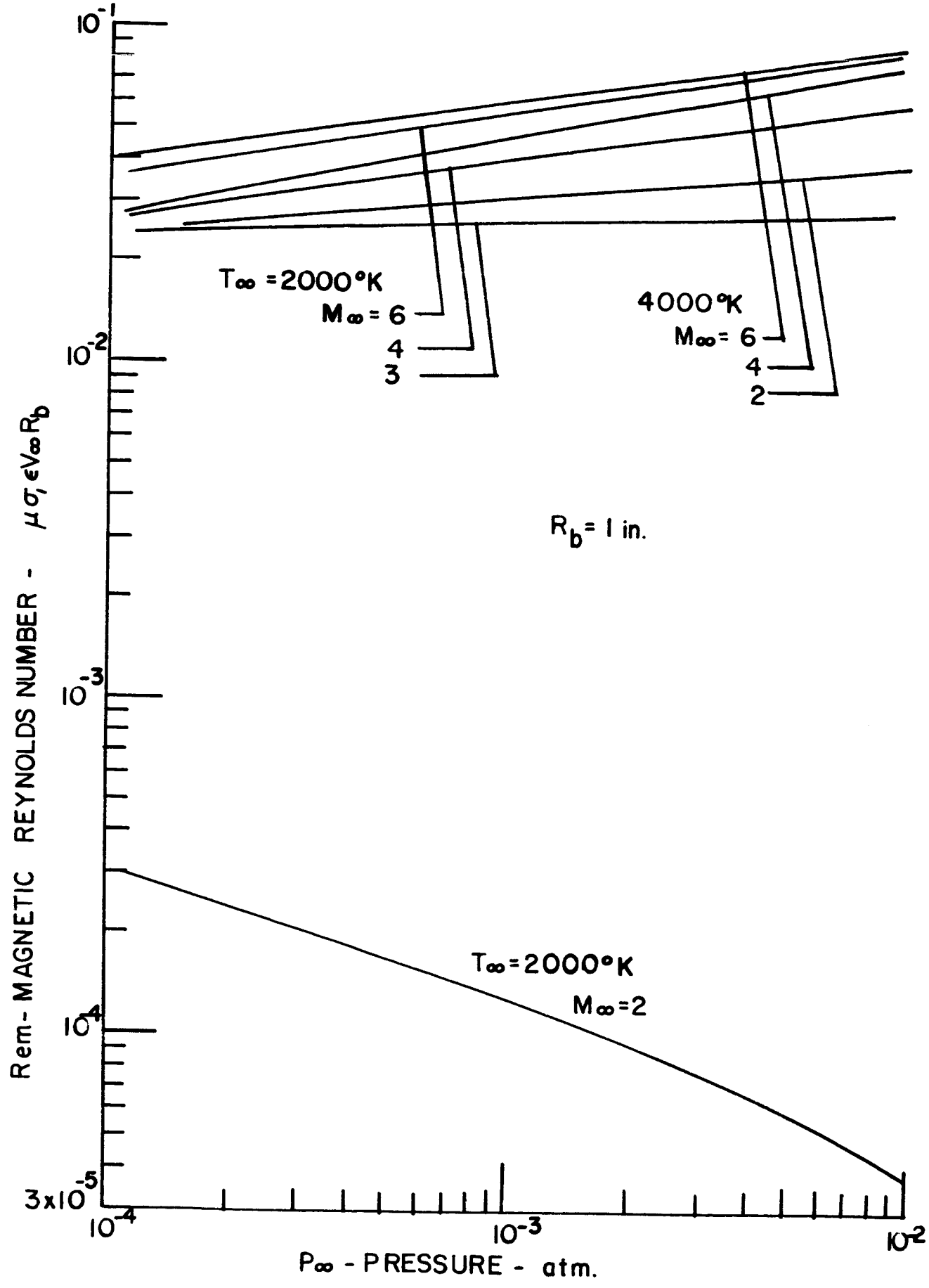

FIGURE 16. MAGNETIC REYNOLDS NUMBER - ARGON PLASMA

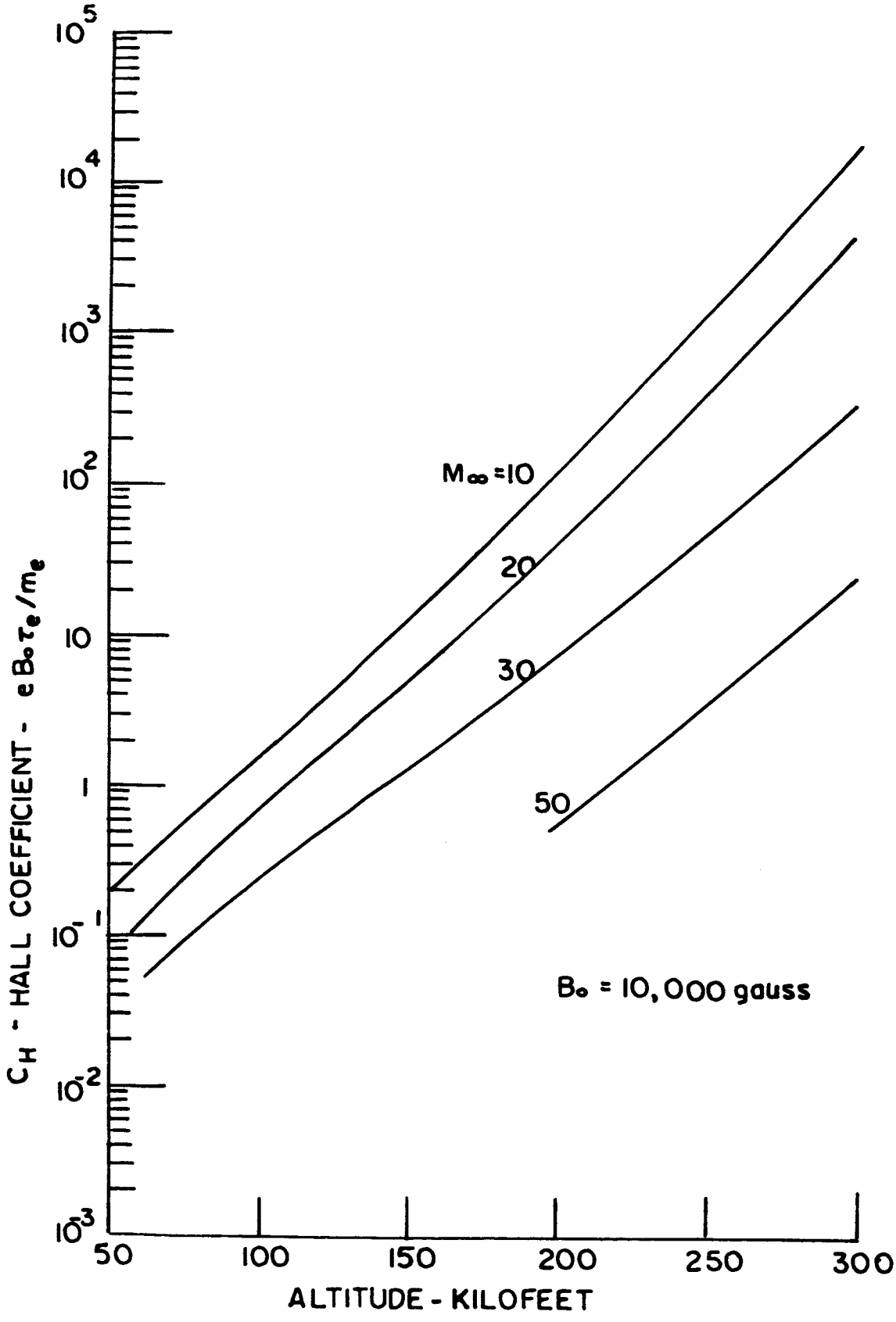

FIGURE 17. HALL COEFFICIENT - ENTRY FLIGHT

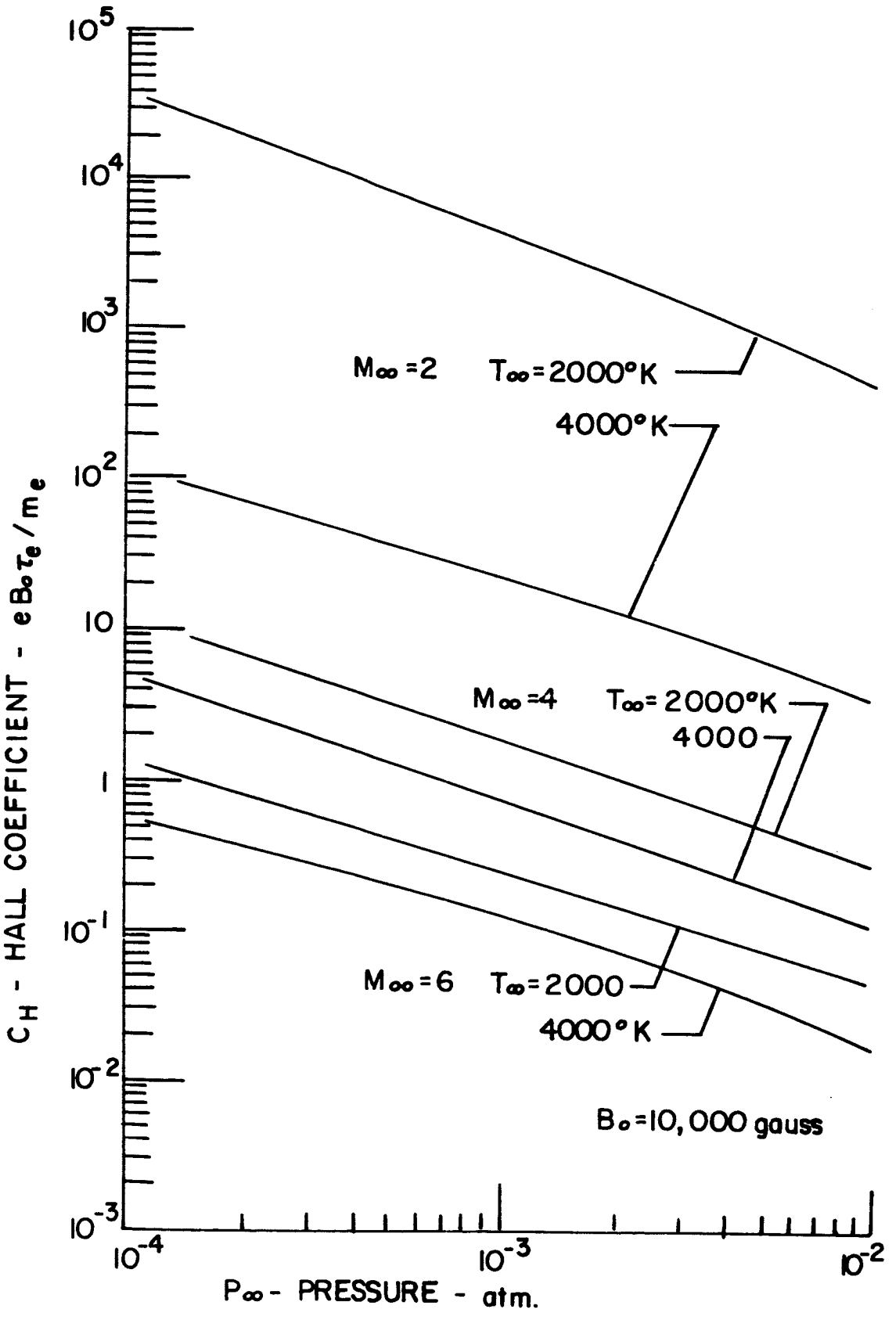

FIGURE 18. HALL COEFFICIENT - ARGON PLASMA

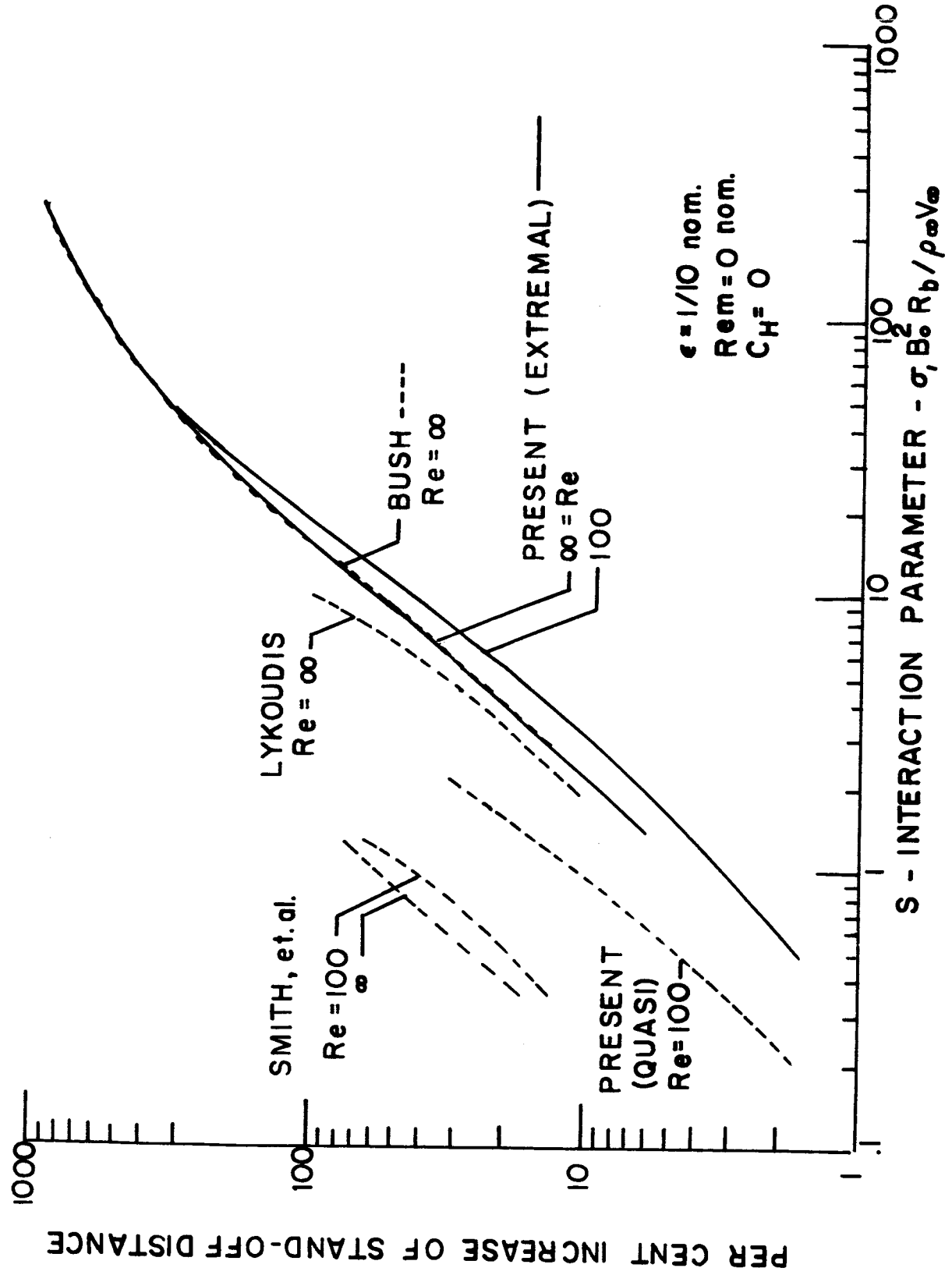

FIGURE 19. COMPARISON OF THEORIES FOR SHOCK STAND-OFF

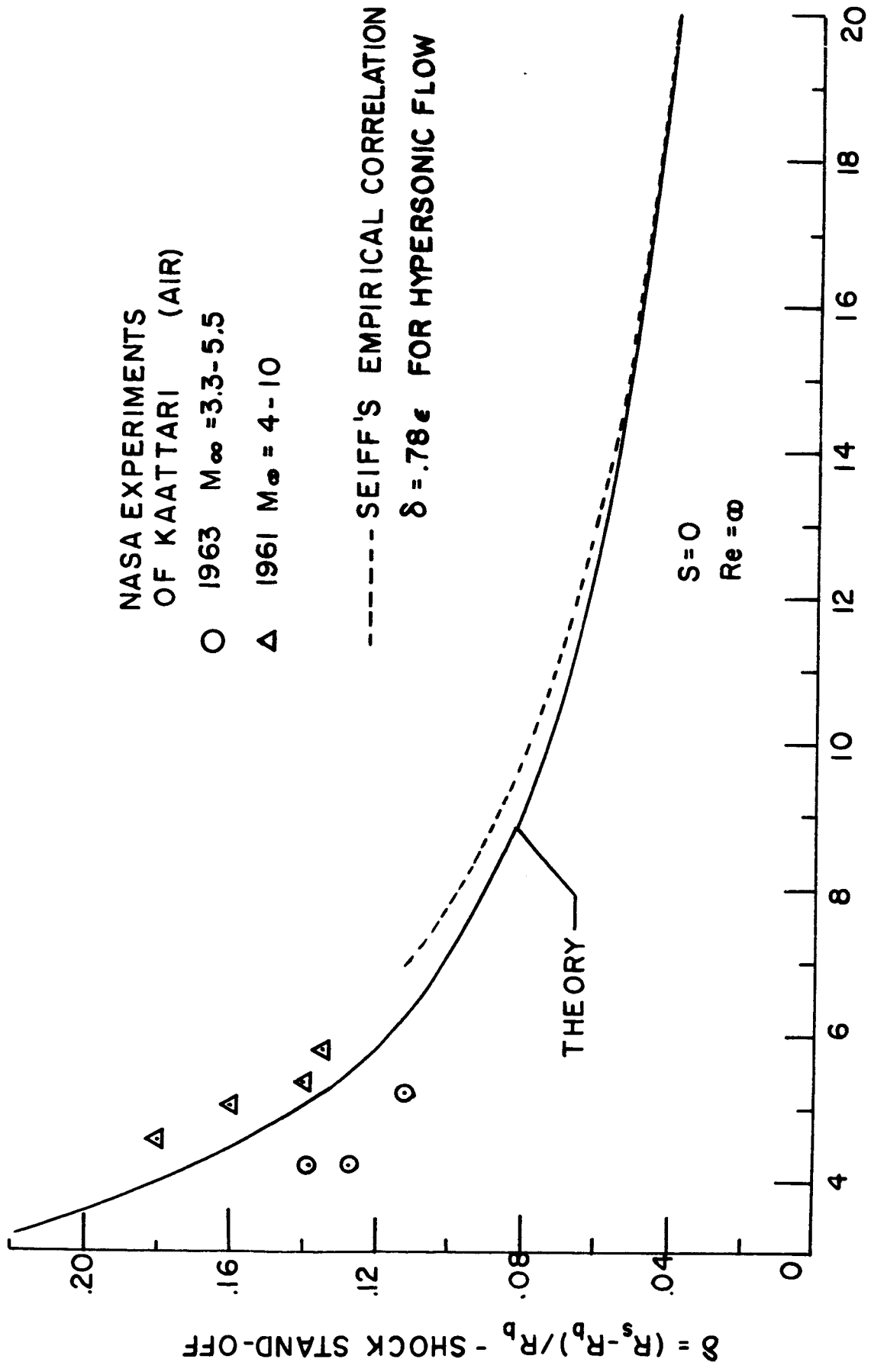

FIGURE 20. SHOCK STAND-OFF DISTANCE

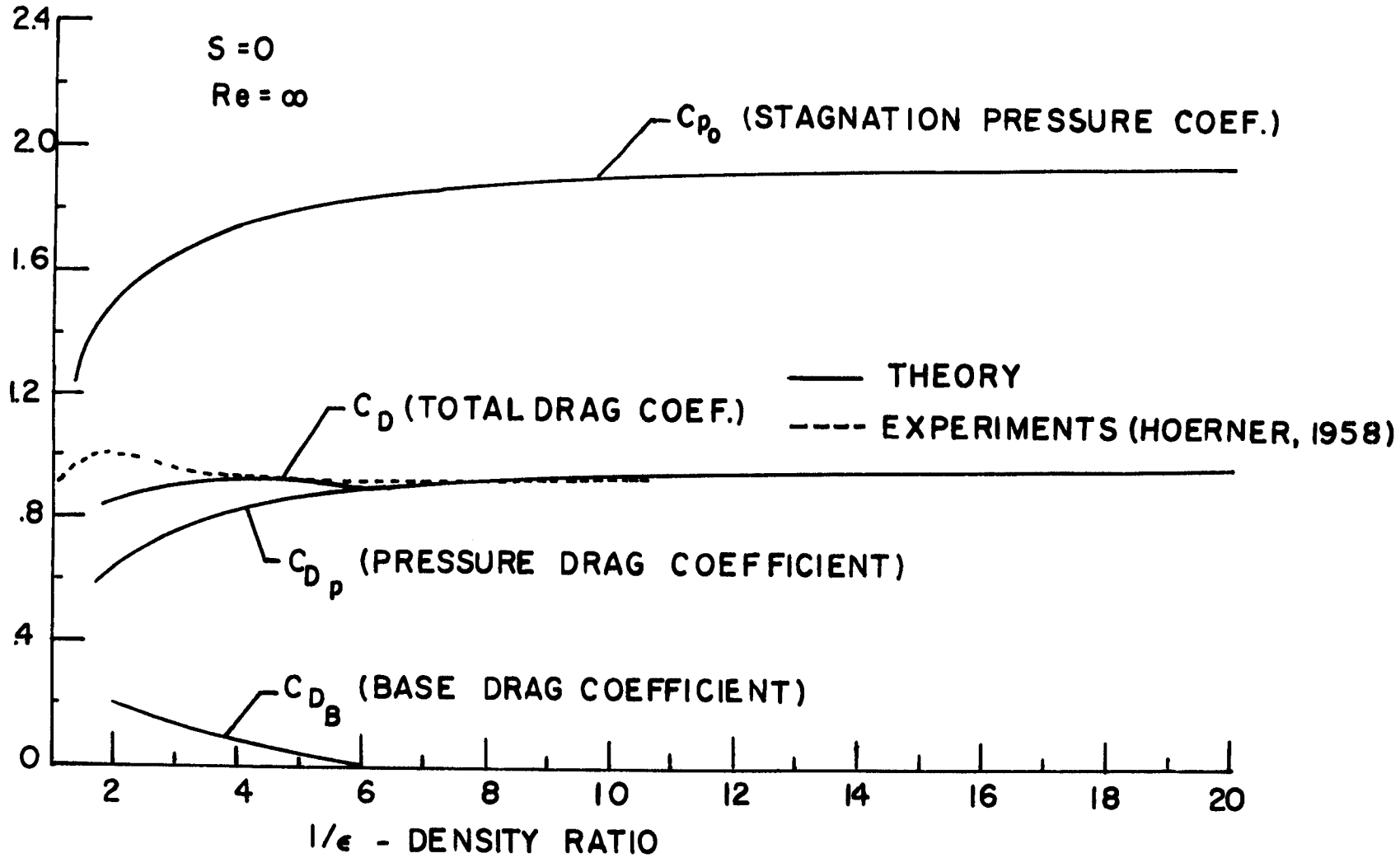

FIGURE 21. AERODYNAMIC COEFFICIENTS

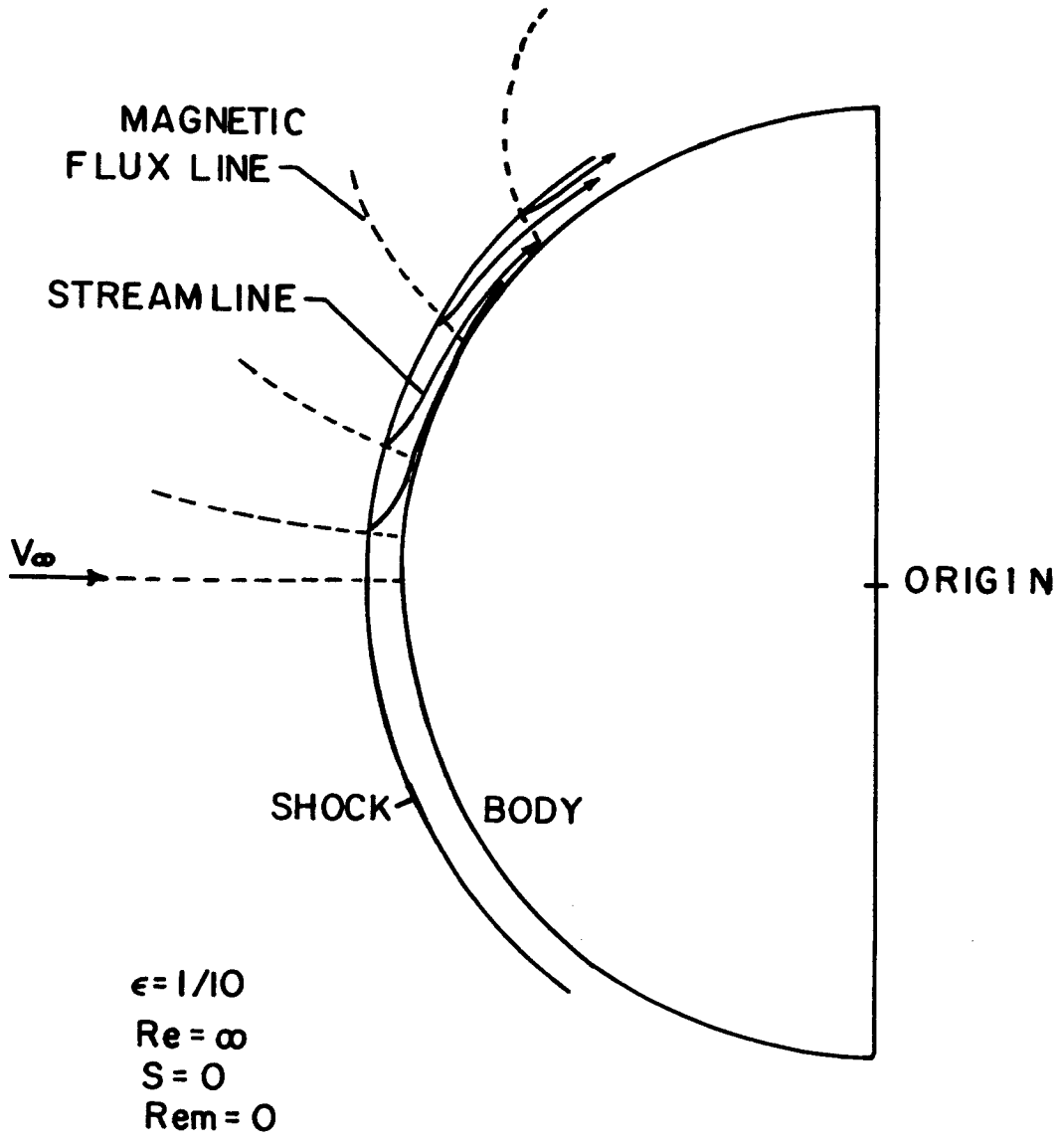

FIGURE 22. STREAM LINES & MAGNETIC FLUX LINES

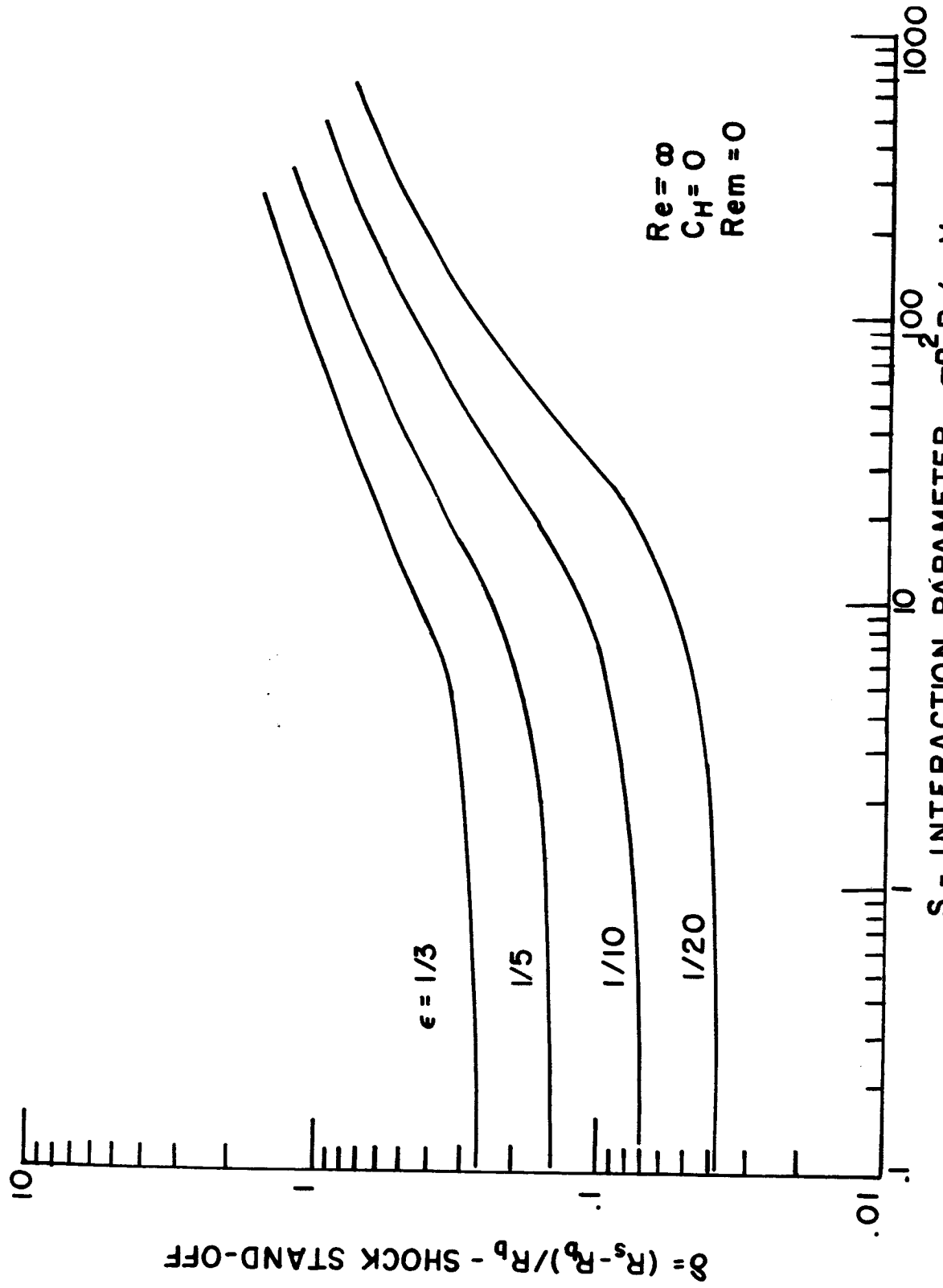

FIGURE 23. STAND-OFF DISTANCE WITH INTERACTION

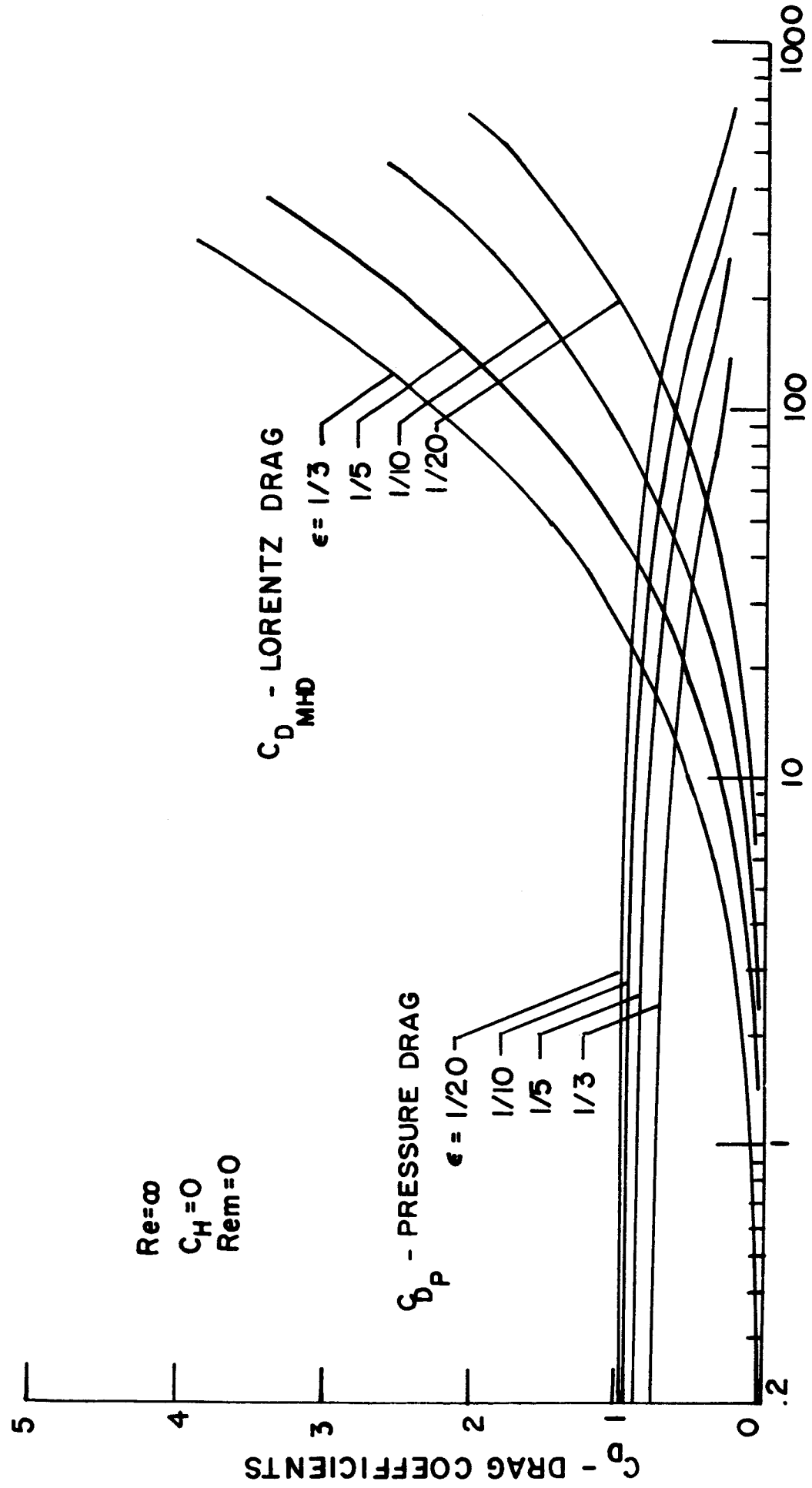

FIGURE 24. PRESSURE AND LORENTZ DRAG WITH INTERACTION

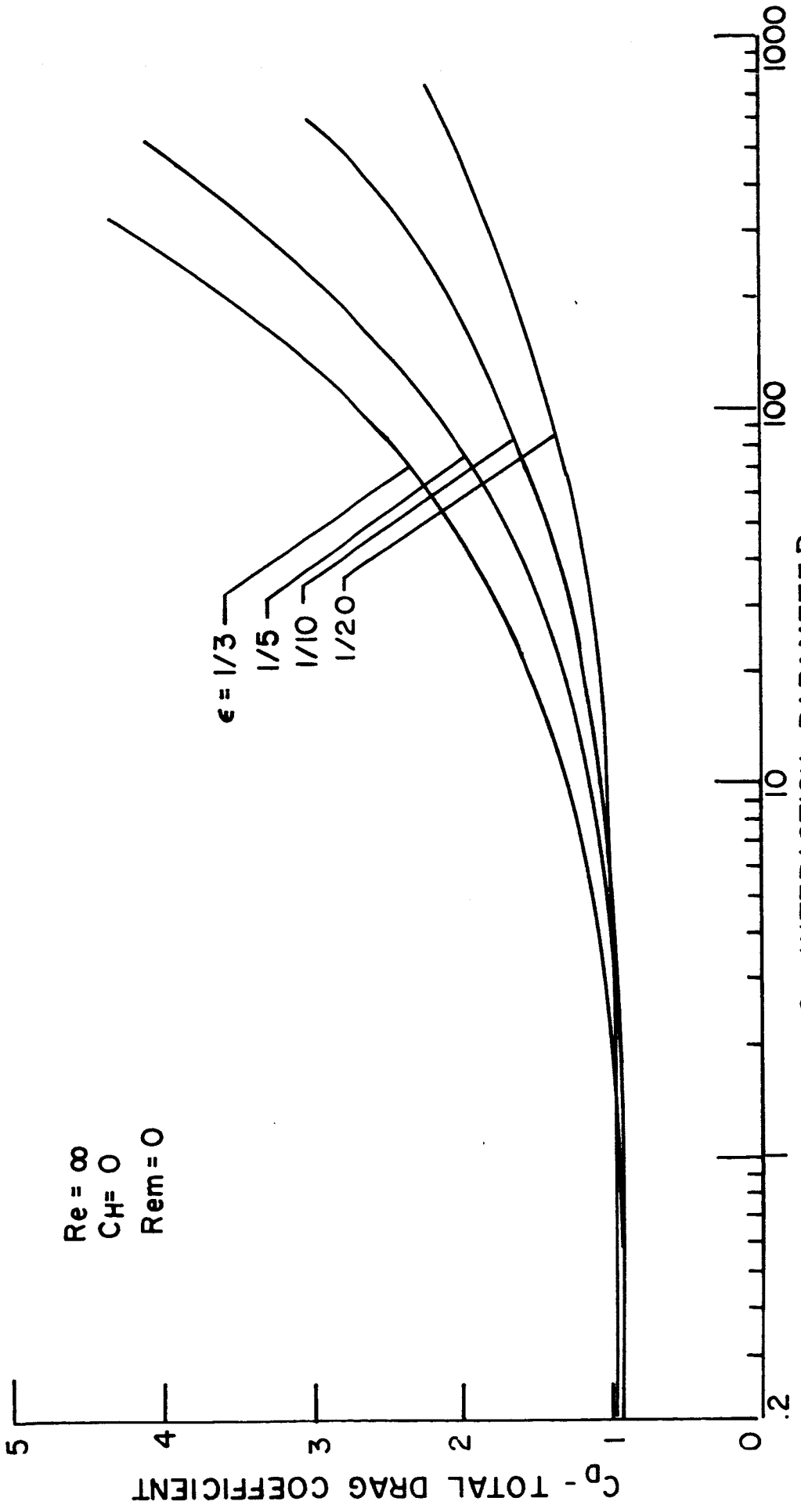

FIGURE 25. TOTAL DRAG WITH INTERACTION

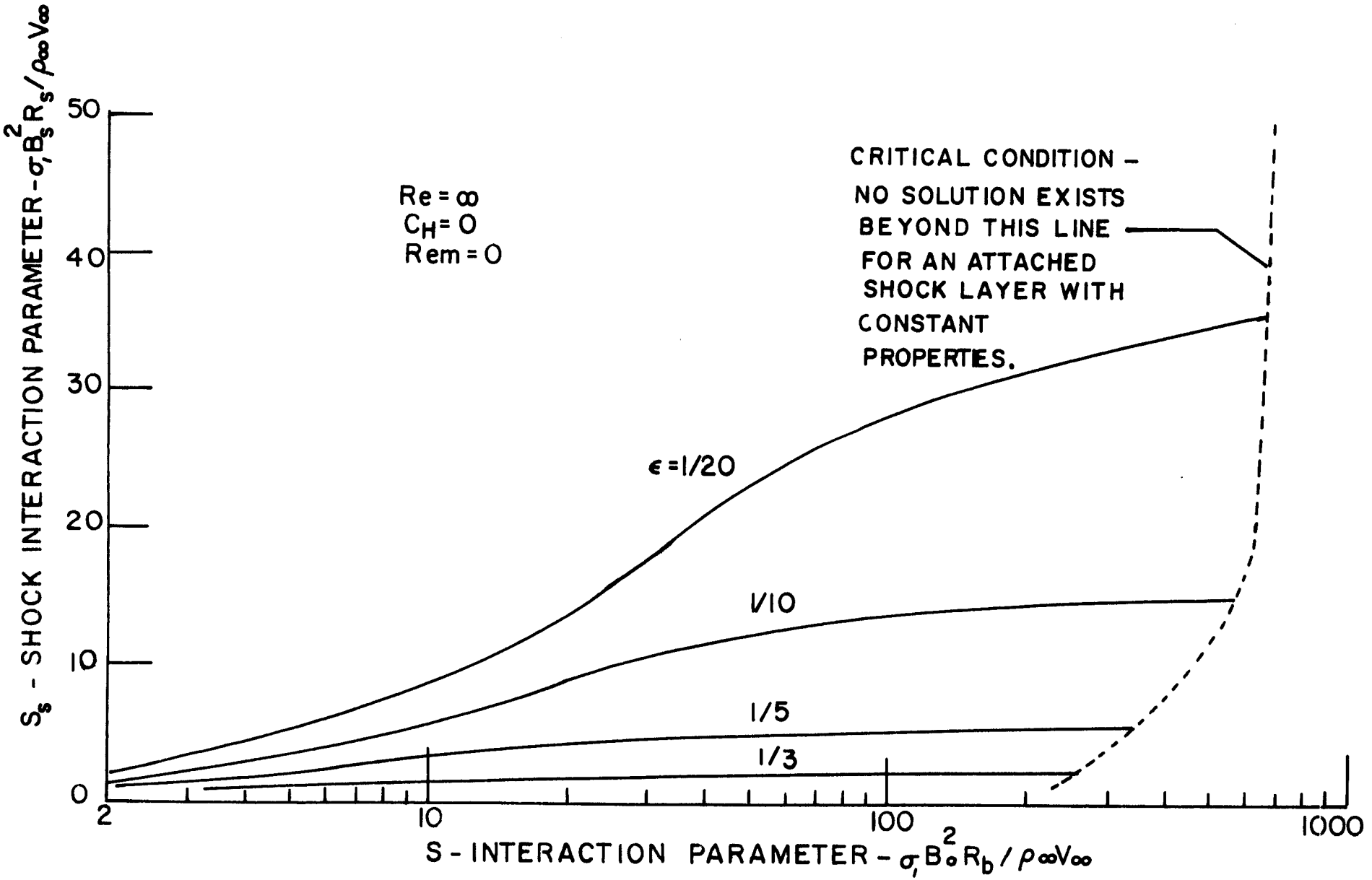

FIGURE 26. SHOCK INTERACTION PARAMETER

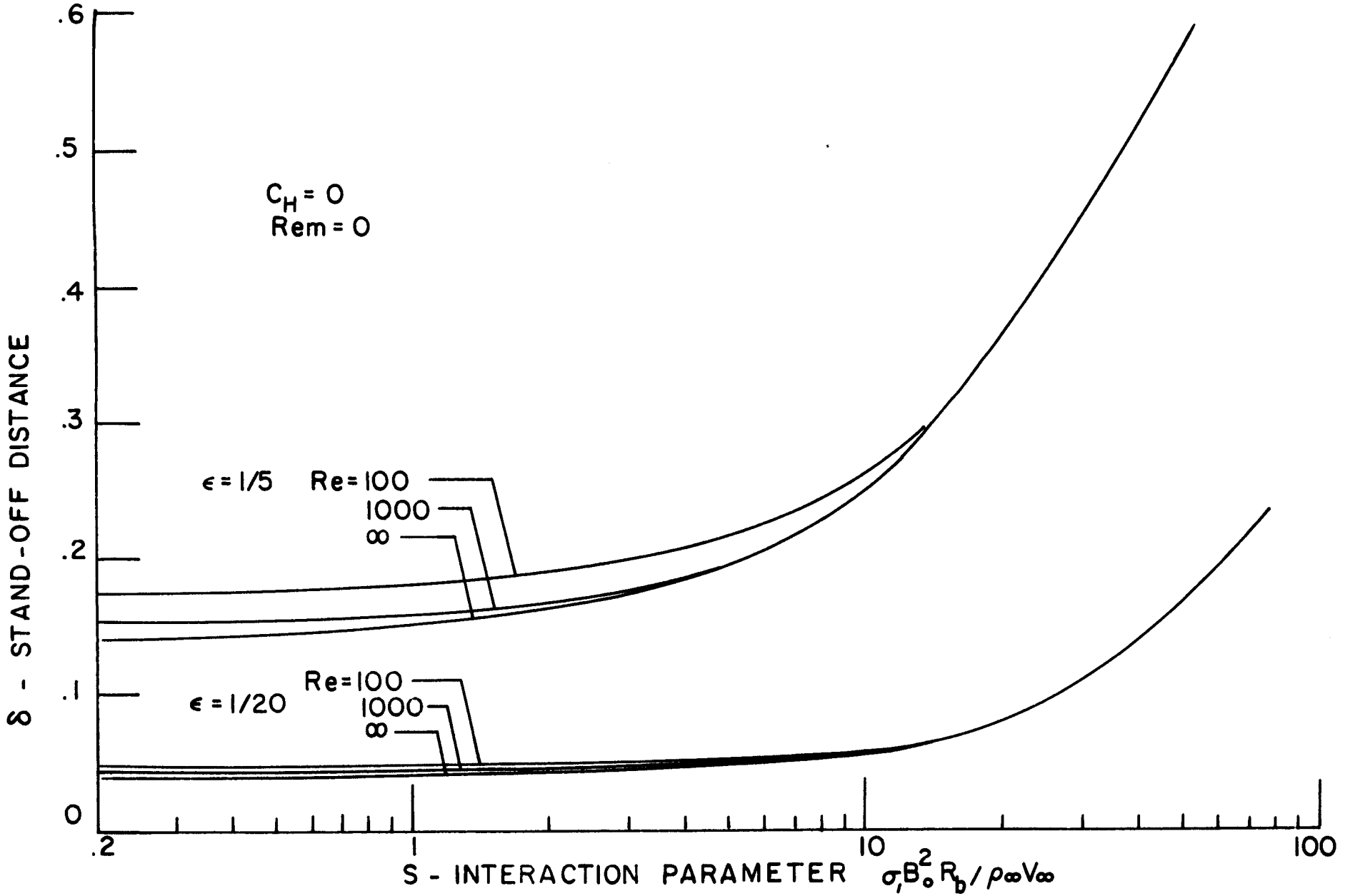

FIGURE 27. STAND-OFF WITH VISCOSITY

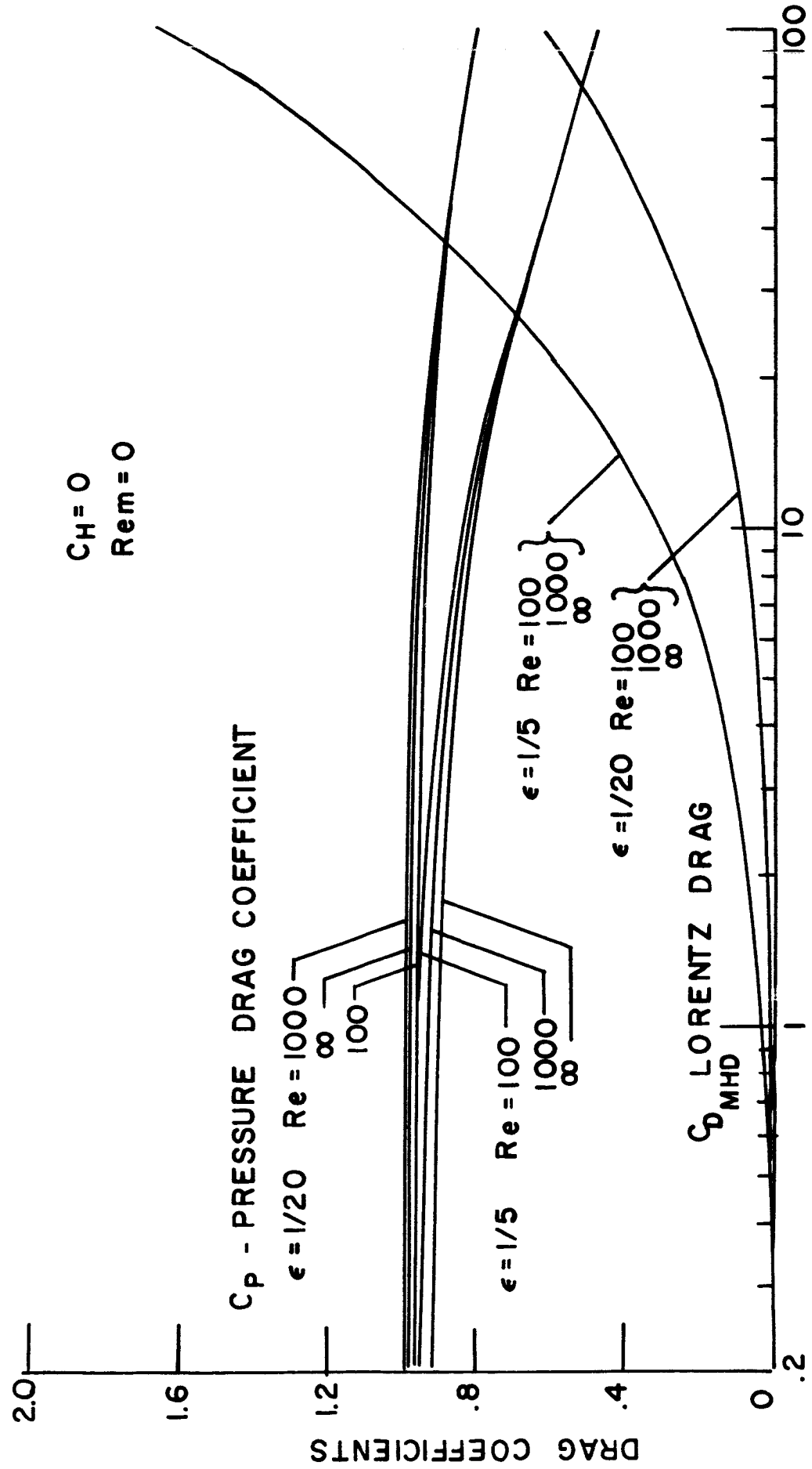

FIGURE 28. PRESSURE AND LORENTZ DRAG WITH VISCOSITY

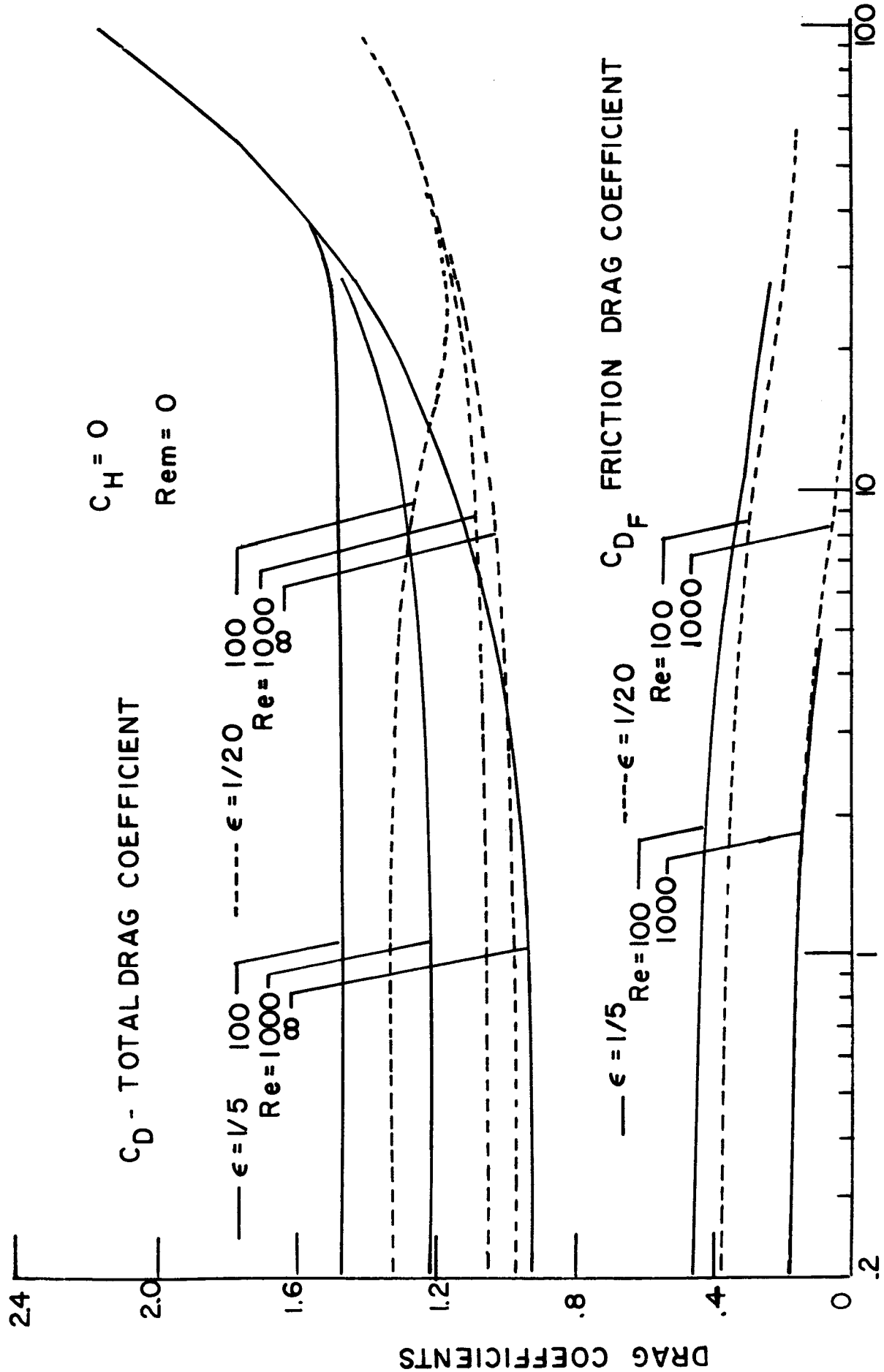

FIGURE 29. VISCOUS AND TOTAL DRAG WITH INTERACTION

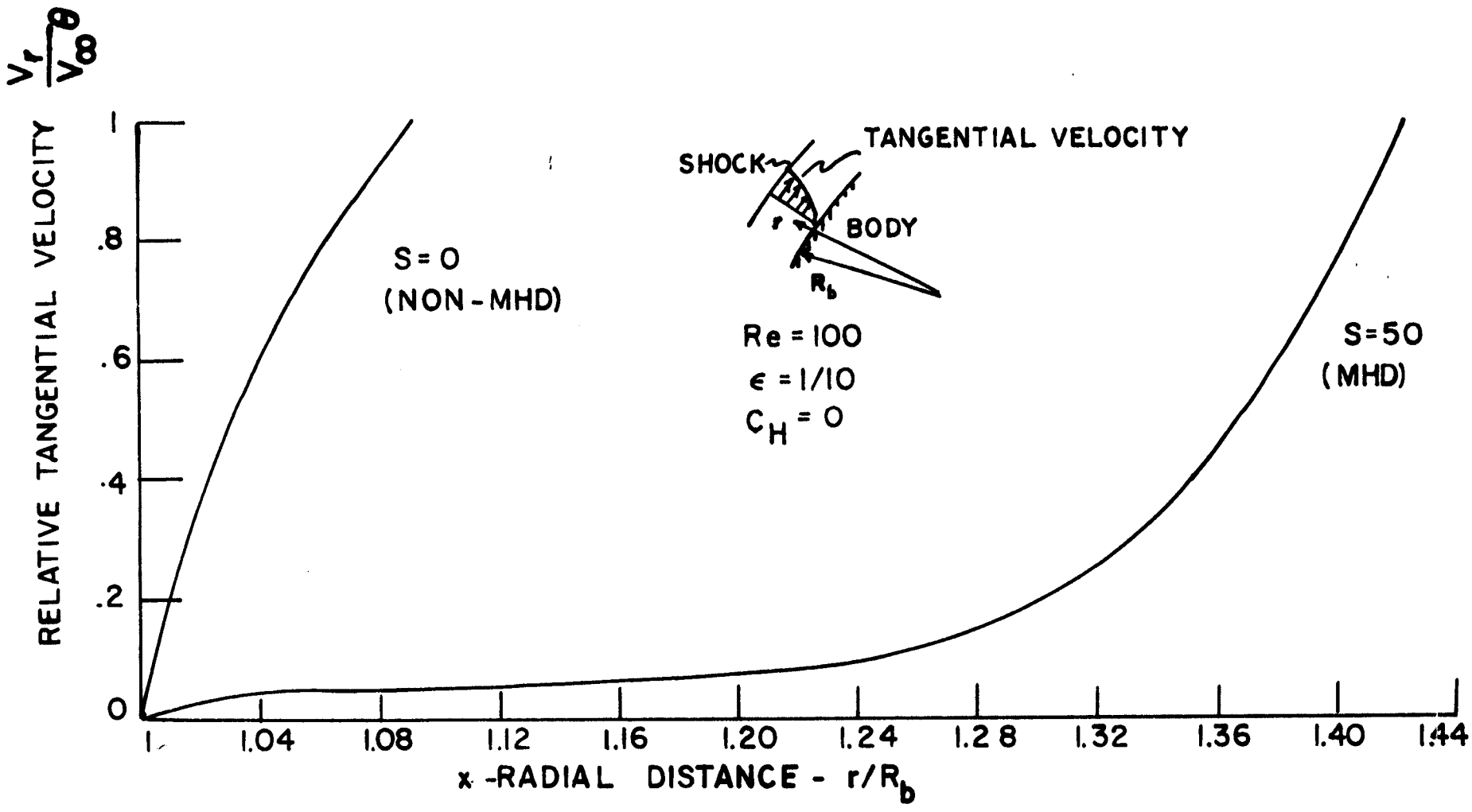

FIGURE 30. VELOCITY PROFILE WITH VISCOSITY

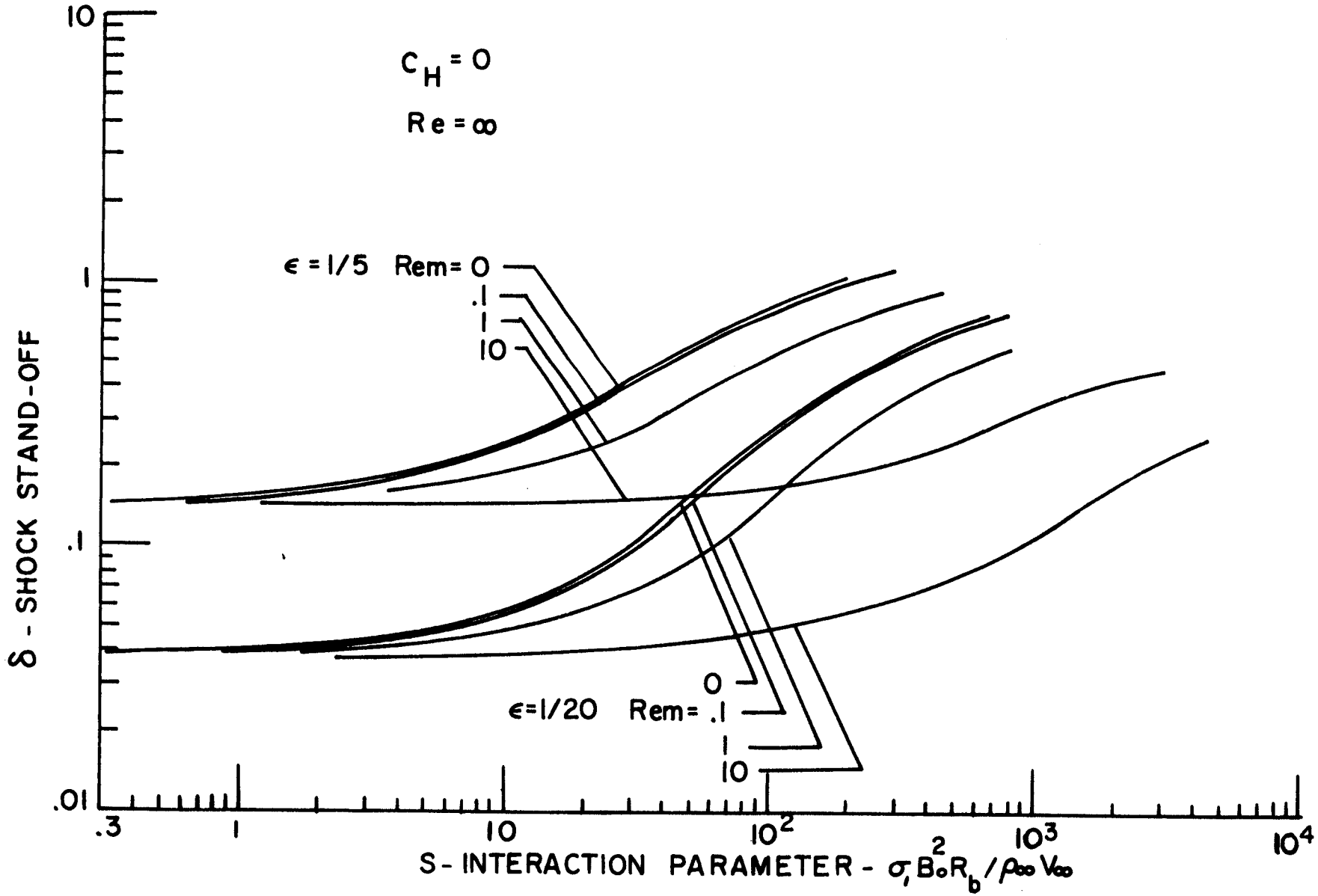

FIGURE 31. SHOCK STAND-OFF WITH MAGNETIC FIELD DEFORMATION

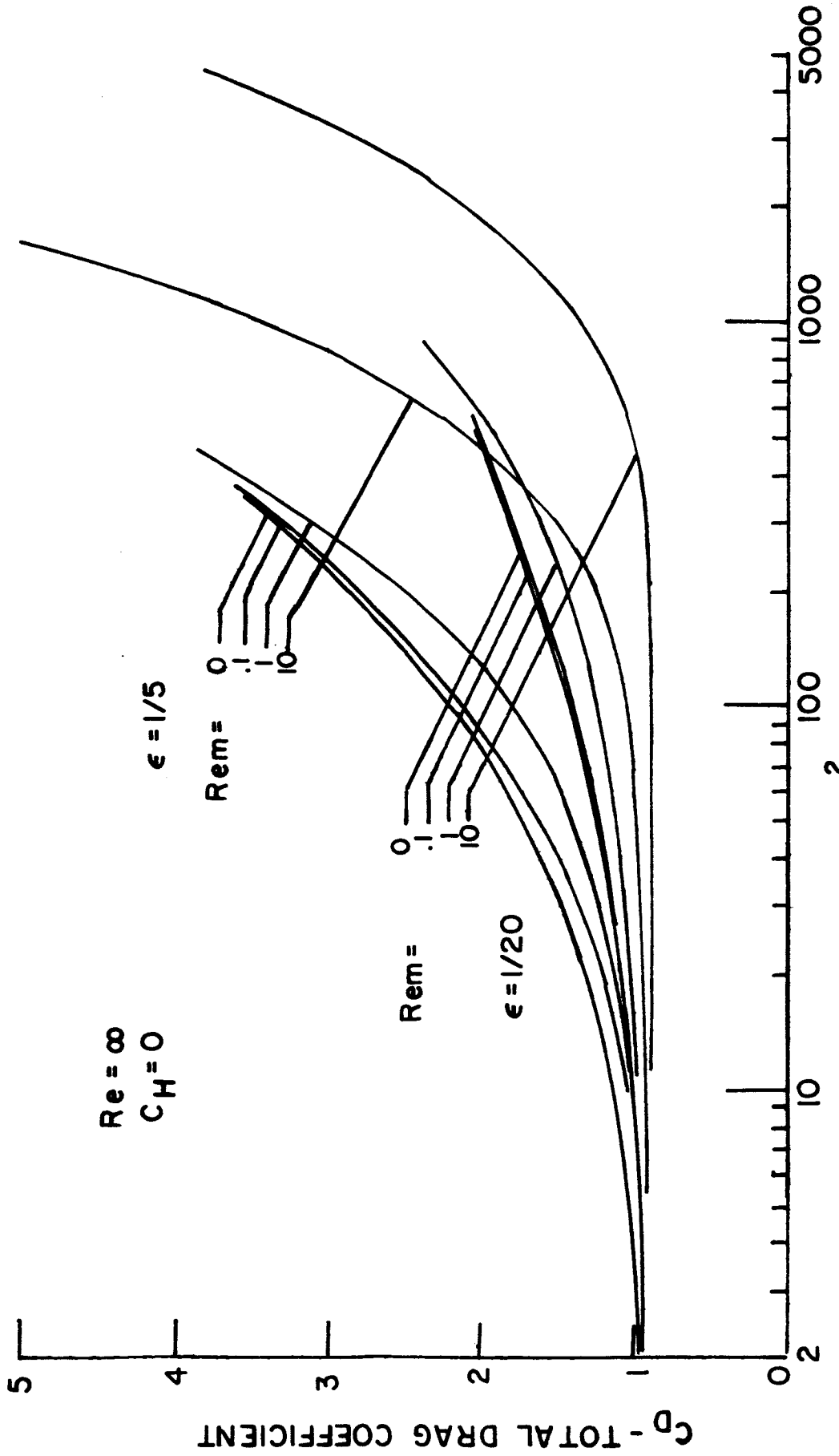

FIGURE 32. TOTAL DRAG WITH MAGNETIC FIELD DEFORMATION

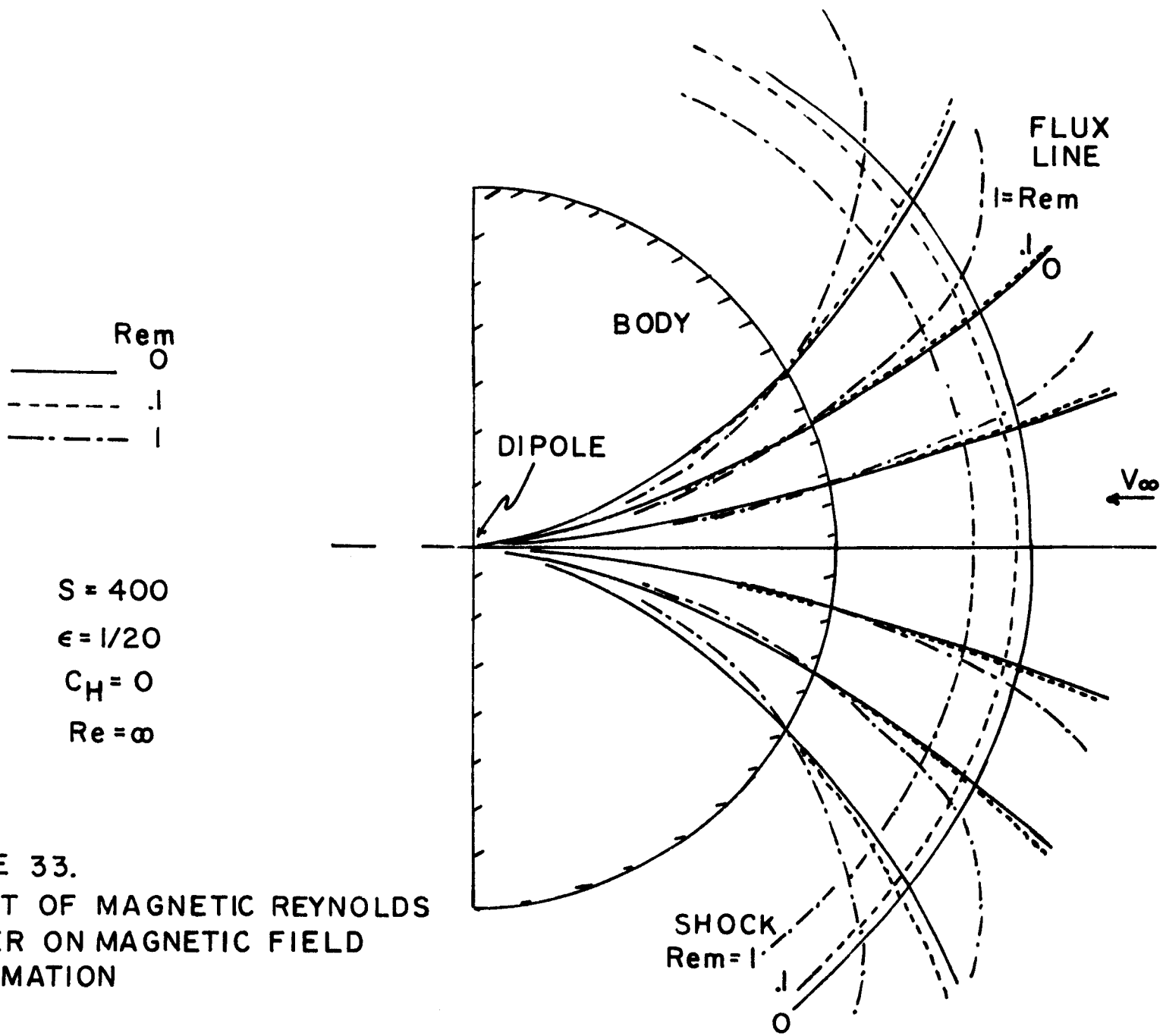

FIGURE 33.
EFFECT OF MAGNETIC REYNOLDS NUMBER ON MAGNETIC FIELD DEFORMATION

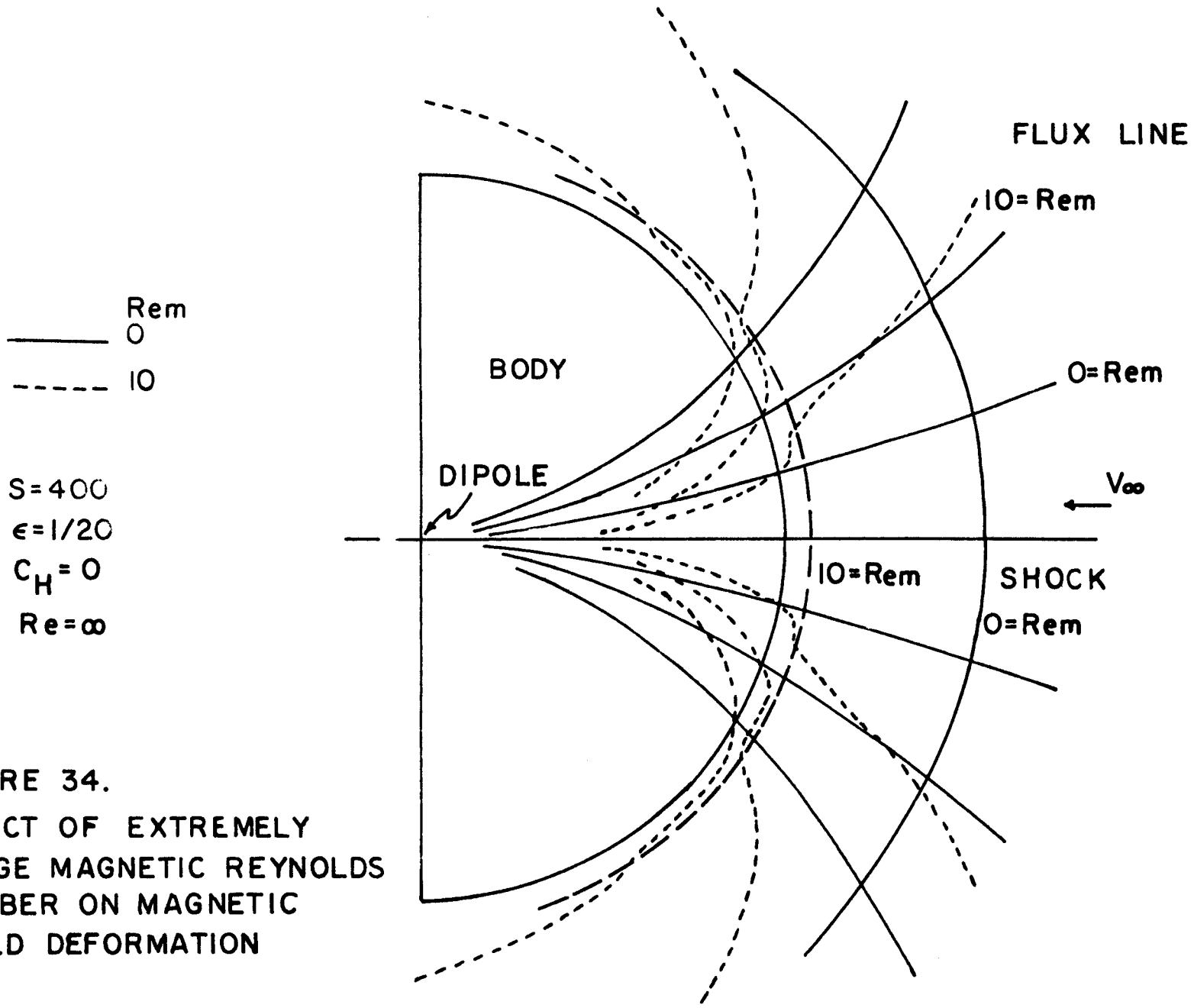

FIGURE 34.
EFFECT OF EXTREMELY LARGE MAGNETIC REYNOLDS NUMBER ON MAGNETIC FIELD DEFORMATION

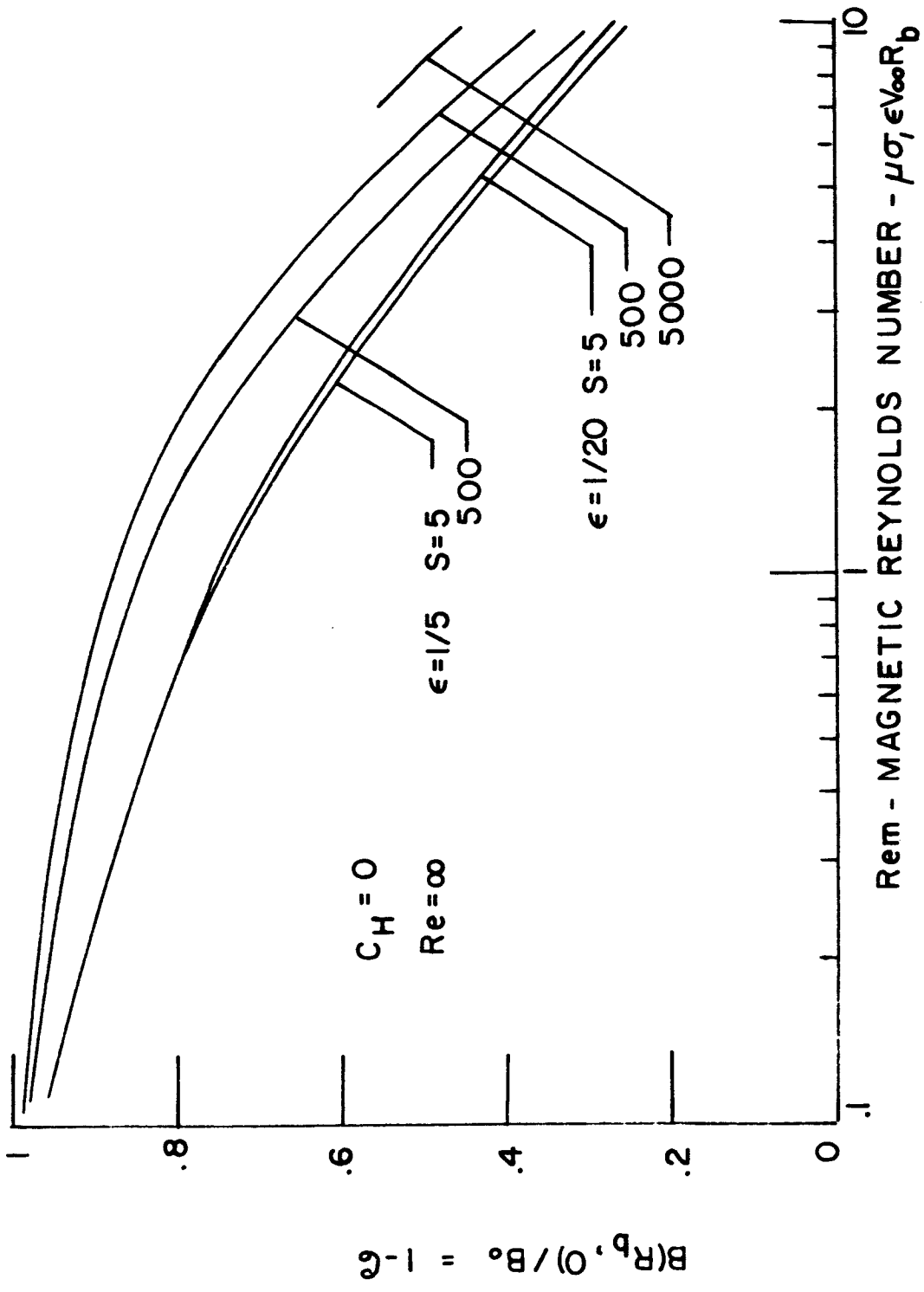

FIGURE 35. REDUCTION OF STAGNATION FIELD STRENGTH

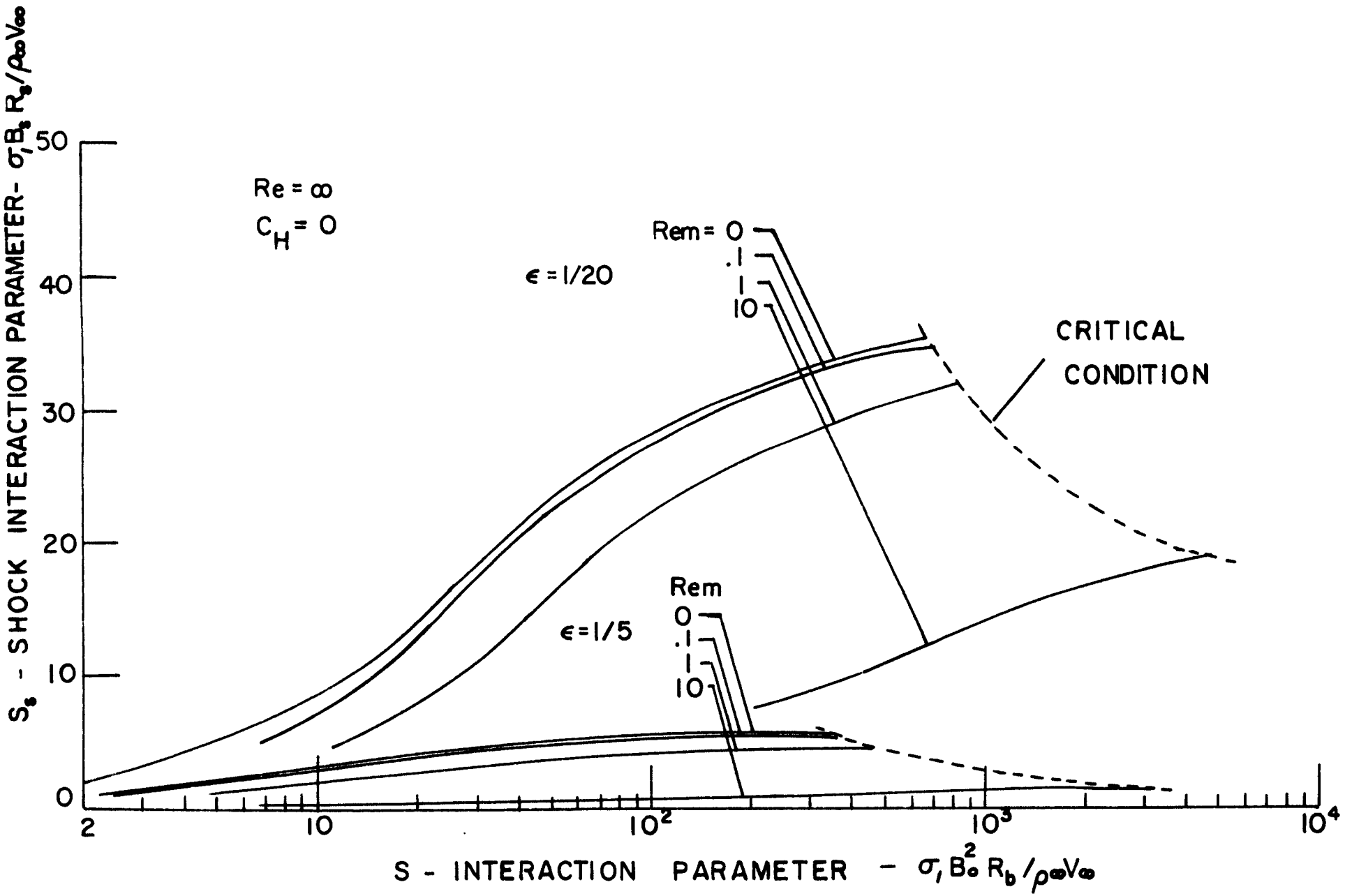

FIGURE 36. EFFECT OF Rem ON SHOCK INTERACTION PARAMETER

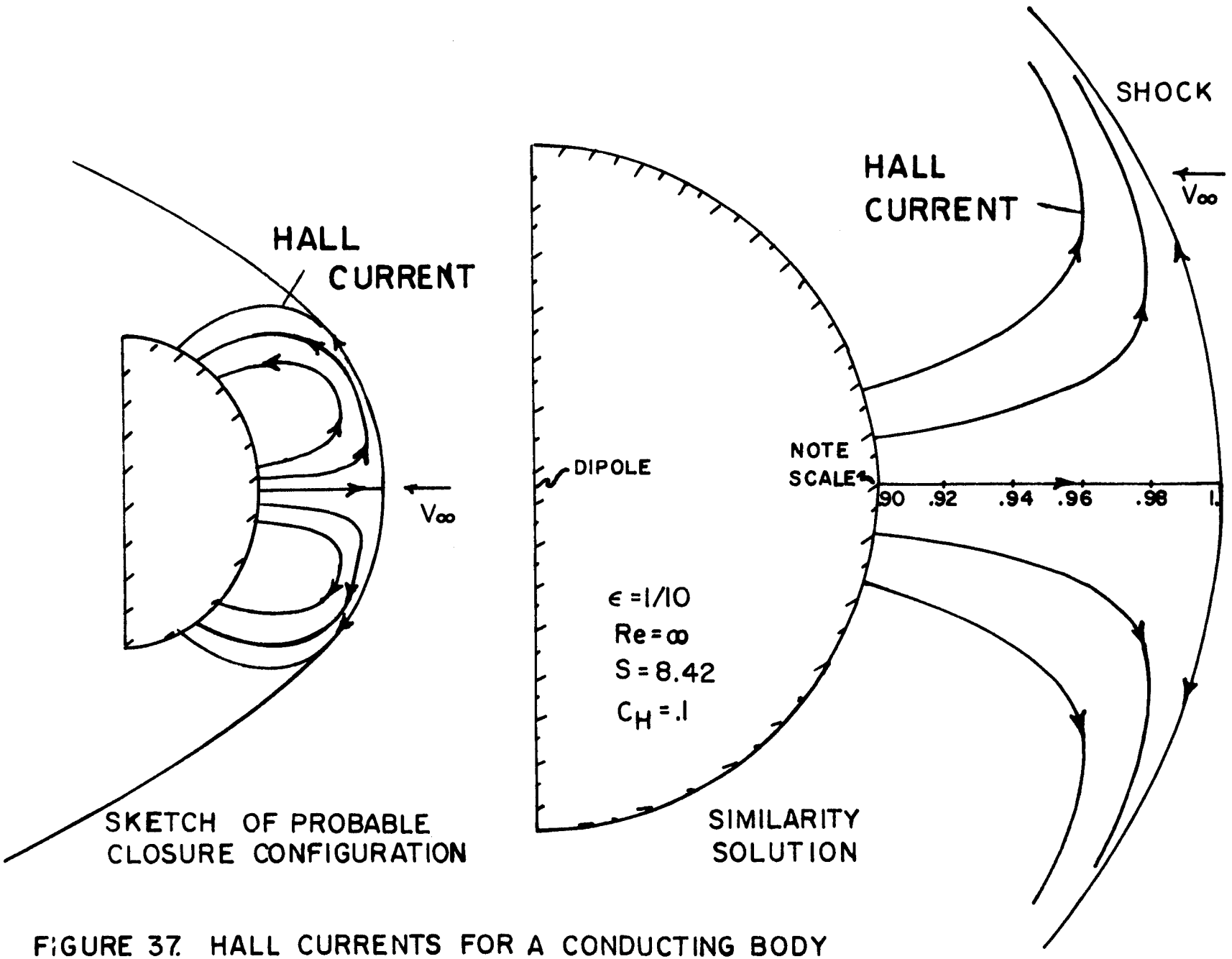

FIGURE 37. HALL CURRENTS FOR A CONDUCTING BODY

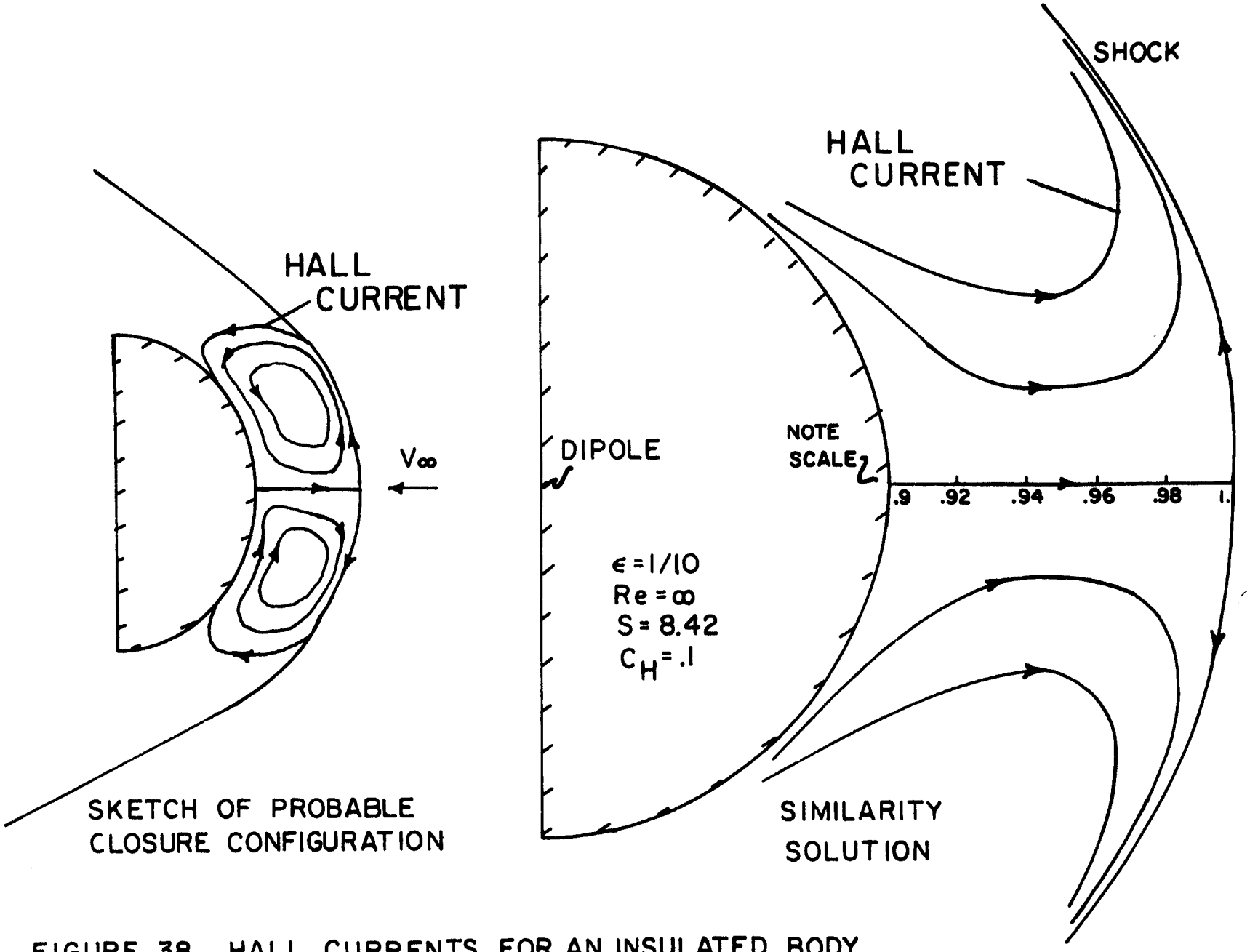

FIGURE 38. HALL CURRENTS FOR AN INSULATED BODY

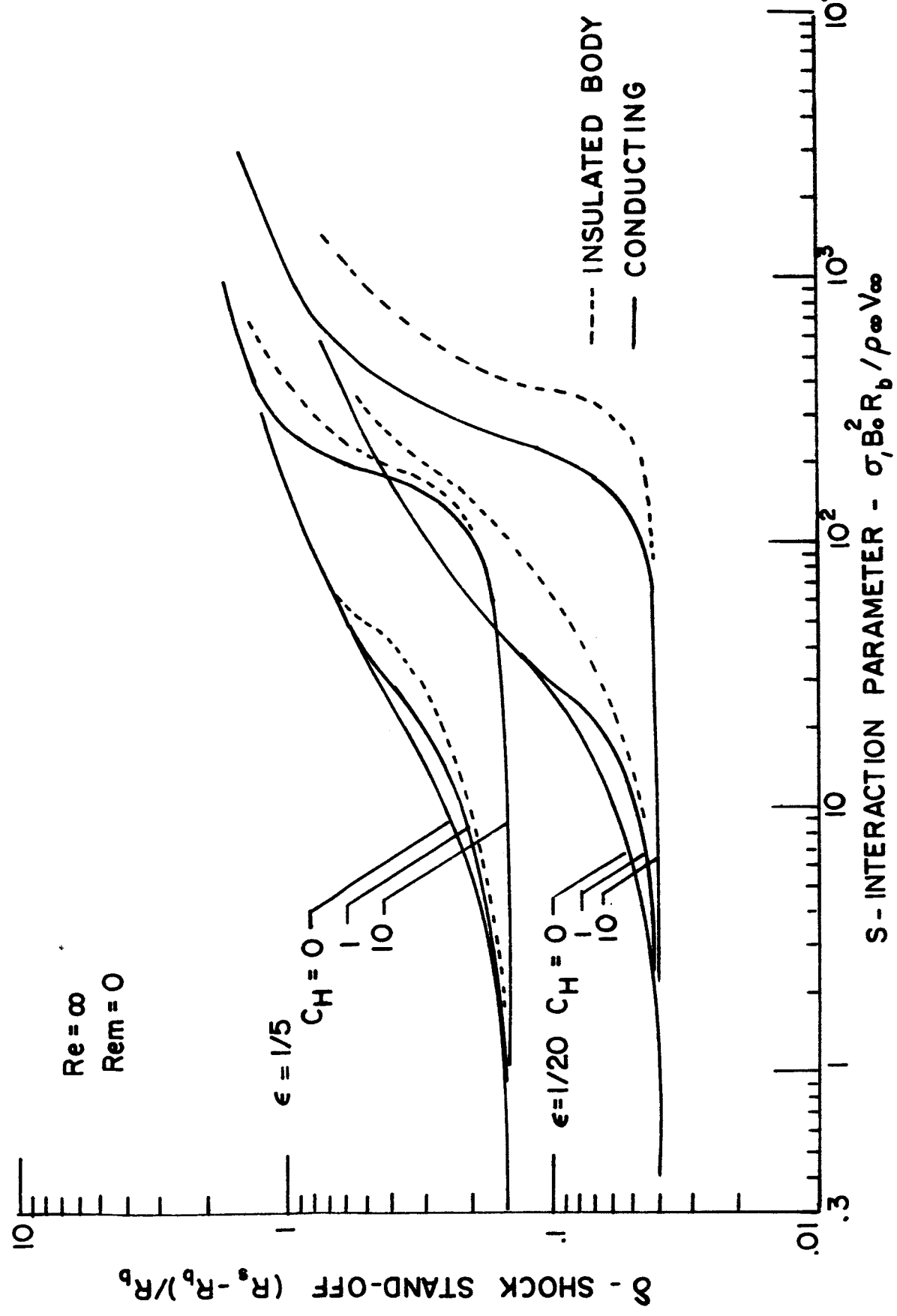

FIGURE 39. SHOCK STAND-OFF WITH HALL EFFECT

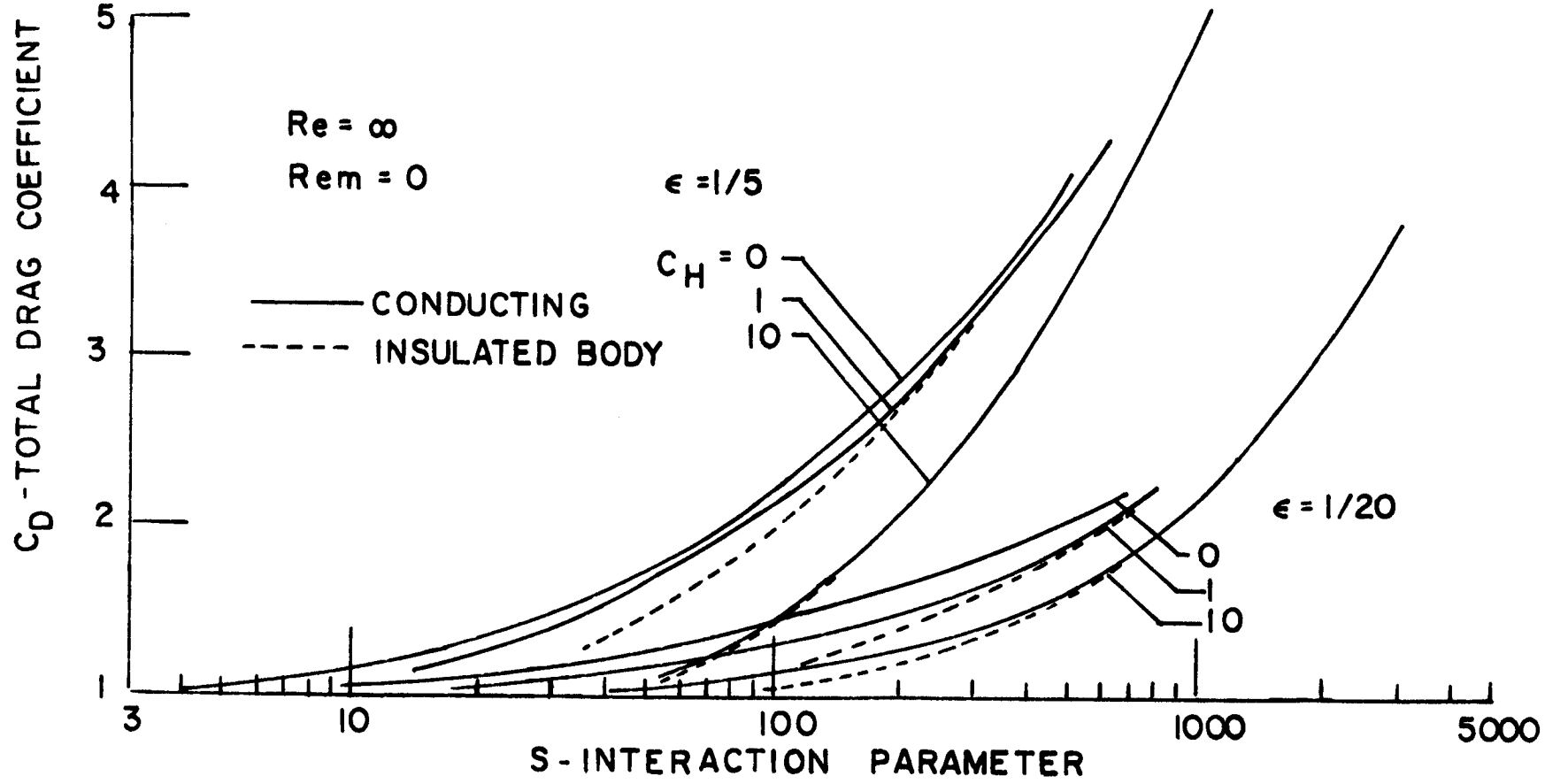

FIGURE 40. TOTAL DRAG WITH HALL EFFECT

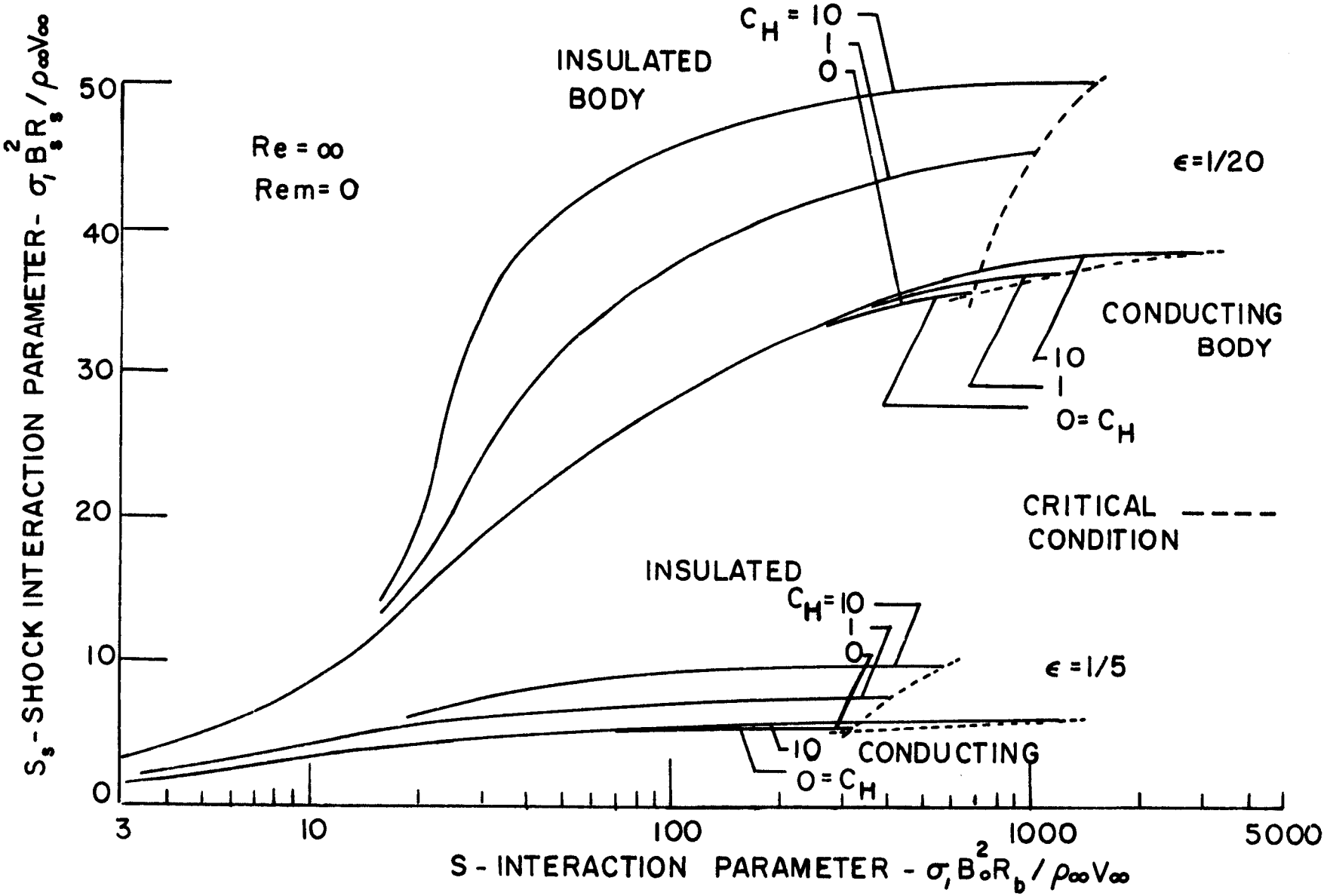

FIGURE 41. SHOCK INTERACTION PARAMETER WITH EFFECT

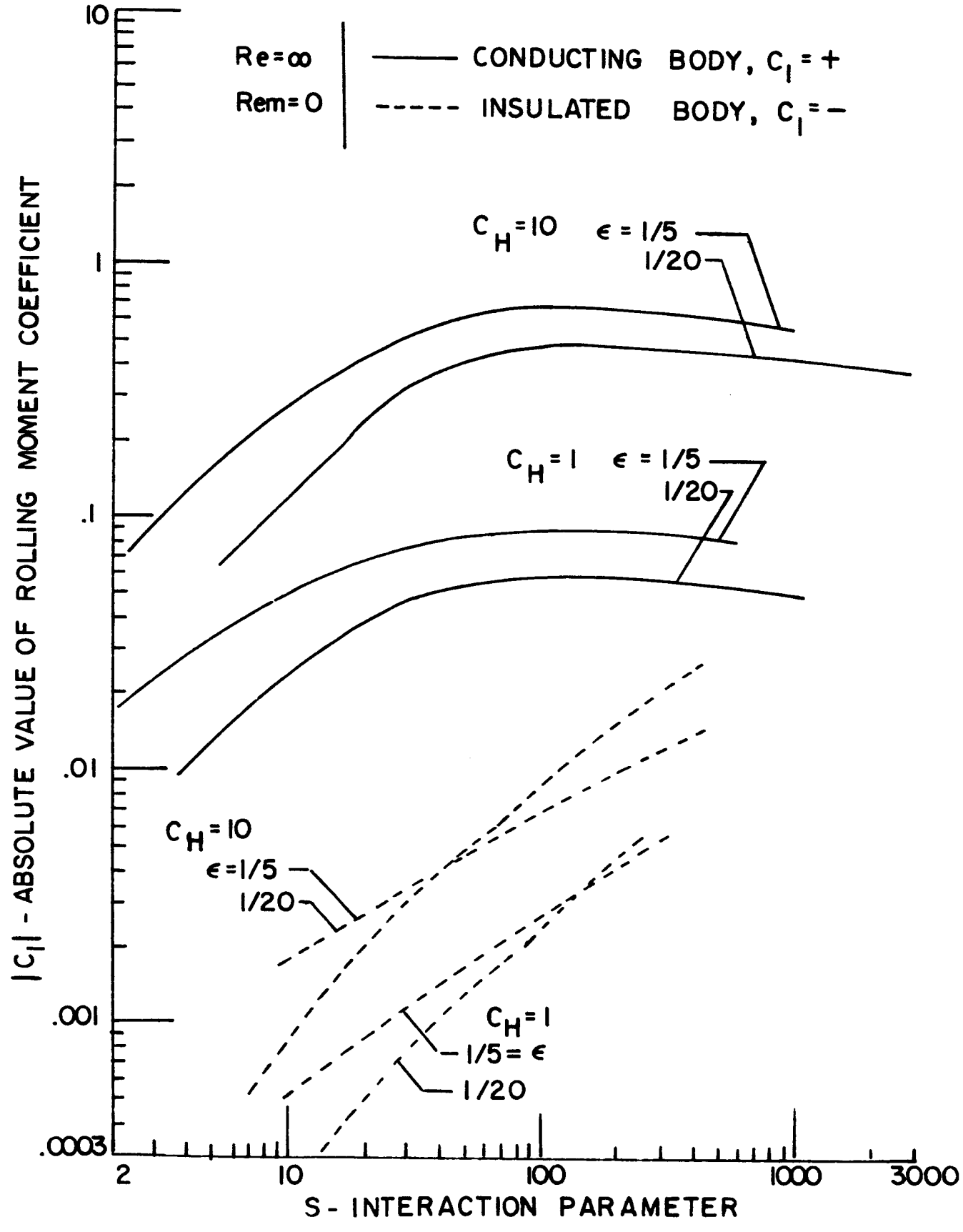

FIGURE 42. ROLLING MOMENT COEFFICIENT WITH HALL EFFECT

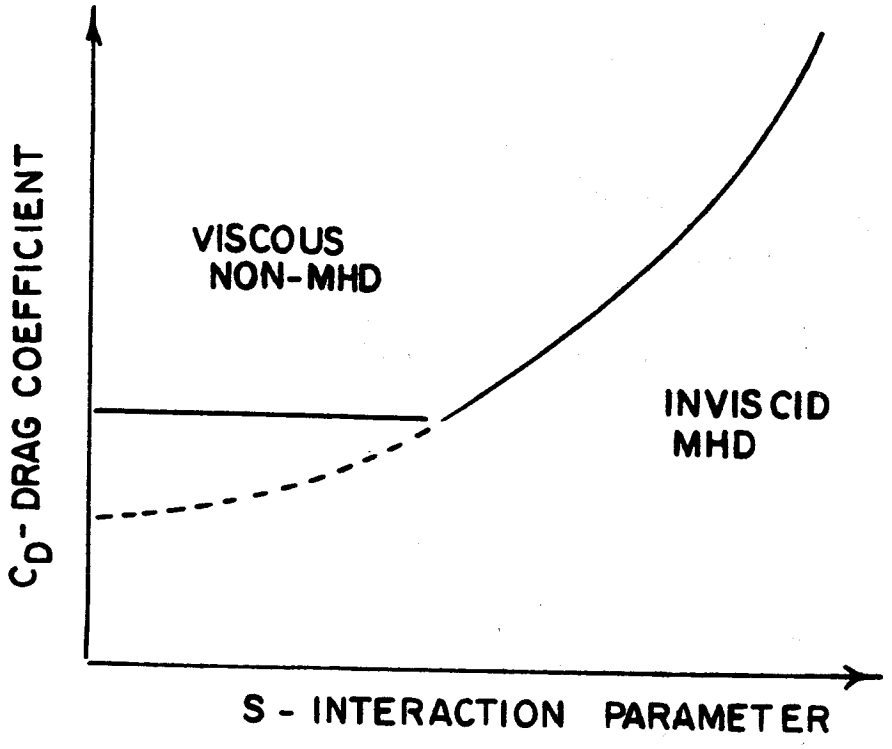

FIGURE 43. SKETCH OF APPROXIMATE THEORY

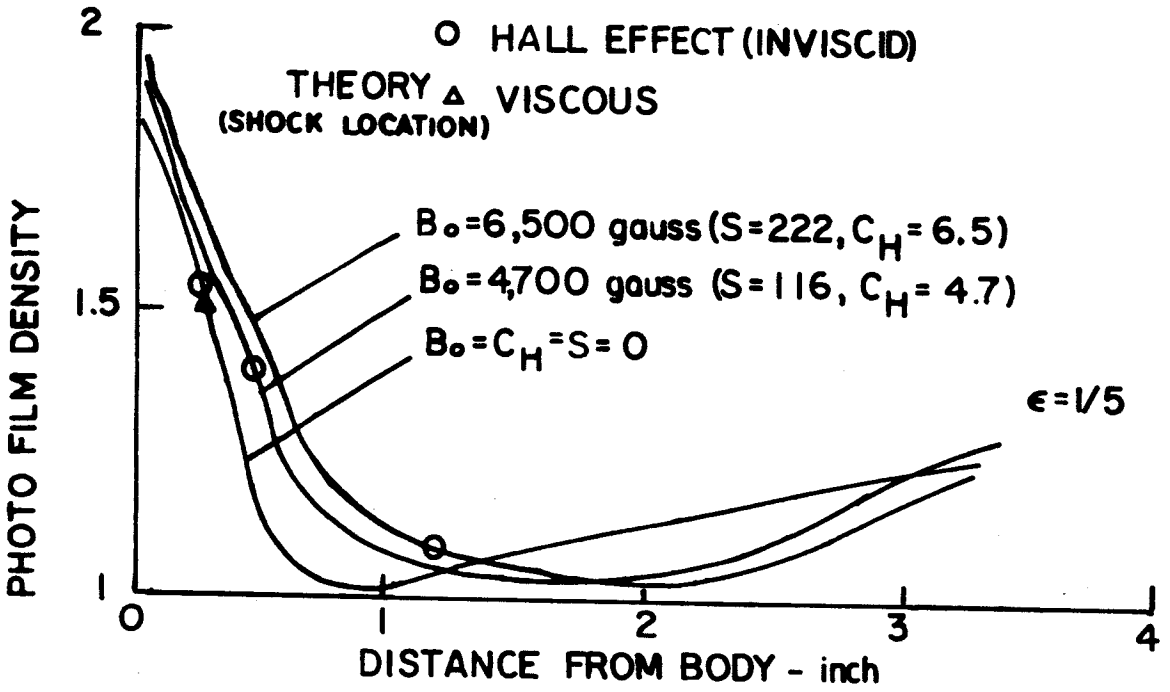

FIGURE 44. FILM DENSITY VS. DISTANCE FROM BODY

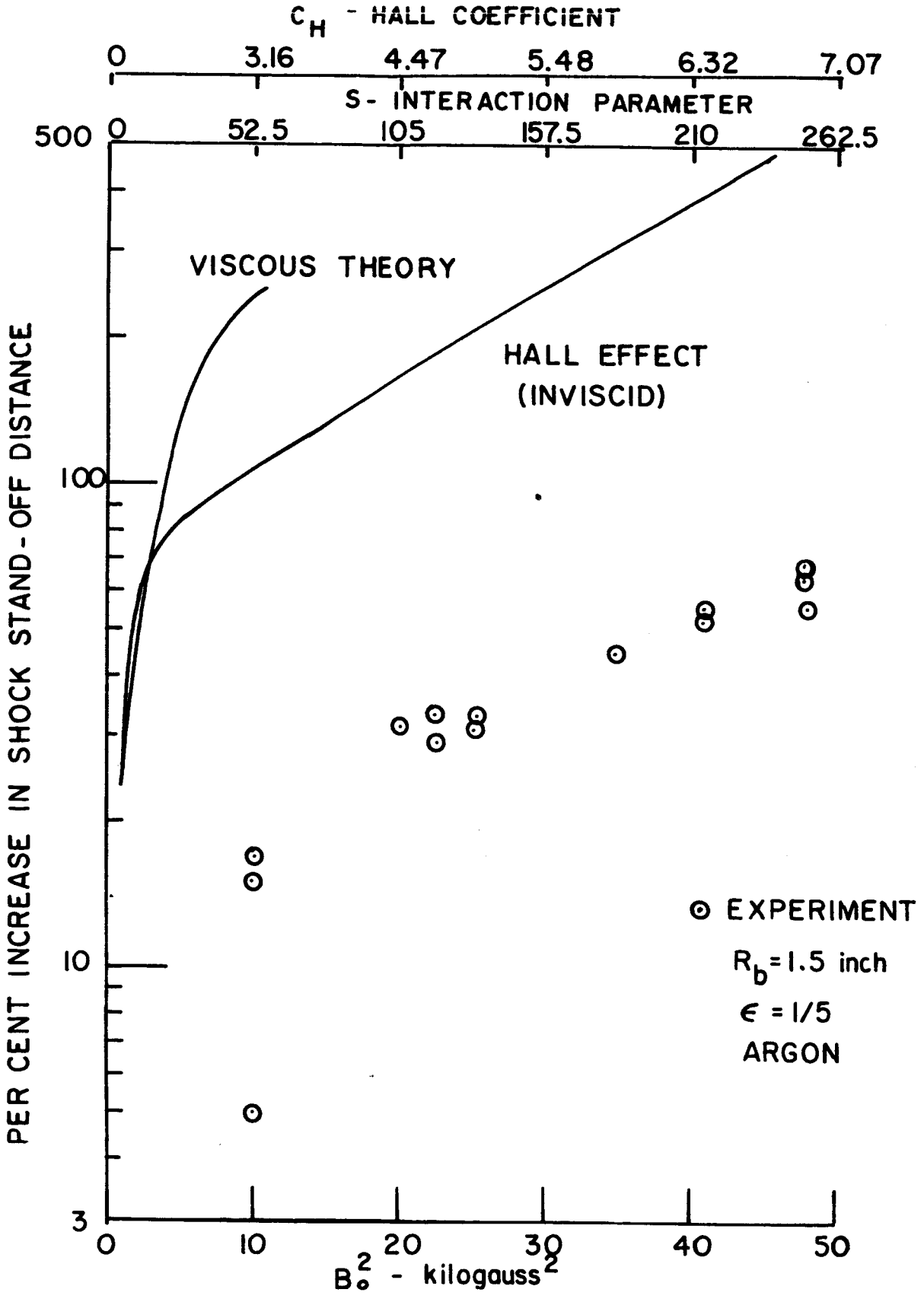

FIGURE 45. EXPERIMENTAL SHOCK STAND-OFF (REF. 33)

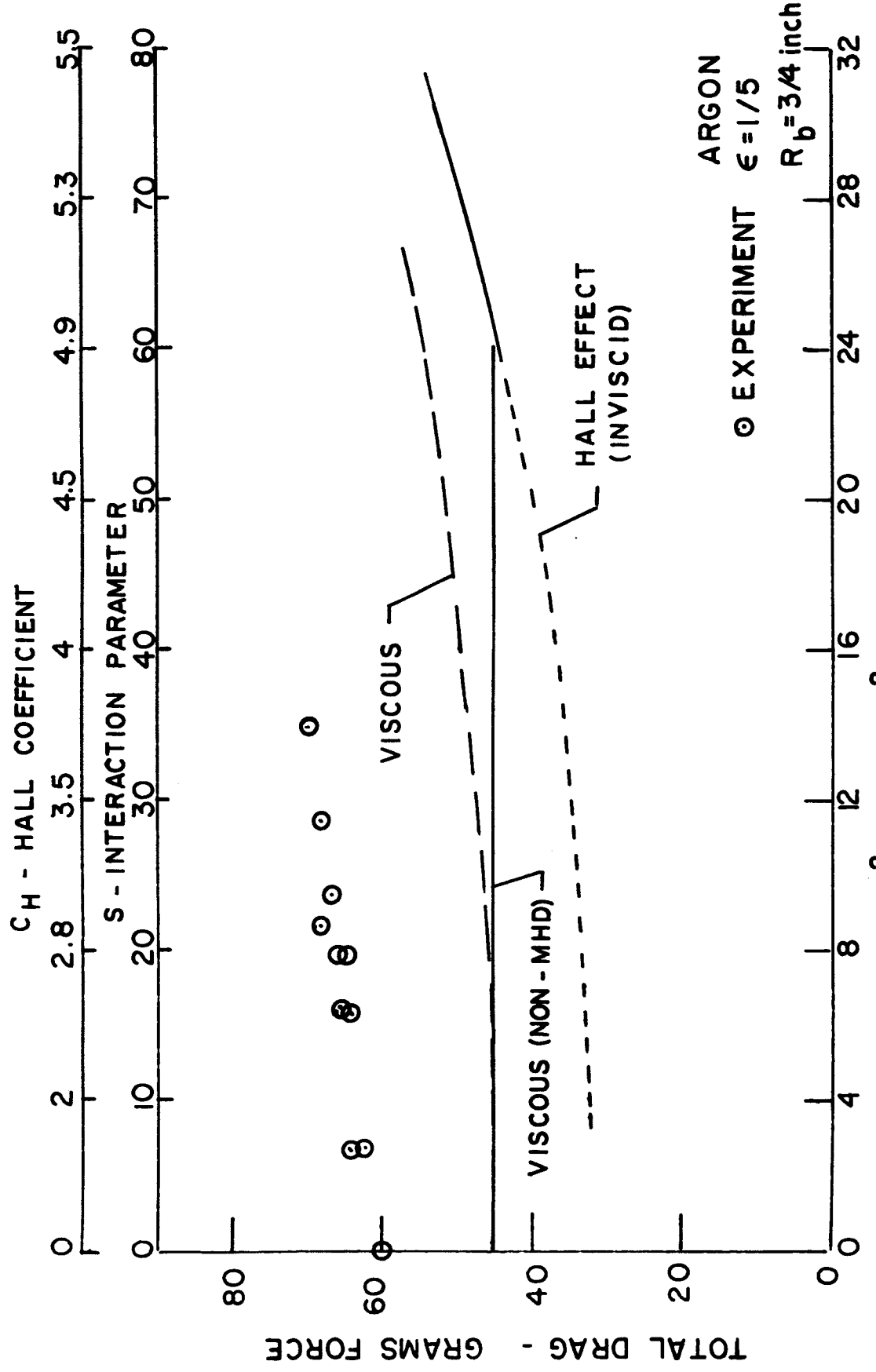

FIGURE 46. THEORETICAL & EXPERIMETAL DRAG

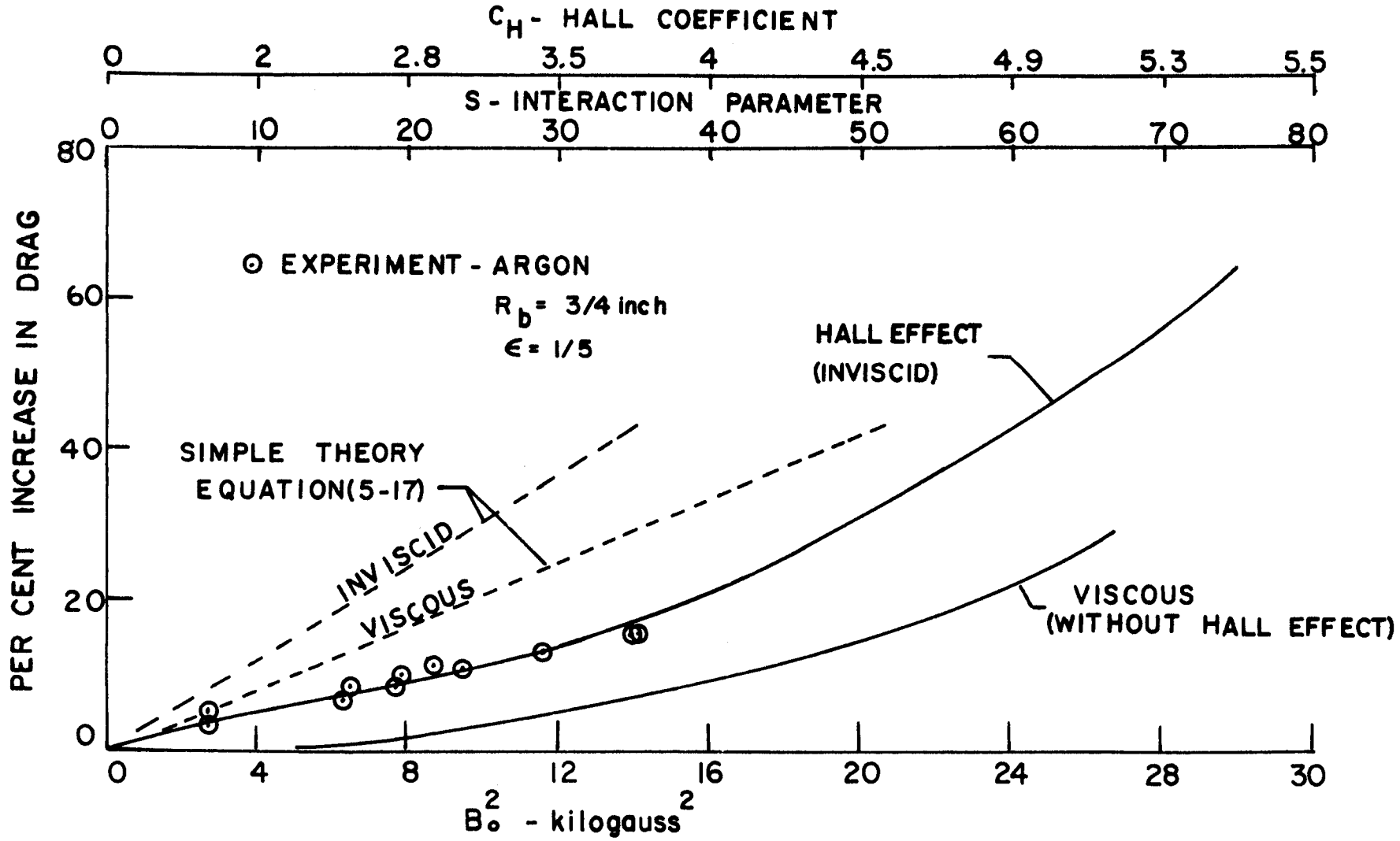

FIGURE 47. PER CENT INCREASE IN DRAG